Universitat Autònoma de Barcelona

Printing of organic semiconductors: morphology, crystal structure and interfaces

Adrián Tamayo Serra

ADVERTIMENT. L'accés als continguts d'aquesta tesi doctoral i la seva utilització ha de respectar els drets de la persona autora. Pot ser utilitzada per a consulta o estudi personal, així com en activitats o materials d'investigació i docència en els termes establerts a l'art. 32 del Text Refós de la Llei de Propietat Intel·lectual (RDL 1/1996). Per altres utilitzacions es requereix l'autorització prèvia i expressa de la persona autora. En qualsevol cas, en la utilització dels seus continguts caldrà indicar de forma clara el nom i cognoms de la persona autora i el títol de la tesi doctoral. No s'autoritza la seva reproducció o altres formes d'explotació efectuades amb finalitats de lucre ni la seva comunicació pública des d'un lloc aliè al servei TDX. Tampoc s'autoritza la presentació del seu contingut en una finestra o marc aliè a TDX (framing). Aquesta reserva de drets afecta tant als continguts de la tesi com als seus resums i índexs.

ADVERTENCIA. El acceso a los contenidos de esta tesis doctoral y su utilización debe respetar los derechos de la persona autora. Puede ser utilizada para consulta o estudio personal, así como en actividades o materiales de investigación y docencia en los términos establecidos en el art. 32 del Texto Refundido de la Ley de Propiedad Intelectual (RDL 1/1996). Para otros usos se requiere la autorización previa y expresa de la persona autora. En cualquier caso, en la utilización de sus contenidos se deberá indicar de forma clara el nombre y apellidos de la persona autora y el título de la tesis doctoral. No se autoriza su reproducción u otras formas de explotación efectuadas con fines lucrativos ni su comunicación pública desde un sitio ajeno al servicio TDR. Tampoco se autoriza la presentación de su contenido en una ventana o marco ajeno a TDR (framing). Esta reserva de derechos afecta tanto al contenido de la tesis como a sus resúmenes e índices.

WARNING. The access to the contents of this doctoral thesis and its use must respect the rights of the author. It can be used for reference or private study, as well as research and learning activities or materials in the terms established by the 32nd article of the Spanish Consolidated Copyright Act (RDL 1/1996). Express and previous authorization of the author is required for any other uses. In any case, when using its content, full name of the author and title of the thesis must be clearly indicated. Reproduction or other forms of for profit use or public communication from outside TDX service is not allowed. Presentation of its content in a window or frame external to TDX (framing) is not authorized either. These rights affect both the content of the thesis and its abstracts and indexes.

Printing of organic semiconductors: morphology, crystal structure and interfaces

Adrián Tamayo Serra

Doctoral Thesis

Physics and Chemistry Department

Universidad Autónoma de Barcelona

PhD Programme in Materials Science

Supervisor/Director: Prof. Marta Mas Torrent

Molecular Nanoscience and Organic Materials (NANOMOL)

Institut de Ciència de Materials de Barcelona (ICMAB-CSIC)

May, 2022

Memòria presentada per aspirar al Grau de Doctor per:

Adrián Tamayo Serra

Vist i plau:

Prof. Marta Mas Torrent

Bellaterra, 4 de maig del 2022

MARTA MAS TORRENT, Research Scientist of the Spanish Council of Research (CSIC) at the Materials Science Institute of Barcelona (ICMAB)

CERTIFIES

That Adrián Tamayo Serra has performed, under her supervision, the research work entitled “Printing of organic semiconductors: morphology, crystal structure and interfaces”. This work has been carried out under the framework of the Materials Science PhD programme of the Physics and Chemistry Department of the Autonomous University of Barcelona.

And in witness whereof this is signed by

Director:

Prof. Marta Mas-Torrent

Bellaterra, May 4th, 2022

ACKNOWLEDGEMENTS

Hace ya 6 años y medio que empecé esta larga aventura que llega a su fin. Echando la vista atrás, este ha sido un viaje irregular en que ha habido buenos y malos momentos de los que aprender y evolucionar. Durante este largo trayecto han pasado muchas personas por mi vida y cada una de ella ha aportado su granito de arena en la consecución de esta tesis.

Primero de todo me gustaría agradecer a la Prof. Marta Mas por darme la oportunidad de entrar en este grupo cuando solo era un estudiante de grado. Ella me ha ayudado y guiado durante este largo camino que finaliza con la presentación de esta tesis doctoral, y me abrió la puerta de un grupo increíble de personas que me introdujeron en el mundo de la investigación. También me gustaría agradecer a Jaume Veciana y Concepció Rovira, por darme la oportunidad de realizar los proyectos de grado, máster y tesis en su grupo, y aunque no he convivido mucho con ellos, he agradecido enormemente todas sus sugerencias y consejos estos años.

Del mismo modo me gustaría agradecer a todos los post-doc que durante este tiempo han compartido su conocimiento conmigo. Quiero agradecer al Dr. Sergi Riera-Galindo por guiarme en mis primeros años en el mundo de la investigación. Sus consejos y su dedicación me ayudaron a entrar en un mundo nuevo para mí.

También agradecer a la Dra. Francesca Leonardi, por sus enseñanzas y su apoyo durante este largo viaje, fue un place trabajar contigo en el laboratorio y fuera de él. Al Dr. Stefano Casalini, que, aunque convivimos poco tiempo, aprendí mucho de tu forma de trabajar y me ayudaste siempre que lo necesité. También al Dr. Jose Muñoz por todos sus consejos y ayudarme en el desarrollo de esta tesis.

No quiero olvidarme de los Dres. Tommaso Salzillo y Raphael Pfattner que probablemente sean con los que más tiempo he convivido, quiero agradeceros la paciencia que tuvisteis conmigo. Han sido muchos años de escuchar mis lamentaciones y problemas, pero siempre habéis estado para darme buenos consejos y aportar nuevas ideas.

The work carried out in this thesis would not have been possible without collaborations with other research groups. Because of that, I would like to thank all the collaborators which have contributed to the research done in this thesis.

I would like to thank, Dr. Roland Resel from the University of Graz and his group, for their collaboration in the study of the crystal structure of my organic thin films.

I would like to thank Prof. Beatrice Fraboni from the University of Bologna and her group, for collaboration in the study of the relationship between the x-ray sensitivity and the morphology of my organic thin films.

I would also like to thank Dr. Emanuele Orgiu from the Institut National de la Recherche Scientifique (INRS) in Quebec, for accepting me during a 3 month, although in the end I could not work alongside them. Also, thanks to all the collaborators from his group that were part of this thesis.

Finally, thank you all the members of the OFET team, I have spent most of the time with you talking and working in the lab. Thanks to Dr. Ines Temiño, Dr. Simona Ricci, Dr. Antonio Campos and Dr. Qiaoming Zhang for sharing with me the first years of my thesis. They taught me many of the things that I have taught new members. Also, thanks to Dr. Carme Martinez for helping me to close this stage of my professional life.

And thanks to Jinghai Li, Sara Ruiz, Lamiaa Fijahi and Maria Elisabetta Giglio, I have really enjoyed the time that I have shared in the laboratory with you, although due to the pandemic it was not as much as I would have liked.

Dejando de lado la parte científica de mi etapa en el ICMAB, tengo que agradecer a todos los compañeros del grupo NANOMOL, por esos momentos de desconexión. He conocido a mucha gente durante mi estancia en el ICMAB y de cada uno de ellos he aprendido algo nuevo. Especialmente quiero agradecer a mis compañeros de oficina con los que he disfrutado de infinidad de desayunos, largas charlas a última hora de la tarde y compartido grandes momentos. Esta tesis también en vuestra (Lidia, Guillem, Pilar, Songabi, Arnau, Judit, David, Albert, Ángel, Nathalie, Dolores, Ramon, Lijia, Jose Catalán, Fabiao, Nere, Edu, Marc, y mucha más gente).

Por último y no menos importante, gracias a mi familia por su apoyo durante esta etapa de mi vida. Entendieron en todo momento que para mí esto no era trabajo sino algo más y me apoyaron en todo momento. Y una mención especial para Mariel Ruiz Kubli, que me ha aguantado durante la escritura de artículos y esta tesis. Sé que ha sido difícil adaptarte a mis horarios de trabajo y mis sesiones de trabajo en horas intempestivas.

ABSTRACT

Organic electronics is raising a lot of interest in low-cost and large area applications. Organic semiconductors (OSCs) can be deposited from solution techniques compatible with roll-to-roll processes at low temperatures and on flexible substrates. The transport in OSCs is determined by the electronic overlap between molecules, and hence, the morphology and structure of the OSC films has a crucial effect in the device performance. Organic field-effect transistors (OFETs) are suitable platforms to study the transport properties of OSCs. In addition, these devices show great potential in sensing devices, such as for the development of photodetectors or in bio-sensing by using electrolyte-gated OFETs (EGOFETs). In this thesis, we have fabricated OFETs and EGOFETs using the bar-assisted meniscus shearing (BAMS) technique to deposit the OSC layer, which is a high throughput low cost printing technique. In addition, to process the OSCs, we used blends of these materials with polystyrene (PS) to enhance the OSC processability and crystallinity.

In Chapter 2, the influence of the coating parameters and solution formulation on the thin film morphology and structure was investigated using the OSCs dibenzotetrathiafulvalene, 6,13-Bis(triisopropylsilylethynyl)pentacene, and 2-Decyl-7-phenyl[1]benzothieno[3,2-b][1]benzothiophene. The modification of these parameters permitted to control the formation of kinetic or thermodynamic polymorphs and also the thin films anisotropy. The films were optimised to achieve an enhanced OFET performance.

Chapter 3 is devoted to the application of OFETs based on pentacene derivatives as X-ray photodetectors. The X-ray response was optimised by controlling the thin morphology, by reducing the majority of charge carrier traps using blends of the OSC with PS, and by improving the device mobility. Record photoresponses were achieved surpassing that of commercial inorganic detectors.

In Chapter 4, we studied different aspects related to the modification of the gate electrode/electrolyte interface in EGOFETs. We investigated how the functionalisation of the gate electrode with molecular self-assembled monolayers or the use of carbon paste electrodes with different carbon fillers can be useful tools to tune the device response. In addition, EGOFETs were exploited to monitor the formation of a surfactant monolayer on the gate metal.

PUBLICATIONS INCLUDED IN THIS THESIS

[I] **Control of polymorphism and morphology in solution sheared organic field-effect transistors**

Sergi Galindo, Adrián Tamayo, Francesca Leonardi and Marta Mas-Torrent

Advanced Functional Materials 27 (25), 1700526 (2017)

[II] **Role of polymorphism and thin-film morphology in organic semiconductors processed by solution shearing**

Sergi Riera Galindo, Adrián Tamayo and Marta Mas-Torrent

ACS omega 3 (2), 2329 (2018)

[III] **Modification of the gate electrode by self-assembled monolayers in flexible electrolyte-gated organic field effect transistors: work function vs. capacitance effects**

Francesca Leonardi, Adrián Tamayo, Stefano Casalini and Marta Mas-Torrent

RSC advances 8 (48), 27509 (2018)

[IV] **Impact of the ink formulation and coating speed on the polymorphism and morphology of a solution-sheared thin film of a blended organic semiconductor**

Adrián Tamayo, Sergi Riera Galindo, Andrew OF Jones, Roland Resel and Marta Mas-Torrent

Advanced Materials Interfaces 6 (22), 1900950 (2019)

[V] **Electronic performance of polymer carbon-paste nanoallotropes from 0D to 3D as novel gate electrodes in water-gated organic field-effect transistors**

Adrián Tamayo, Jose Muñoz and Marta Mas-Torrent

Advanced Electronic Materials 6 (7), 2000431 (2020)

[VI] Morphology and mobility as tools to control and unprecedentedly enhance X-ray sensitivity in organic thin-films

Inés Temiño, Laura Basiricò, Ilaria Fratelli, Adrián Tamayo, Andrea Ciavatti, Marta Mas-Torrent and Beatrice Fraboni

Nature Communications 11 (1), 2136 (2020)

[VII] Molecular disorder in crystalline thin films of an asymmetric BTBT derivative

Sebastian Hofer, Johanna Unterkofler, Martin Kaltenegger, Guillaume Schweicher, Christian Ruzié, Adrián Tamayo, Tommaso Salzillo, Marta Mas-Torrent, Alessandro Sanzone, Luca Beverina, Yves Henry Geerts, Roland Resel

Chemistry of Materials 33 (4), 1455 (2021)

[VIII] Mobility anisotropy in the herringbone structure of asymmetric Ph-BTBT-10 in solution sheared thin film transistors

Adrián Tamayo, Sebastian Hofer, Tommaso Salzillo, Christian Ruzié, Guillaume Schweicher, Roland Resel, Marta Mas-Torrent

Journal of Materials Chemistry C 9, 7186 (2021)

[IX] Interplay between electrolyte-gated organic field-effect transistors and surfactants: a surface aggregation tool and protecting semiconducting layer

Qiaoming Zhang, Adrián Tamayo, Francesca Leonardi, Marta Mas-Torrent

ACS Applied Materials & Interfaces 13 (26), 30902 (2021)

[X] Low activation energy field-effect transistors fabricated by bar-assisted meniscus shearing

Michael Berteau-Rainville, Adrián Tamayo, Tim Leydecker, Atiye Pezeshki, Ingo Salzmann, Marta Mas-Torrent, Emanuele Orgiu

Applied Physics Letters 119 (10), 103301 (2021)

[XI] Organic Field Effect Transistors based on Ternary Blends including a Fluorinated Polymer for Achieving Enhanced Device Stability

Adrián Tamayo, Tommaso Salzillo, and Marta Mas-Torrent

Advanced Materials Interfaces 9 (6), 2101679 (2022)

PUBLICATIONS NOT INCLUDED IN THIS THESIS

[I] **Charge transfer complexes of a benzothienobenzothiophene derivative and their implementation as active layer in solution-processed thin film organic field-effect transistors**

Lamiaa Fijahi, Tommaso Salzillo, Adrián Tamayo, Marco Bardini, Christian Ruzié, Claudio Quarti, David Beljonne, Simone D'Agostino, Yves Geerts, Marta Mas-Torrent

Journal of Material Chemistry C, Accepted (2022)

DOI: 10.1039/D2TC00655C

CONFERENCE CONTRIBUTIONS

[I] **Control of morphology and polymorphism in DB-TTF thin films**

Adrián Tamayo, Sergi Galindo, Francesca Leonardi and Marta Mas-Torrent

XVII Escuela Nacional de Materiales Moleculares, Málaga (Spain), poster presentation (2018).

[II] **Control of polymorphism and morphology in DB-TTF thin films by solution shearing**

Adrián Tamayo, Sergi Riera-Galindo, Francesca Leonardi and Marta Mas-Torrent

14th International Conference on Organic Electronics (ICOE), Bordeaux (France), poster presentation (2018).

[III] **Control of morphology and polymorphism in organic semiconductor thin films**

Adrián Tamayo, Sergi Riera-Galindo, Francesca Leonardi and Marta Mas-Torrent

4th Scientific Meeting of BNC-b Students, Bellaterra (Spain), oral presentation (2019).

[IV] **Control of morphology and polymorphism in a thin film of a blended organic semiconductor by tuning the solution shearing parameters**

Adrián Tamayo, Sergi Riera-Galindo, Francesca Leonardi, Inés Temiño and Marta Mas-Torrent

15th European Conference on Molecular Electronics (ECME), Linköping (Sweden) poster presentation.

[V] **Morphology and mobility as tools to control and unprecedentedly enhance X-ray sensitivity in organic thin-films**

Inés Temiño, Laura Basiricò, Ilaria Fratelli, Adrián Tamayo, Andrea Ciavatti, Marta Mas-Torrent and Beatrice Fraboni

2020 Express Conference on the Physics of Materials and Their Applications in Energy and Environment, Online, poster presentation (2020).

[VI] Mobility anisotropy in the herringbone structure of asymmetric Ph-BTBT-10 in solution sheared thin film transistors

Adrián Tamayo, Sebastian Hofer, Tommaso Salzillo, Aleix Quintana, Roland Resel and Marta Mas-Torrent

Spring Meeting of the European Materials Research Society (E-MRS), Online, poster presentation (2021).

LIST OF ABBREVIATIONS AND SYMBOLS

Abbreviations

1DT	1-dodecanethiol
AFM	atomic force microscopy
ATP	4-aminothiophenol
AUT	11-amino-1-undecanol
BAMS	bar-assisted meniscus shearing
C8-BTBT	2,7-dioctyl[1]benzothieno[3,2-b][1]benzothiophene
C8-O-BTBT	2,7-bis(octyloxy)[1]benzothieno[3,2-b]-benzothiophene
CPE	carbon paste electrode
BGBC	bottom-gate bottom-contact
BGTC	bottom-gate top-contact
CRP	c-reactive protein
D	drain
DB-TTF	dibenzotetrathiafulvalene
DIF-TES-ADT	2,8-difluoro-5,11-bis(triethylsilylethynyl)anthradithiophene
EDL	electrical double layer
EGOFET	electrolyte-gated organic field-effect transistor
F_4-TCNQ	2,3,5,6-tetrafluoro-7,7,8,8-tetracyanoquinodimethane
FTP	4-fluorothiophenol
G	gate
HOMO	highest occupied molecular orbital
KPFM	Kelvin probe force microscopy
LED	light-emitting diode
LUMO	lowest unoccupied molecular orbital
METP	4-methylthiophenol
MHD	16-mercaptohexadecanoic acid
MOSFET	metal-oxide-semiconductor field-effect transistor
N2200	polynaphtalene-bithiophene
OFET	organic field-effect transistor
OLED	organic light-emitting diode
OPV	organic photovoltaic
OSC	organic semiconductor
P3HT	poly(3-hexylthiophene-2,5-diyl)

PDI8CN2	n,n'-bis(n-octyl)-x:y,dicyanoperylene-3,4:9,10-bis(dicarboximide)
PDMS	Poly(dimethylsiloxane)
PEDOT:PSS	poly(3,4-ethylenedioxythiophene) polystyrene sulfonate
PFBT	2,3,4,5,6-Pentafluorothiophenol
PFDT	2h,2h-perfluorodecanethiol
Ph-BTBT-C_{10}	2-decyl-7-phenyl[1]benzothieno[3,2-b][1]benzothiophene
PFS	poly(pentafluorostyrene)
PMA	poly(methyl acrylate)
PMMA	poly(methyl 2-methylpropenoate)
PS	polystyrene
PVA	poly(vinyl alcohol)
PVD	vapor phase deposition
S	source
SAM	self-assembled monolayer
TGBC	top-gate bottom-contact
TGTC	top-gate top-contact
TIPS-pentacene	6,13-bis(triisopropylsilylethynyl)pentacene
TLM	transfer-length method
TMTES-pentacene	1,4,8,11-tetramethyl-6,13-triethylsilylethynyl pentacene
TOF-SIMS	time-of-flight secondary ion mass spectrometry
TTF-TCNQ	tetrathiafulvalene-tetracyanoquinodimethane

Symbols

C	capacitance
D	drain
E_F	fermi level
E_g	band gap
ϕ	work-function
G	gate
I_{DS}	drain-source current
I_{GS}	gate-source current
L	channel length
μ	field-effect mobility
N_T	density of charge carrier traps
On/Off	on/off current ratio
Q	charge
R_C	contact resistance
R_{CH}	channel resistance
S	source
SS	sub-threshold swing
V_{FB}	flat-band voltage
V_{on}	on voltage
V_{DS}	drain-source voltage
V_{GS}	gate-source voltage
V_{TH}	threshold voltage
W	channel width

CONTENTS

CHAPTER I

INTRODUCTION

1.1. ORGANIC ELECTRONICS

In 1948, one of humanity's greatest achievements of the 20th century was developed at Bell Laboratories. John Bardeen, Walter H. Brattain and William Shockley created the first operative transistor based on germanium.[1] These three researchers are considered the fathers of microelectronics. The first silicon-based transistor was developed in 1958 also at Bell Laboratories. Silicon-based transistors are the cornerstone of today's microelectronics. The enormous improvement in transistor fabrication technology has permitted to move from integrated devices based on only 4 transistors in 1958[2] to 54 billion transistors in 2020.[3] This has been achieved by reducing the size and increasing the density of transistors per unit area. Transistors have changed the way people work, live, and communicate in the last century, since they are present in all the equipment that we use daily, from the electronics of cars or cell phones to glucose or blood sensors in the hospitals.

Silicon-based transistors exhibit high mobility and therefore high speed devices can be fabricated with them. However, their high manufacturing costs and poor scalability are their big handicap.[4] In the last two decades, there has been a high demand for silicon-based transistors for Internet-of-Things. The stock of semiconductor devices in the world has been steadily worsening since the start of the pandemic. A new surge in demand driven by changing habits fuelled by the pandemic has led to a critical point of a global shortage in semiconductors.[5] Thus, low-cost alternatives to electronics based on silicon are being sought.

Organic electronics represents a viable alternative to silicon-based electronics since they can provide new applications horizons and production methods. Organic-based devices are not suitable for high-speed circuits, but they can be potentially manufactured at reduced costs, with methodologies compatible with roll-to-roll processes and at low temperature, making them compatible with flexible substrates.[6–11] Further, organic materials offer greater biocompatibility.

Organic semiconductors (OSCs) are based on molecules and polymers composed mainly of carbon (C) and hydrogen (H), and also of other heteroatoms such as nitrogen (N), phosphorus (P), oxygen (O), sulphur (S) as well as halogens or transition metals.[6,12] Organic materials display excellent and tuneable mechanical, electrical and optical properties which are of great interest for numerous applications. Hence, they have become very attractive for their integration in electronic devices.

The birth of organic electronics took place in the 70's with the discovery of the first small molecule organic metal, tetrathiafulvalene-tetracyanoquinodimethane (TTF-TCNQ),[13] and the first highly conducting conjugated polymer, chemically doped polyacetylene.[14] These achievements led to a huge research interest and promoted the development of new organic conducting materials and organic semiconductors. OSCs have been implemented into a variety of electronic devices such as organic light-emitting diodes (OLEDs),[15–17] organic solar cells or photovoltaic devices (OPVs)[18–22] and organic field-effect transistors (OFETs).[23–26]

OLEDs are electronic devices that convert current into light. The basic structure of OLEDs consists in two sandwiched OSC layers (**Figure 1.1a**). One of the layers acts as electron transporting layer, while the second one acts hole transporting layer. The recombination of the injected electrons and holes at the interface produces excitons. The decay of the exciton to the ground state results in the radiation emission. The wavelength of the emitted light (UV, VIS or IR) is modulated by selecting the appropriate OSC pair. The main advantages of OLEDs with respect to conventional LEDs are they low consumption and ease of turning off the devices. Due to the impressive advances in these devices, commercial products based on OLEDs have been launched to the market as an OLED LG which shows an excellent contrast and colour display (**Figure 1.1b**).

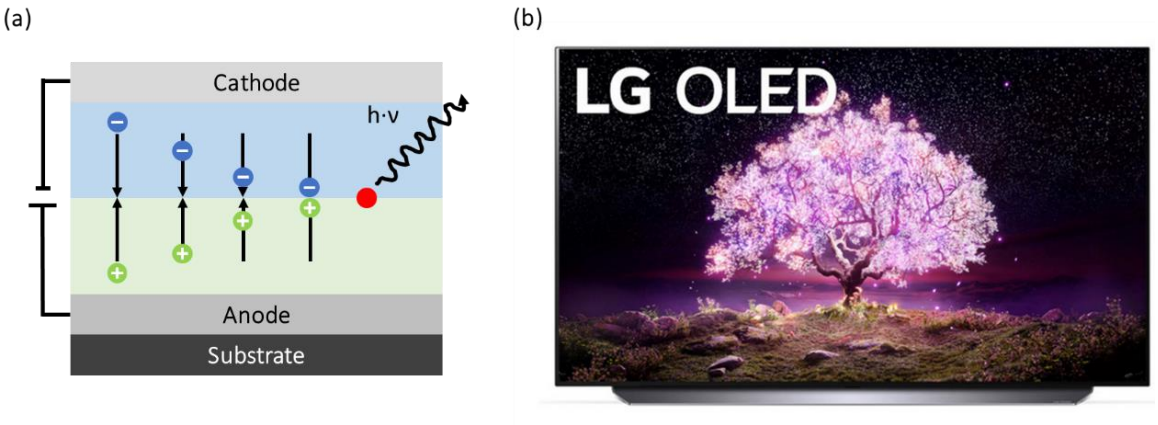

Figure 1.1. (a) Schematic illustration of a typical OLED architecture. **(b)** OLEDs display of LG C1 Class 4K Smart OLED TV. Image taken from the website of LG (https://www.lg.com/us/tvs/lg-oled55c1pub-oled-4k-tv).

In contrast, OPVs are devices devoted to convert sunlight radiation into electrical power. In this case, the semiconductors are responsible for the sunlight radiation absorption instead of the emission. The mechanism behind the operation of OPVs is the generation of excitons at the interface between two p- and n-type OSC layers which are then dissociated into free electrons and free holes (**Figure 1.2a**) that diffuse towards the electrodes generating an electric current. Although OPVs exhibit an acceptable power conversion efficiency (around 18 %),[18] their low stability is currently their main disadvantage. Today,

OPVs are not yet competitive for the PV market, however, OPV provide certain advantages to the photovoltaic sector such as low-cost fabrication, flexibility and the possibility of manufacturing tandem solar cells to maximize the sunlight radiation absorption (**Figure 1.2b**).[20,27,28]

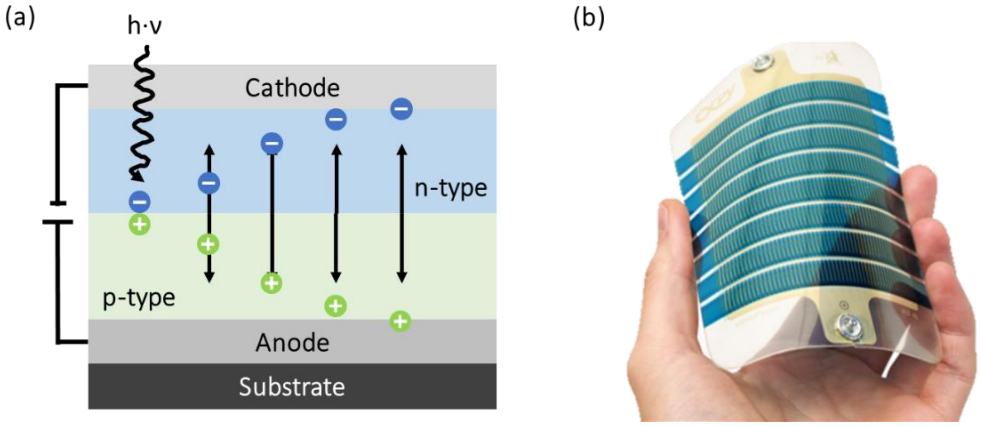

Figure 1.2. (a) Schematic illustration of a typical OPV architecture. **(b)** OPVs modules of infinity PV. Image taken from the website of infinity PV (https://infinitypv.com/products/opv/demonstrator).

Lastly, OFETs are current modulating devices which use an electric field to control the flow of current in an OSC. The current flowing between two electrodes (source and drain) through the semiconductor is modulated by the strong electric field created by a third electrode (gate) (**Figure 1.3a**). The gate electrode is separated from the other electrodes by an insulating layer. This insulating layer acts as a dielectric material and is typically a metal-oxide or a polymer (**Figure 1.3b**).

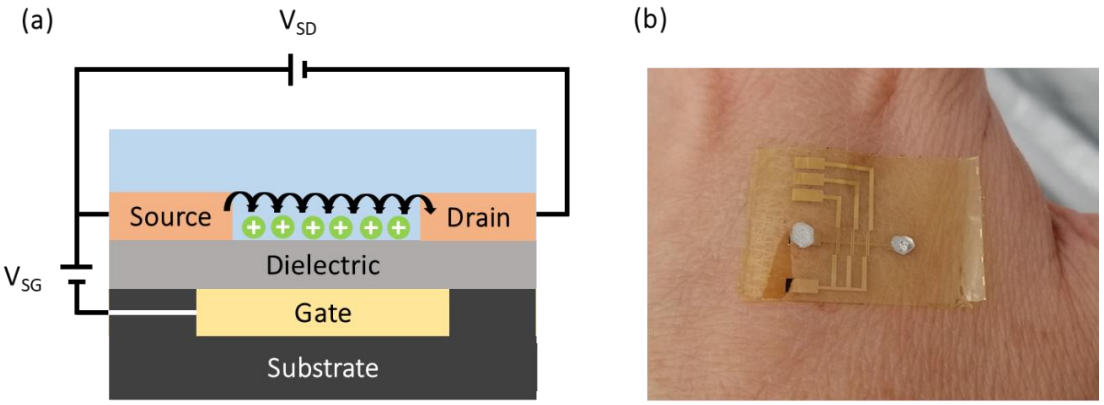

Figure 1.3. (a) Schematic illustration of a typical OFET architecture. **(b)** Photograph of an ultrathin organic OFET fabricated on a polyamide substrate.

The first OFETs were reported in 1987 by Koezuka *et al.* and by Tsumura *et al.* in 1986. Polythiophene was used as organic semiconductor giving mobilities on the order of 10^{-5} $cm^2 \cdot V^{-1} \cdot s^{-1}$.[29,30] Nowadays, the best performance OFET devices display mobilities around 10-20 $cm^2 \cdot V^{-1} \cdot s^{-1}$.[31–35] These mobility values surpass those of amorphous silicon transistors (typically ~1 $cm^2 \cdot V^{-1} \cdot s^{-1}$),[36] which makes OSCs competitive for applications in certain sectors of consumer electronics.

However, the implementation of organic devices into real applications requires to fabricate devices with high-reproducibly, high-performance and high stability. Thus, the research community are devoting intensive efforts to develop organic electronics in order to set up a viable alternative for silicon-based devices.

1.2. Organic Semiconductors

Organic and inorganic materials can be divided into three groups according to their electrical properties, namely insulators, semiconductors, and metals. Inorganic semiconductors are materials formed by a net of covalently bonded atoms (i.e., Si, Ge, GaAs, etc.) that exhibit a strong interaction enabling the formation of long-range delocalized electronic bands extended along the semiconductor material. In inorganic semiconductor materials, the valence band is the ground state which is filled with electrons, while the conduction band is empty. The energy required to move electrons form the valence band to the conduction band is called the band gap (E_g). The band gap is a forbidden energy band without any energy state, and, thus, this is a characteristic parameter of the semiconductor material. Typically, inorganic semiconductors show an electrical conductivity lower than that of a metal (10^6 $S \cdot m^{-1}$) but higher than that of an insulator (10^{-6} $S \cdot m^{-1}$).

On the other hand, organic conductors/semiconductors are hold together by weak van der Waals interactions and usually show much higher resistivity values compared to their inorganic counterparts. Typically, the dependence of their conductivity with temperature is employed to classify them. Organic metals decrease their conductivity when the temperature is increased because the vibration of the crystal structure increases with the temperature scattering the electrons. In contrast, organic semiconductors show an exponential increase of the electrical conductivity as the temperature rises due to an increase of the number of free charges carriers.

OSCs are carbon-based conjugated small molecules or polymers rich in π-orbitals that are delocalized along the backbone of the molecule.[36] They interact with each other are by π-π stacking, van der Waals forces or hydrogen bonding depending on their molecular and supramolecular structure.[6,37] The electrical properties of OSCs are defined by the interactions of the π-orbitals within the molecule/polymer (delocalisation of the π-orbitals

around the molecule) and between the neighbouring molecules. When two sp^2 carbon atoms are bonded along a common axis, molecular delocalized π-orbitals are formed (**Figure 1.4a**). The interaction of the π-orbitals of the semiconductor molecules leads to splitting of the binding and anti-binding energy levels of the OSC. The energy levels of OSCs are characterized by the highest occupied molecular orbital (HOMO) and the lowest unoccupied molecular orbital (LUMO).[38] There is no a long-range electron delocalization like in inorganic semiconductors. In the ground state, all the energy levels below the HOMO are fully filled with electrons and all the energy levels above the LUMO are empty (**Figure 1.4b**). Generally, in OSCs the resulting HOMO-LUMO energy gap is in the range between 1 and 4 eV. This energy gap has a critical role for many optoelectronic properties.[12]

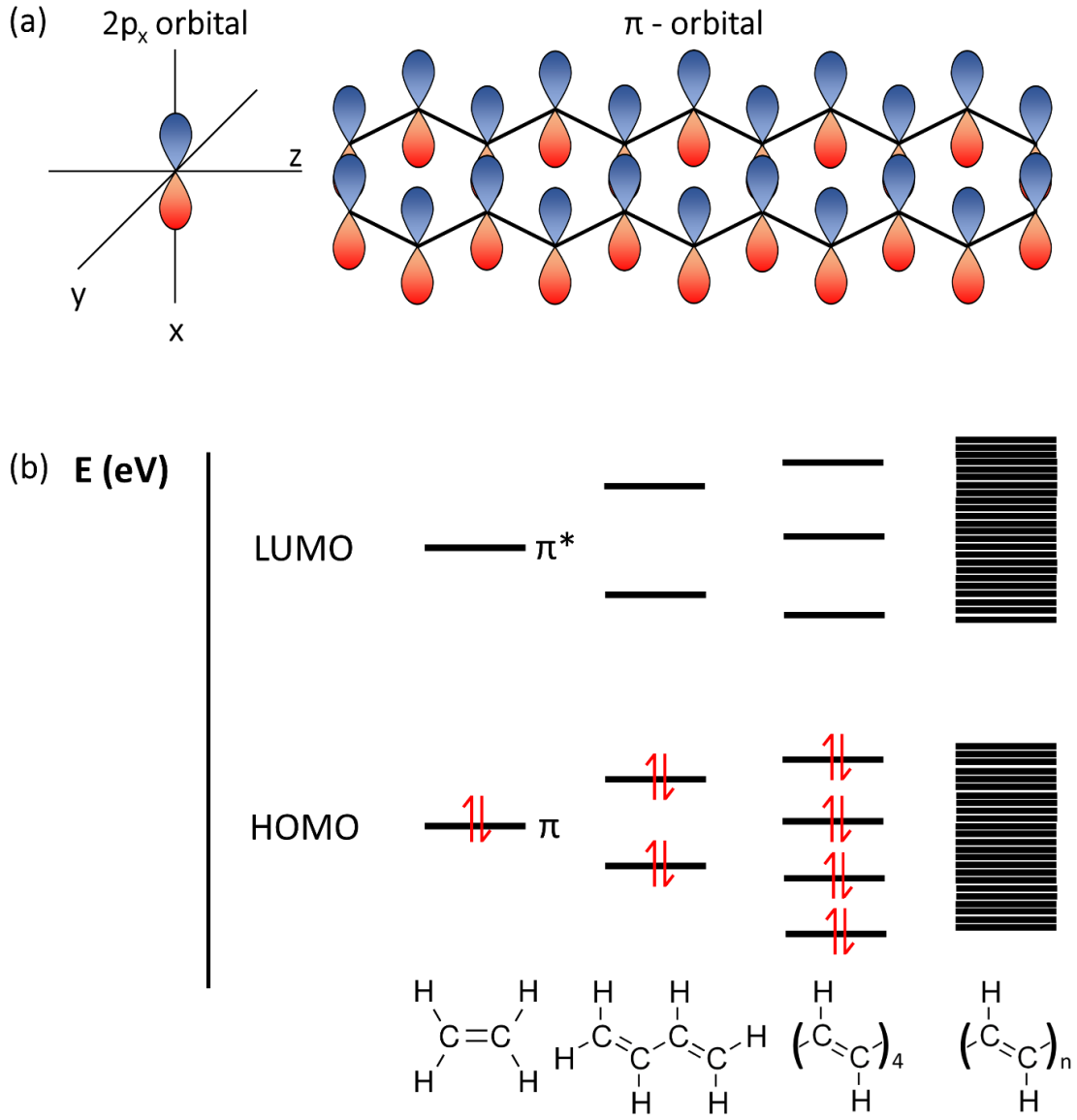

Figure 1.4. (a) Carbon $2p_x$ orbital and π-orbitals in a pentacene molecule. **(b)** Scheme of the energetic diagram of π orbitals for a single double bond, a conjugated molecule, and an organic semiconductor crystal.

OSCs, like inorganics semiconductors, can be classified according to their polarity as p-type, n-type or ambipolar OSCs. P-type OSCs are electron donor organic molecules/polymers that can be easily oxidised, while n-type OSCs are electron acceptor organic molecules/polymers that can be easily reduced. Finally, ambipolar OSCs are both electron donor and acceptor materials that can transport holes or electrons depending on the electric field applied.

The ability of OSCs to be oxidized and reduced is determined by the energy of their HOMO and LUMO orbitals. HOMO and LUMO energy levels are also crucial parameters for understanding the OSCs environmental stability and resistance to water, oxygen and other external agents.[38–41] P-type OSCs display high HOMO energy levels around -5.0 eV, which makes them more stable in environmental conditions. On the contrary, n-type OSCs show low LUMO energy levels around -4.0 eV, and are normally more sensitive to water, oxygen, and light.

OSCs can be also classified accordingly to their molecular structure into small conjugated molecules and conjugated polymers. Conjugated polymers are defined as long chains of interconnected electroactive and aromatic groups, which present inter- and intra-molecular interactions. Some of the most studied organic semiconductor polymers are poly(3-hexylthiophene-2,5-diyl) (P3HT), polynaphtalene-bithiophene (N2200 or PNDI(2OD)2T) and poly(2,5-bis(2-octyldodecyl)-3,6-di(pyridin-2-yl)-pyrrolo[3,4-c]pyrrole-1,4(2H,5H)-dione-alt-2,2'-bithiophene) (PDBPyBT) (Figure 1.5a). On the other hand, small conjugated molecule semiconductors are discrete molecular units that self-assemble through inter-molecular interactions, such as dibenzotetrathiafulvalene (DB-TTF), 2,7-bis(octyloxy)[1]benzothieno[3,2-b]-benzothiophene (C_8-O-BTBT), 2,7-Dioctyl[1]benzothieno[3,2-b][1]benzothiophene (C_8-BTBT), 2-decyl-7-phenyl[1]benzothieno[3,2-b][1]benzothiophene (Ph-BTBT-C_{10}), 2,8-difluoro-5,11-bis(triethylsilylethynyl)anthradithiophene (diF-TES-ADT), 6,13-bis(triisopropylsilylethynyl)pentacene (TIPS-pentacene), N,N'-bis(n-octyl)-x:y,dicyanoperylene-3,4:9,10-bis(dicarboximide) (PDI8CN2), 2,3,5,6-tetrafluoro-7,7,8,8-tetracyanoquinodimethane) (F_4-TCNQ) and 1,4,8,11-tetramethyl-6,13-triethylsilylethynyl pentacene (TMTES-pentacene) (Figure 1.5b). Importantly, small molecules can be deposited by thermal evaporation or solution techniques. Although many rigid small molecules generally show poor solubility, the addition of pendant solubilising groups has been exploited to gain higher solubility.[42–44] In contrast, conjugated polymers due to their high molecular weight cannot be deposited by evaporation and they are deposited using solution-based techniques. Further, small molecules can form more ordered crystalline structures which typically lead to higher charge carrier mobilities. Polymers, on the other hand, commonly form films with semicrystalline and amorphous regions.

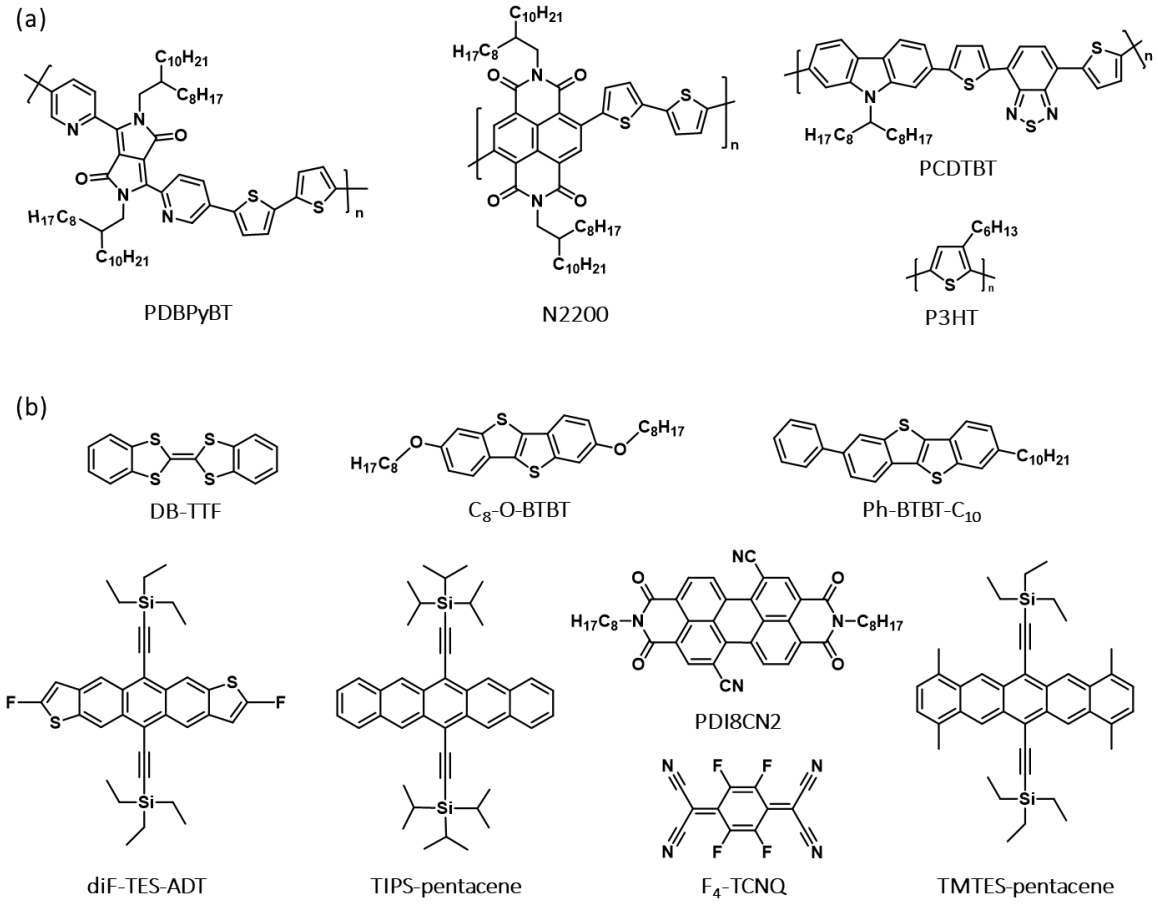

Figure 1.5. Chemical structures of (a) conjugated polymer OSCs and (b) small conjugated molecule OSCs.

1.2.1. Polymorphism and structure-performance relationship in OSCs

Polymorphism is the capacity of a specific molecule to crystallize in more than one form. The weak intermolecular interactions (van der Waals, π-π stacking or hydrogen bond) make small molecule OSCs prone to crystallise into a large number of crystal structures, called polymorphs. The crystal packing of each polymorph provides specific optoelectronic properties to the OSC.[45–53] The formation of one specific polymorph will be determined by the crystallisation experimental conditions, such as the temperature, crystallisation speed, solvent, concentration, etc. In Figure 1.6 some of the most characteristic packings observed in OSCs are shown, like the cofacial, brickwork and herringbone motifs. Noticeably, the last two structures exhibit a 2-dimensional (2D) electronic character, whereas the cofacial packings are electronically 1D and might be more sensitive to defects. Hence, the anisotropy in the optoelectronic properties is a direct consequence of the packing dimensionality of non-symmetric 3D molecules.

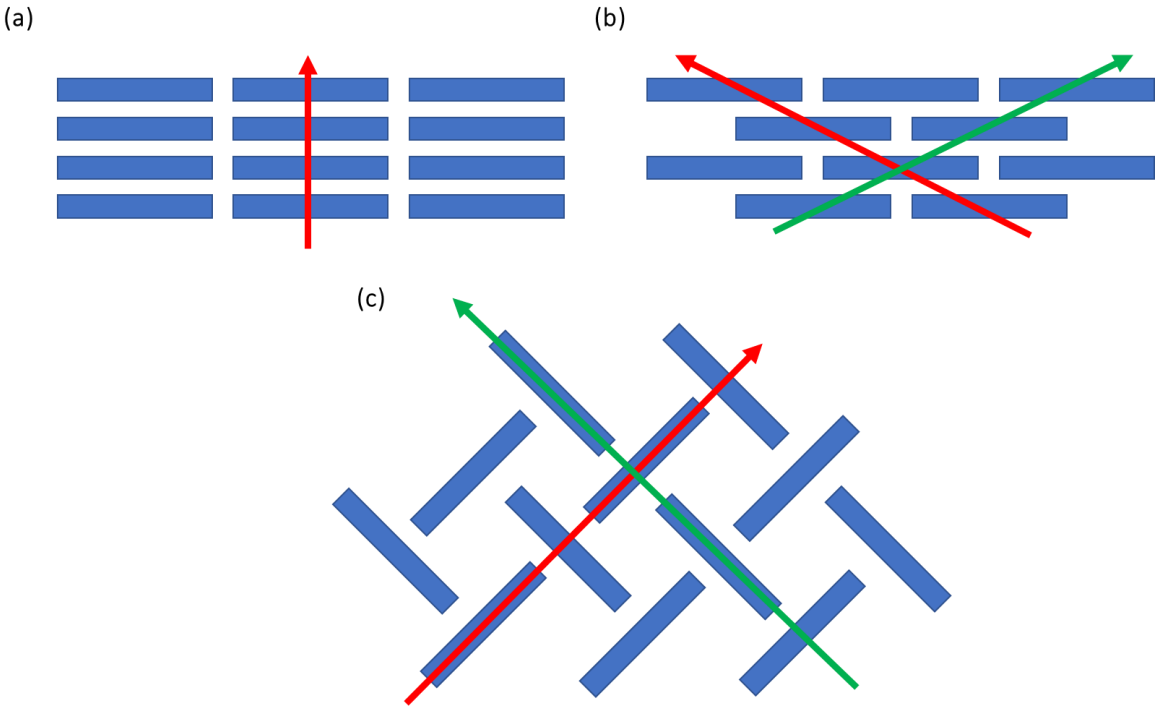

Figure 1.6. Scheme of some of the most characteristic crystal packings found in OSCs: **(a)** cofacial or 1D brick wall, **(b)** 2D brick wall, and **(c)** herringbone. The arrows indicate possible transport pathways.

1.2.2. CHARGE TRANSPORT IN ORGANIC SEMICONDUCTOR MATERIALS

Due to the nature of organic crystals, charge transport in organic semiconductor materials does not follow the behaviour observed in inorganic semiconductors. In inorganic semiconductors, charge carriers freely move through delocalized energy states (i.e., band transport).[54] In contrast, charge transport in OSCs usually takes place via thermally activated hopping between nearby molecules,[55–58] although for a very few highly ordered OSCs band-like transport has been reported.[59–61] Several transport mechanisms have been proposed for organic materials depending on their structural order, which ranges from amorphous films to single crystals.[12,62]

BAND TRANSPORT

For highly ordered systems like single crystals, charge-carriers can be delocalized along the material following a classic band-like model. In a band-like model, an enhancement of the charge-carrier mobility with decreasing temperature is found due to the reduction of the lattice vibrations. For instance, band-transport has been reported by Mori *et al.* for single crystals of C_8-BTBT.[63]

MULTIPLE TRAPPING

In the case of polycrystalline organic semiconductor films, grain boundaries act as charge traps. Charge carriers travel along narrow delocalised bands but are trapped and released in the traps. In this model, trapping and thermally activated release of the charge carriers establishes the effective mobility and their thermally activated behaviour. Noticeably, crystalline defects and impurities can also act as traps.

HOPPING TRANSPORT

Finally, the hopping transport mechanism is associated to amorphous or highly structural or energetic disordered systems. In contrast to the band transport mechanism, hopping is thermally activated since the lattice vibrations enhance the movement of the charge-carriers by providing the energy necessary to overcome the energetic barrier. Ideally, the charge transport in semiconductor materials is governed by the Marcus theory for chemical reactions.[55] Marcus theory describes the charge carrier mobility (μ) as a thermally activated parameter that follows the Arrhenius dependency:[62]

$$\mu \sim e^{-\frac{E_A}{k_B T}} \quad (1.1)$$

Where E_A is the activation energy, k_B is the Boltzmann constant and T is the temperature. In OSCs, the charge carrier strongly interacts with the carrying molecule, forming a polaron. The charged molecule couples to the surrounding ones promoting inter-molecular displacements and polarisation, altering hence the crystalline structure. The hopping of the charge carrier along the semiconductor material is ruled by the transfer integral and the reorganisation energy. The latter considers the conformational changes caused by acceptance or release of a charge carrier, while the transfer integral provides information about the electronic coupling between neighbouring molecules and, hence, is highly dependent on the crystal structure and the direction (anisotropic property).[64–66] The mobility of the charge carriers is proportional to the transfer integral and inversely proportional to the reorganisation energy.

1.3. ORGANIC SEMICONDUCTOR PROCESSING TECHNIQUES

As transport properties are greatly influenced by the microstructure of the organic layer, the processing of organic semiconductors is critical to obtain optimum performance devices. However, finding a compromise between electrical performance and manufacturing costs is also crucial for practical applications. The deposition techniques that

can be employed to prepare OSCs thin films can be divided into two main groups: 1) physical vapor deposition (PVD) techniques and 2) solution-based deposition techniques.

1.3.1. VAPOR PHASE DEPOSITION TECHNIQUES (PVD)

Vapor phase deposition (PVD) techniques are well established techniques for the growth of thin film layers. PVD technique consists of the sublimation of a semiconductor powder, which is then deposited on the surface of a substrate (**Figure 1.7**). The organic semiconductor material is evaporated typically inside a vacuum chamber with a pressure ranging from 10^{-6} to 10^{-8} mbar.

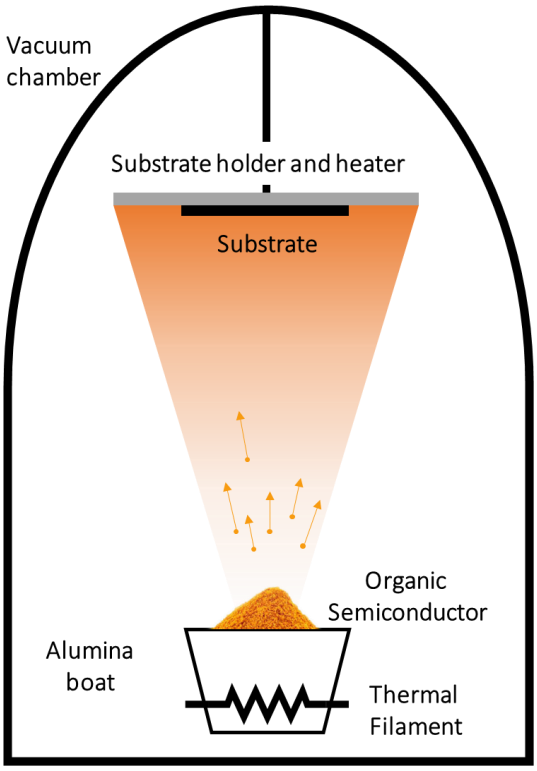

Figure 1.7. Scheme of a physical vapor deposition process. The organic semiconductor material is placed in an aluminium boat with a thermal filament. The semiconductor material is sublimed and subsequently deposited on the substrate.

PVD technique is compatible with all small molecule semiconductors with high thermal stability. The vapor phase techniques provide layers with the highest purity and with high control and reproducibility in terms of film thickness. The films produced give rise to crystallites with random orientation and usually with a small domain size. The crystallinity

and morphology of the semiconductor films are controlled by the evaporation rate of the semiconductor material and the substrate temperature. PVD also offers the possibility of tandem deposition and co-deposition of different materials.

Vapor phase techniques are ideal for the deposition of poorly soluble semiconductors. Nevertheless, the main disadvantages are the lack of large-scale manufacturing techniques, the need of expensive equipment and difficulty to increase the control over the growth of crystal domains.

1.3.2. Solution-processed deposition techniques

Solution processing techniques are generally preferred for the deposition of organic semiconductors at low cost. Initially, the main difficulty in using solution processing techniques was that there were only a few small molecule OSCs available which were soluble enough in common organic solvents. However, today there is a large number of soluble OSCs available.[41,42,44,67,68]

Drop-casting

Drop-casting consists in dropping an OSC solution on a substrate and then letting the solvent to evaporate, which leads to the precipitation of crystals on the substrate surface (**Figure 1.8**).[69,70] Drop-casting is the simplest technique for the deposition of OSCs, and is traditionally used to determine the viability of a material to act as semiconductor. Nevertheless, the potential of preparing OSC films by drop-casting is limited due to the lack of control and reproducibility, as well as the impossibility of its implementation for large scale manufacturing.

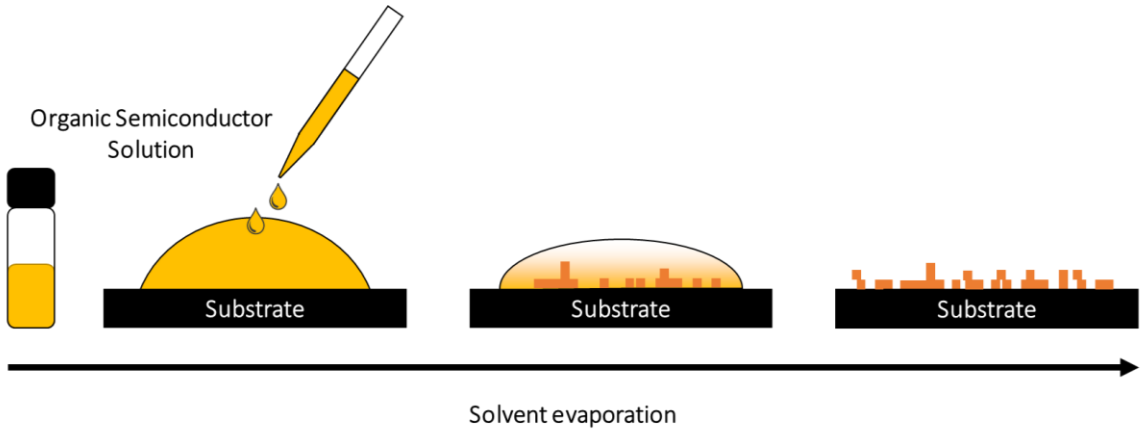

Figure 1.8. Schematic representation of the drop-casting technique.

SPIN-COATING

Spin coating is one of the most common techniques used to prepare OSC thin films at laboratory scale. Spin coating is a simple and quick technique. Some drops of the OSC solution are cast on the substrate, which is subsequently spun at high speed to uniformly spread the solution. Afterwards, the solvent evaporates, and a thin layer is formed, as depicted in **Figure 1.9**.[71–74] Due to its fast-drying time period and unidirectional centrifugal force, often the molecules do not have enough time to achieve high crystalline order and the films present high alignment along the centrifugal force direction. For this reason, in some cases, to achieve high-performance devices is mandatory to realise post thermal treatments to enhance the crystallinity of the OSC film.

The thickness of OSC film can be easily adjusted by changing the solution employed (i.e., concentration and viscosity), and also by modifying the spin-coater deposition parameters (mainly the angular speed, time and the spin speed). Although spin coating is widely used for academic purposes due to its versatility to produce nanometer thick OSC films, it cannot be easily up-scaled and, therefore, it is not a suitable technique for large-area applications.

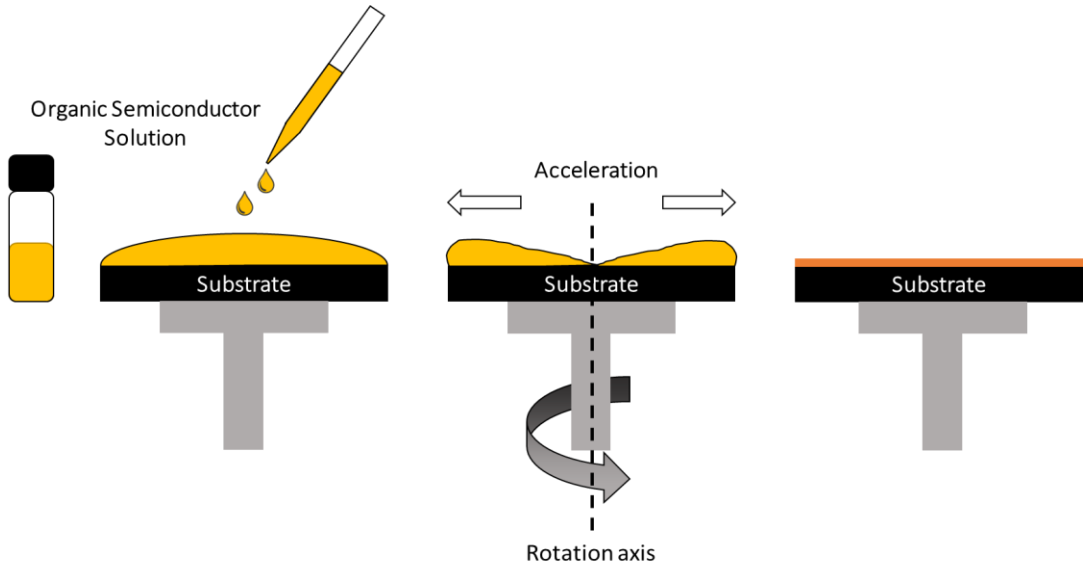

Figure 1.9. Schematic representation of the spin coating technique.

SPRAY COATING

Spray coating is based on the vaporisation of an OSC solution. The high pressure of a gas carrier transports small droplets of the OSC from the reservoir boat to the surface of the substrate (**Figure 1.10**).[75,76] Spray coating is compatible with large areas coverage. However, the resulting films typically show higher roughness and lower performance compared to other solution-based techniques.

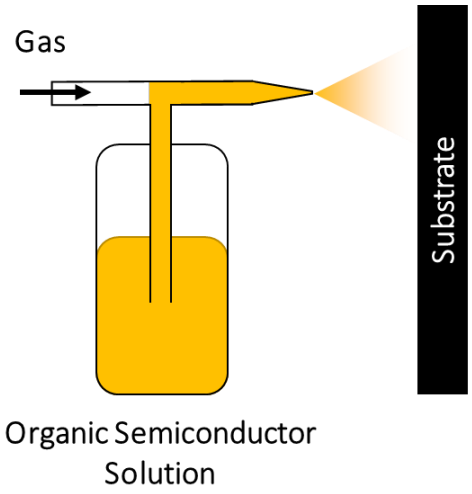

Figure 1.10. Schematic representation of the spray coating technique.

INKJET PRINTING

Inkjet printing is based on the formation of drops of an OSC solution by fluid surface tension (Figure 1.11). The flux of drops is expelled from a jet nozzle covering the desired surface area of the substrate.[77,78] Inkjet printing permits to deposit all kinds of materials and generate multilayers and patterning structures. However, the control of the droplets by formulation is extremely challenging.

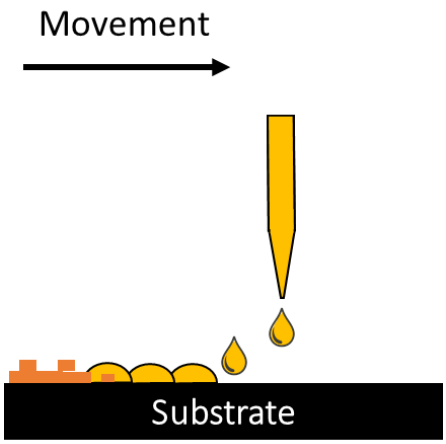

Figure 1.11. Schematic representation of inkjet printing.

MENISCUS-GUIDED TECHNIQUES

Meniscus-guided techniques are the group of techniques that use the translation of a solution meniscus along a substrate to induce the growth of a thin film. The OSC ink displacement and solvent evaporation results in the over-concentration of the semiconductor material inside the solution. Once the supersaturation point is reached, the

organic semiconductor material precipitates and starts to crystallize along the evaporation line front.[10,79–83]

There are different approaches depending on how the meniscus is created and confined (Figure 1.12). The most common meniscus-guided techniques are dip-coating, zone-casting, and blade coating or bar-assisted meniscus shearing (BAMS), which will be briefly described in the following:

Dip-coating consists in the immersion of the substrate in an ink solution bath. Then, the substrate is pulled upwards dragging the OSC that forms a uniform film on the surface of the substrate (Figure 1.12a).[84,85] The solvent evaporation rate and crystallisation can be adjusted by changing the solvent, concentration, the temperature of the solution bath and the withdrawal speed. Although this technique is used as a starting point for large-scale manufacturing due to its facility to cover large areas, its implementation is quite expensive due to the need of using a large volume of the OSC solution.

Zone-casting consists in the continuous deposition of an OSC solution by a slot-die (nozzle) on a moving substrate. The nozzle drags a meniscus across the substrate and then the evaporation of the solvent occurs forming a crystalline thin film (Figure 1.12b).[86–89] The film formation is adjusted by the temperature of the substrate, the coating speed, the solvent supply rate and the ink concentration. During the deposition process the slot-die ensures that the volume of the meniscus does not change while coating is taking place. This technique has been applied using low deposition speeds (< 1 $mm \cdot s^{-1}$) leading to highly anisotropic films.

Blade coating consists in the spreading of an OSC solution meniscus by a blade. The movement of either the blade or the substrate leaves a uniform film, and the evaporation of the solvent can be assisted by heating the substrate (Figure 1.12c).[47,60,79,82,90–92] The control of the thickness can be ruled by the distance between the substrate and the blade. Again, temperature and coating speed affect the crystallinity and anisotropy of the resulting films. In blade coating larger deposition speeds compared to zone casting are usually used (from a few $mm \cdot s^{-1}$ to 10 $cm \cdot s^{-1}$).

Finally, BAMS is a variation of the blade-coating approach developed in our research group. Here, instead of a blade, a cylindrical bar is used to drag the solution over the substrate (Figure 1.12d). This technique has been successfully employed to process a large variety of OSCs and blends of OSCs with insulating polymers.[81,93–97] In this thesis, the effect of the ink composition and deposition parameters (temperature and coating speed) on the OSC thin film formation is widely investigated.

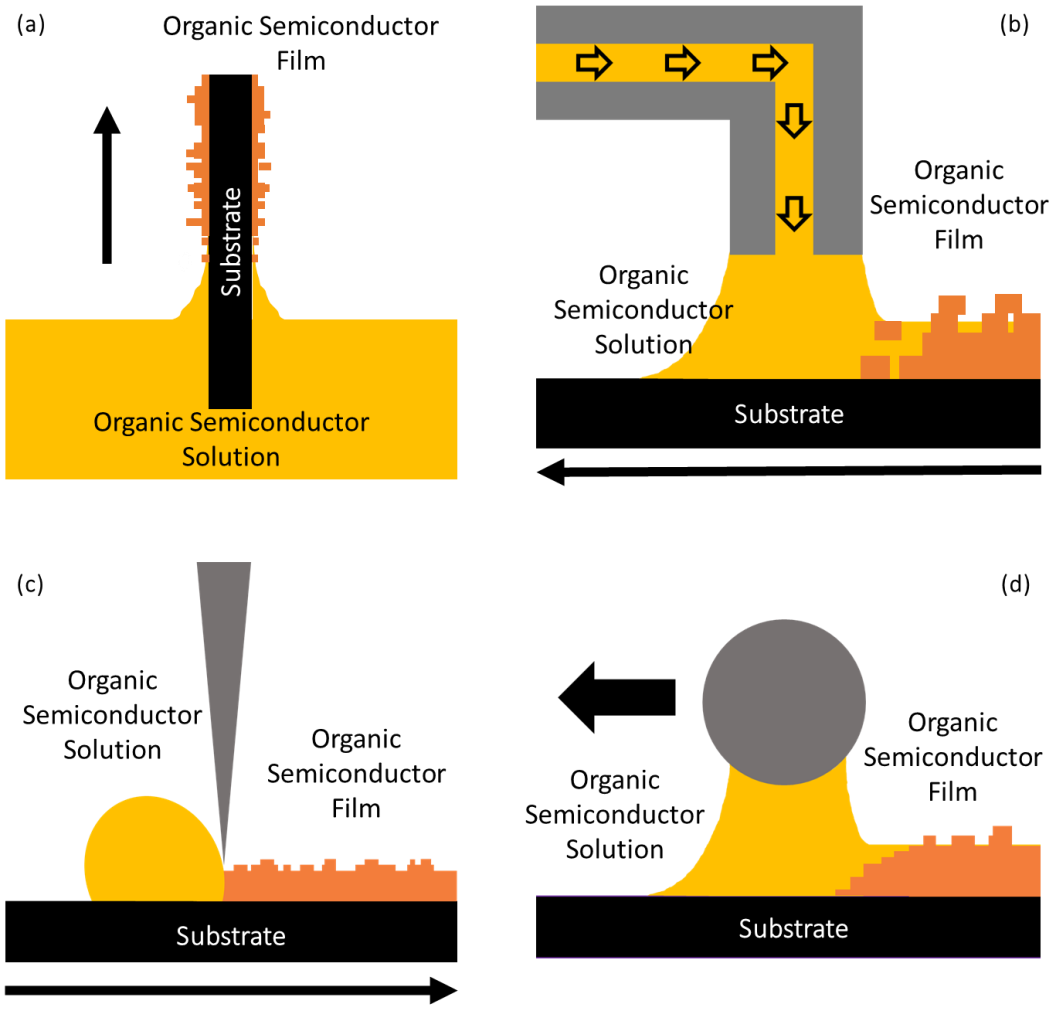

Figure 1.12. Overview of different meniscus-guided coating techniques: **(a)** dip-coating, **(b)** zone-casting, **(c)** blade coating and **(d)** BAMS.

1.4. CRYSTALLISATION PROCESSES INVOLVED IN SOLUTION SHEARING TECHNIQUES

The use of printing techniques compatible with up-scaling or roll-to-roll processes represent a promising strategy to reduce the production costs.[48,51,98–102] In this direction, solution shearing techniques are raising a lot of interest. The performance of a film depends on the structural order of the film, both at the molecular scale and up to the crystal scale. The organization of crystalline grains and domains in a film is considered to be one of the main parameters governing the charge carrier transport. For this reason, it is important to be aware of the crystallisation processes that are taking place during the thin film preparation. Further, since the formation of thin films of small molecules is challenging due to the low viscosity of their solutions, a promising approach that has been used is to blend the small molecule OSC with an insulating polymer. These two issues are discussed below.

1.4.1. CRYSTALLISATION REGIMES

The first report about the use of a solution shearing method to deposit a small molecule semiconductor was in 2008 by Becerril *et al*.[9] They reported the preparation of uniform crystalline 20–50 nm thick films composed by aligned ribbon-like crystals. The OFET devices displayed little mobility anisotropy and charge carrier mobility values of an order of magnitude higher than the previous ones reported for films deposited by non-solution shearing techniques. Subsequently, Le Berre *et al.* and Marco Faustini *et al*. investigated the growth mechanisms in the films deposited by solution shearing.[103,104] In these experiments, the effect of the temperature, shearing speed and solution properties (viscosity, surface tension) were explored. They identified two growth regimes in solution shearing: the evaporation regime and the Landau-Levich regime. The different regimes depend on competing forces: the evaporative force of the meniscus and the viscous drag out of the meniscus.

i) In the evaporation regime, there are fast-drying conditions and the evaporation force is predominant, and hence, the crystallization initiates at the contact line. In this regime, the thickness of the film is inversely proportional to the shearing speed. The increment of thickness is due to the feeding with molecules from the bulk of the solution which permits the deposition of more material.

ii) In the Landau-Levich regime, the meniscus moves faster than the evaporation rate, leaving a wet film along the surface of the substrate. The film thickness in the Landau-Levich regime depends on the capillary properties of the solution (viscosity, surface tension of the liquid and substrate characteristics). In contrast to the evaporation regime, the thickness of the film is proportional to the shearing speed.

Finally, there is a region where the viscous forces and evaporation forces are compensated. Under these conditions it has been observed that the thickness of the films is minimum and independent of the shearing speed.

The crystallisation of small-molecule semiconductors is highly dependent of deposition regime. The films prepared at evaporation regime tend to form big crystals, being even possible to fabricate single-crystalline domains. However, the deposition of OSCs at the Landau-Levich regime tend to give rise to polycrystalline films with a high dispersion of crystal domain sizes. The shearing speed is an ideal parameter to control the nucleation and crystal growth through the solvent evaporation. Giri *et al*. reported the effect of the shearing speed on the nucleation and crystal growth of thin films based on the small molecule TIPS-pentacene.[47] They found that lattice strain was introduced at higher coating speeds diminishing the π–π stacking distance, which led to a greater electronic overlap between the molecules. This resulted in devices exhibiting higher field-effect mobility.

In general terms, the deposition of small molecule OSCs by solution processing techniques, especially at high speed, is often quite challenging. The low viscosity of the solutions and limited solubility of the molecules has pushed the development of new approaches to overcome these limitations.

1.4.2. Organic semiconductor:polymer blends

The use of inks based on small semiconducting molecules blended with insulating polymers was proposed as excellent strategy to facilitate the processability of small molecule OSCs. Interestingly, the use of binder polymers also provided additional advantages, such as lower manufacturing cost (by reducing the amount of semiconductor), a higher device-to-device reproducibility and an improvement in the thin film crystallinity and electrical properties. [81,98,105–107]

It has been demonstrated for various OSCs that when they are blended with an insulating polymer, such as polystyrene (PS), a vertical stratification of the two materials takes place in the films, in which the OSC lies on top of a PS layer. This helps the crystallisation of the OSC and also results in the passivation of the dielectric interface traps with polystyrene.[98,108–112] Generally, the dielectric material is silicon oxide (SiO_x), which is known for its capacity to adsorb water on its surface and generate a large density of interfacial charge carrier traps. The passivation effect of the insulating polymer prevents the dewetting of the organic film and reduces the density of interfacial charge carrier traps. Thus, the use of blends of OSCs with insulating polymers is appealing for achieving devices with a higher performance and stability.

1.5. Organic field-effect transistors (OFETs)

A field-effect transistor (FET) is a three-terminal device which uses an electric field to control the flow of current in a semiconductor layer. The current flowing from the source (S) to the drain (D) electrodes is controlled by the application of a voltage at the gate (G) electrode.[38,113,114] The G electrode is isolated from the semiconductor and S/D electrodes by a dielectric material. The application of a voltage between S and G electrodes induces the accumulation of charge carriers at the semiconductor/dielectric interface. The accumulated charges at the interface produce a conductive channel along the semiconductor. It is important to note that the thickness of the conductive channel is only of a few nanometres thick.[115,116]

OFETs are a special kind of FETs, where at least the active semiconducting material is an organic semiconductor. The basic structure and operation principle are the same as that of conventional FETs based on metal-oxide-semiconductors (MOSFET). In OFETs, the

dielectric layer is typically a metal-oxide (most commonly SiO_2 or Al_2O_3) or a polymer (like poly(methyl 2-methylpropenoate) (PMMA), poly(vinyl alcohol) (PVA), Cytop, polystyrene (PS) or polyacrylamide (PAM)).

Depending on the relative position of the OSC, dielectric and contacts, four OFET architectures can be differentiated (**Figure 1.13**). These architectures are called (a) bottom-gate bottom-contact (BGBC), (b) bottom-gate top-contact (BGTC), (c) top-gate bottom-contact (TGBC) and (d) top-gate top-contact (TGTC).

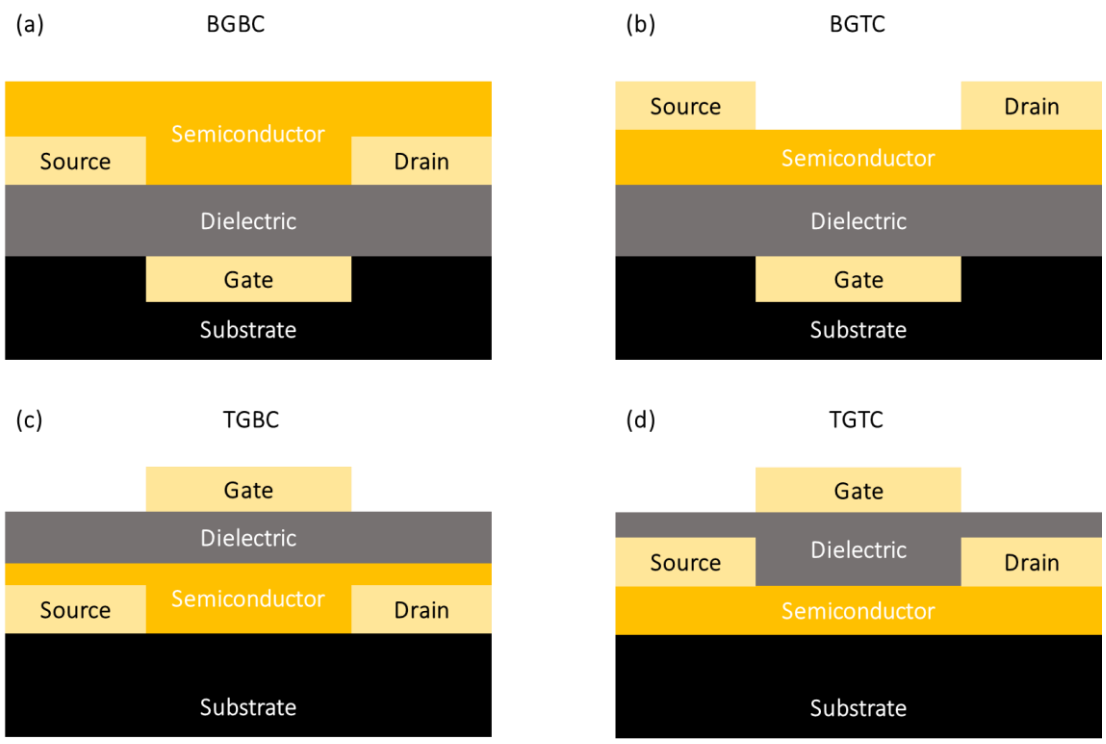

Figure 1.13. Scheme of the four main OFET architectures: **(a)** bottom-gate bottom-contact (BGBC), **(b)** bottom-gate top-contact (BGTC), **(c)** top-gate bottom-contact (TGBC) and **(d)** top-gate top-contact (TGTC).

Each of the device geometries provides some advantages and disadvantages. Thus, the most suitable OFET geometry is selected depending on the employed organic semiconductor material and coating conditions. For example, it has been shown, that BGTC or TGBC are less affected by the contact resistance due to its higher charge transfer area between the conductive channel and the source injecting electrode.[117–119]

Top contact geometry usually presents less contact resistance since the metal source/drain electrodes that are commonly evaporated penetrate the organic semiconductor layer improving the organic semiconductor/metal interface. However, in BGTC it appears an access resistance since charges have to travel from the contact to the first few molecular

layers close to the dielectric. Further, the high temperature of the evaporated conductive materials can damage the OSC layer. The evaporation of additional interlayers might avoid problems of overheating the OSC and can also be employed to dope the contact area and reduce the energy barrier.[120–123] Top gate geometry encapsulates the organic semiconductor, improving its environmental stability.[124,125] However, if the gate dielectric is deposited from solution, an orthogonal solvent with the OSC is required to prevent damaging it.

Bottom gate geometry has the advantage that the gate electrode and gate dielectric is deposited prior to the deposition of the OSC. Consequently, the patterning of the dielectric and gate electrode does not affect the semiconducting layer. Finally, the bottom gate bottom contact structure is typically the choice in terms of ease of fabrication. Principally, in BGBC geometry the deposition of the OSC is the last fabrication step, which allows to optimize and test faster novel OSC materials. For S/D electrodes, gold is typically used due to its deep work function, resulting therefore especially useful for a large number of p-type OSCs.[126] In addition, the use of bottom electrodes permits the control of the work function of the bottom contacts by functionalising them with molecular self-assembled monolayers.[127–129] Organic conductors such as TTF-TCNQ[75] or PEDOT:PSS[130] can also be used as S/D contacts. It should be highlighted though that the protruded patterned electrodes can affect the morphology of the organic semiconductor layer in terms of thickness and roughness in the contact region. This could lead to a worse connectivity between the organic crystals and a deterioration of the electrical performance. As gate material, especially in the bottom contact architecture, silicon from the silicon wafers is the more commonly employed.

1.5.1. Operation principle

In contrast to inorganic FET devices, OFETs generally use undoped semiconductors and operate in the accumulation mode. The accumulation mode is based on the ability to create a conducting channel in the OSC by the application of a source-gate voltage.

The working mechanism of the OFET can be explained by a simplified electronic energy level diagram (**Figure 1.14**). When no voltage is applied to the gate electrode, the OFET is in the off-state and no charges are accumulated at the OSC-dielectric interface, hence, there are no mobile charges. The application of a gate-voltage V_{GS} causes the shifting of the HOMO and LUMO energy levels, so that the HOMO or LUMO become closer to the Fermi energy (EF) level of the source electrode. Hence, holes or electrons are accumulated at the organic semiconductor/dielectric interface. When a source-drain voltage V_{SD} is applied to the drain electrode, the accumulated charge carriers flow from the source to the drain contact and a current between the source and drain electrodes can be measured.

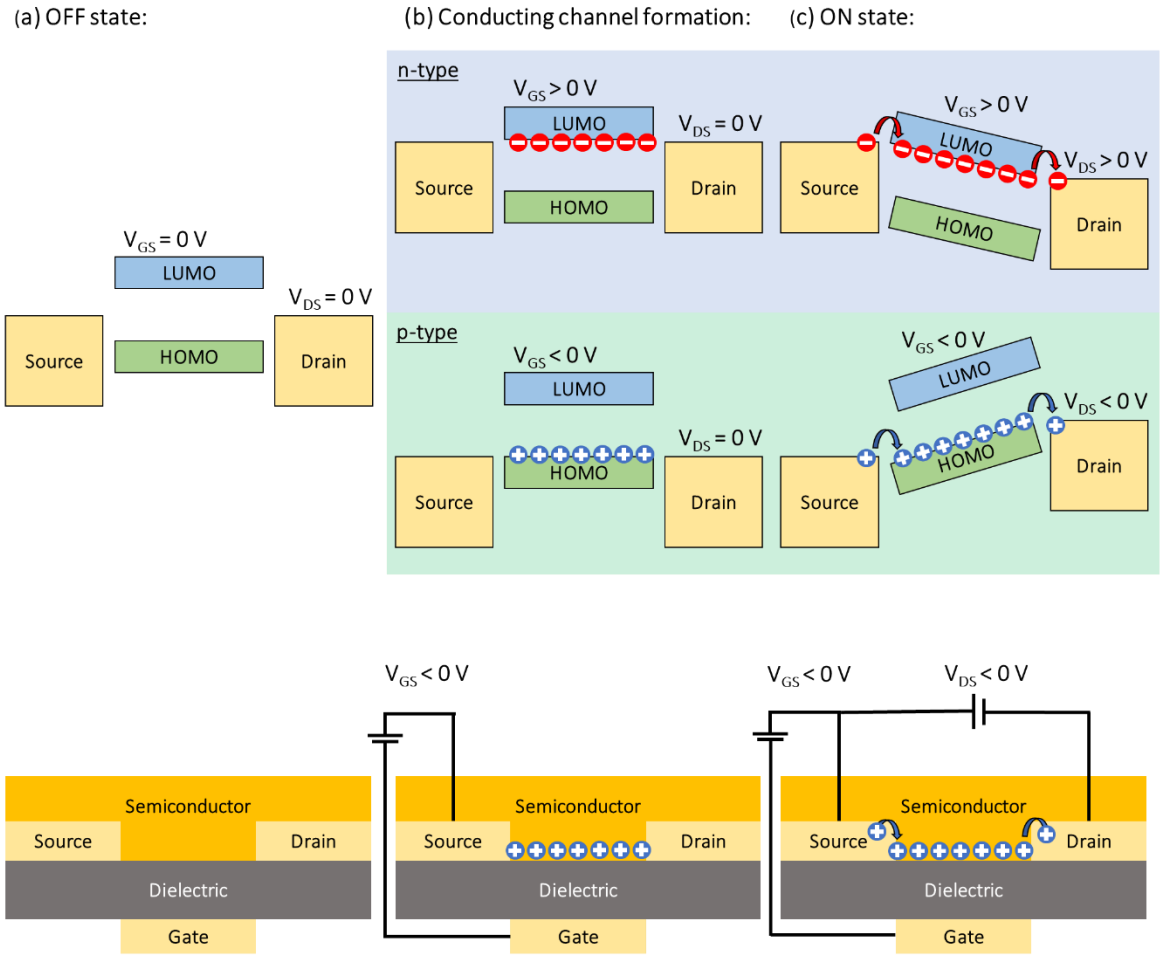

Figure 1.14. Illustration of the working principle of an OFET. **(a)** Ideal device in off-state, when no V_{SD} and V_{SG} are applied. **(b)** Charge accumulation in the channel of the semiconductor when a gate voltage is applied. **(c)** Drain current flowing in the transistor channel after applying a source-drain voltage.

The models used to describe OFETs are the same as the ones developed for inorganic FET devices. Horowitz *et al.* reported a simple model based on the metal-oxide-semiconductor field-effect transistors (MOSFETs) theory to explain the behaviour of the OFETs.[24,25,131] This model considers the following: (a) the charge carrier mobility (μ) is constant, (b) the parasitic contact resistances between the electrodes and the OSC are not considered, and (c) the electric field perpendicular to the channel (created by the gate electrode) has to be significantly stronger than the one parallel to the channel (caused by the source and drain electrodes), which is known as the gradual channel approximation. However, it should be noticed that these conditions are not always met in OFETs, so deviations from the model are often found.

In this model the OFET is described to operate in two distinct regimes: the linear regime and saturation regime.

In the linear regime, the source-drain current (I_{DS}) increases linearly with V_{DS}, accordingly to:

$$I_{DS} = \mu C \frac{W}{L} \left[(V_{GS} - V_{TH}) V_{DS} - \frac{V_{DS}}{2} \right] \quad (1.2)$$

$$\text{for} \quad |V_{GS} - V_{TH}| > V_{DS}$$

In the saturation regime, the source-drain current reaches a value independent on $V_{DS,}$ which is described according to the following equation.

$$I_{DS} = \mu C \frac{W}{2L} (V_{GS} - V_{TH})^2 \quad (1.3)$$

$$\text{for} \quad |V_{GS} - V_{TH}| < V_{DS}$$

Here, I_{DS} corresponds to the source-drain current, V_{GS} the source-gate voltage, V_{TH} the threshold voltage, μ is the charge carrier mobility, C is the gate dielectric capacitance per unit area, W is the channel width and L is the channel length of the transistor. The threshold voltage for an OFET device is defined as the voltage that delimits the transition between two conductive states, the non-conductive and conductive state. Also, the V_{TH} can be defined as the minimum gate voltage required to generate a conductive channel in the OSC.

1.5.2. Main device characterization and parameter extraction

The OFET electrical properties are characterised by the output and transfer curves. The output characteristics (**Figure 1.15a**) are obtained when I_{DS} is measured as a function of the source-drain voltage (V_{DS}) for different constant gate voltages (V_{GS}) values. In contrast, the transfer characteristics (**Figure 1.15b**) are obtained by measuring I_{DS} as a function of V_{GS} at constant V_{DS}. The transfer characteristics can be evaluated in the linear or saturation regimes depending on the choice of the V_{DS}.

OFET devices performance is generally evaluated and compared through the extraction of a series of parameters. In the following, the most important OFET figures of merit, as well as their extraction procedure, are described.

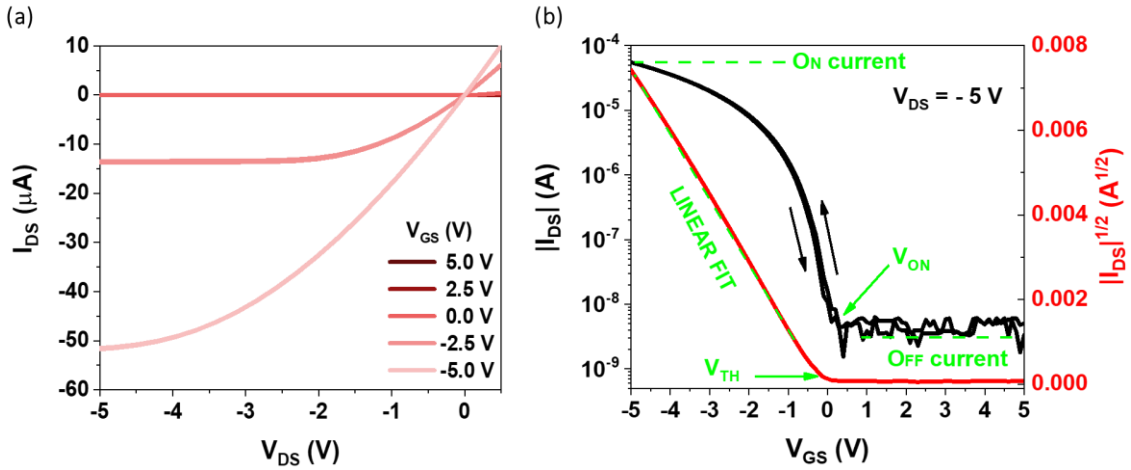

Figure 1.15. (a) Output and (b) transfer characteristics measured in the saturation regime of a typical OFET. The extraction of some OFET parameters are shown.

Charge carrier mobility

The charge carrier mobility (μ) quantifies the capacity of charge carriers to move inside the material when an electric field is applied. It can be calculated from the transfer characteristics from the derivative of the current over V_{GS} for the linear and the saturation regime.

$$\mu = \frac{1}{V_{DS}\,C}\,\frac{L}{W}\,\frac{\partial I_{DS}}{\partial V_{GS}} \qquad (1.4)$$

$$\text{for} \quad |V_{GS} - V_{TH}| > V_{DS}$$

$$\text{(LINEAR REGIME)}$$

$$\mu = \frac{1}{C}\,\frac{2L}{W}\left(\frac{\partial\sqrt{I_{DS}}}{\partial V_{GS}}\right)^2 \qquad (1.5)$$

$$\text{for} \quad |V_{GS} - V_{TH}| < V_{DS}$$

$$\text{(SATURATION REGIME)}$$

However, it should be noticed that the field-effect mobility extracted from the I-V transfer characteristics is not the intrinsic mobility of the OSC material. The μ extracted from I-V characteristics includes defects in the layer, contact resistance and traps. Further, the curves used to extract the mobility usually present low linearity, which could cause mobility overestimation. To ensure a correct mobility extraction, the plot of the mobility in front of the gate voltage V_{SG} is a good strategy to check the gate voltage dependence of the mobility and verify the accuracy in the mobility estimation.

Threshold voltage

The threshold voltage (V_{TH}) quantifies the gate voltage at which current begins to flow. The threshold voltage is extracted from the transfer characteristics and corresponds to the intersection of the fitted mobility with the ordinate axis. However, the low linearity of the fits produce that the value extracted by the fit is clearly dependent on the voltage range that is fitted. Ideally, the threshold voltage should be as low as possible to enable low power operations.

The threshold voltage and field-effect mobility are the two main parameters reported for a basic characterization of an OFET device. Additionally, there are other parameters that are helpful to further characterize the devices such as the ON/OFF ratio, off current, on-voltage subthreshold swing, hysteresis and contact resistance.

On/Off ratio

The ON/OFF ratio is the ratio between the maximum current measured in the on state and in the off state. This parameter depends on the device geometry, the voltage sweep, the field-effect mobility of the semiconductor material, the threshold voltage, and the dielectric capacitance.

Off current

The OFF current is the current measured when the OFET device is in the off state, with typical values in the order of a few nA or pA. This value should be as low as possible to achieve high ON/OFF ratios. The off current is indicative of the quality of the OSC layer and the purity of the material.

On voltage

The ON voltage (V_{ON}) is defined as the point at which the transistor switches from the off state to the on state. V_{ON} is similar to the V_{TH}, but V_{ON} is not extracted from any fit. Instead, V_{ON} is easily extracted from the transfer characteristics in semilogarithmic scale since it is

the voltage at which the current starts to increase with the gate voltage. In an ideal OFET, it should be equal to the threshold voltage.

Sub-threshold swing

The sub-threshold swing (SS) describes how fast the transistor switches from the on state to the off state. SS quantifies the exponential rise of source-drain current with the applied gate voltage. It characterizes the effectiveness of the charge accumulation process upon the application of a gate voltage, and it brings information about the quality of the dielectric-semiconductor interface and the density of traps. Indeed, SS can be correlated with the density of traps as follows:

$$SS = \frac{\partial V_{GS}}{\partial(log\ (|I_{DS}|)} = \frac{k_B T}{e} ln\ 10\ \left(1 + \frac{e}{C} N_T\right) \quad (1.6)$$

where e is the electron charge, k_B is the Boltzmann constant, and T is the temperature.

Hysteresis

The hysteresis is defined by the difference between the forward and backward I-V curves. The hysteresis provides information about the reversibility of the measurements, quality of the film (structural defects), charge trapping and unintentional doping of the semiconductor material.

Contact resistance

Finally, the contact resistance (R_c) is the electrical resistance given by the electrodes/organic semiconductor interface and can limit the charge injection/extraction, reducing the measured device mobility. The origin of contact resistance typically arises from the misalignment of the OSC and the metal electronic levels, which trigger an energy barrier to inject/release charges between the semiconductor and the metal electrode. Contact resistance in OFETs is frequently quite large, from several Ω·cm to kΩ·cm, while contact resistance of MOSFETs is orders of magnitude lower than that of the best OFETs (~0.1 Ω·cm).

Importantly, in OFETs with small channel lengths, the channel resistance (R_{ch}) is reduced and then R_c becomes dominant.

$$R = R_{ch} + R_c \quad (1.7)$$

Consequently, the use of long channel lengths is an excellent strategy to mitigate the negative effects of contact resistance and accurately assess the intrinsic OSC charge carrier mobility.

The contact resistance can be determined by different methods. The more common ones are the Y-function method, the transfer-length method (TLM), the four-point probe method and by Kelvin probe force microscopy. In this thesis, the method used to determine contact resistance has been the transfer-length method (TLM), which is based on the following equation.[121]

$$R = R_C + \frac{L}{W\ C\ \mu\ (V_{GS} - V_{TH})} \qquad (1.8)$$

The TLM method consists in measuring similar OFETs with different channel lengths in the linear regime. Assuming that R_{ch} is proportional to the channel length, R is plotted for different V_{GS} for each channel length, and R_C is then extracted by extrapolating the total device resistance R to zero channel length (L = 0).

1.6. OFETs IN SENSING APPLICATIONS

Nowadays, OFETs are still looking to gain a foothold in the consumer electronics sector. Devices with higher performance have been achieved and low-cost fabrication methods have been developed, making OFETs an excellent platform for electronic applications where low-cost, light-weight, large-area coverage and structural flexibility are desired. In terms of applications, OFETs are expected to have a strong impact in sensing devices since they can offer high sensitivity in addition to the above-mentioned advantages.[132–134] Further, OFETs can also provide a multi-parametric response to changes in the environment. In this direction, OFETs can be exploited in both physical and chemical sensors as it will be discussed below.

1.6.1. PHYSICAL SENSING

The application of OFETs to detect electromagnetic radiation or mechanical stress has attracted plenty of attention in the last two decades.[135–140] Flexible and stretchable sensors based on OFETs exploit the changes in the electrical performance of the devices upon deformation of the crystalline cell or of the film morphology of the OSC layer to develop strain sensors with potential in wearable electronics for human-activity monitoring.[141] In the work of Lai *et al*. the application of compression and elongation stress to OSC thin films

was investigated (**Figure 1.16a**).[136] The reported OSC thin films were deposited using a solution shearing technique and it was found that the films showed different morphology depending on the deposition direction used (i.e., orthogonal or parallel to the channel length). Interestingly, it was found that the morphology of the OSCs influences on the mechanical response of the flexible OFETs. In particular, it was demonstrated that elongation caused a larger stress for OFET devices based on organic films with larger crystallites. Further, films with smaller crystals showed a larger sensitivity to compression.

Alternatively, the development of mechanical sensors based on capacitive changes of the dielectric have also shown to be a viable option.[142,143] For instance, Mannsfeld *et al.* developed a capacitative pressure sensor based on a single crystal of rubrene with exceptional sensitivity and very short response times **(Figure 1.16b)**. A microstructured polydimethylsiloxane (PDMS) film was employed as dielectric, which could elastically deform by the application of pressure. It was found that the change of the PDMS film capacitance upon the application of pressure, was linearly transformed into a change in the transistor's source–drain current.

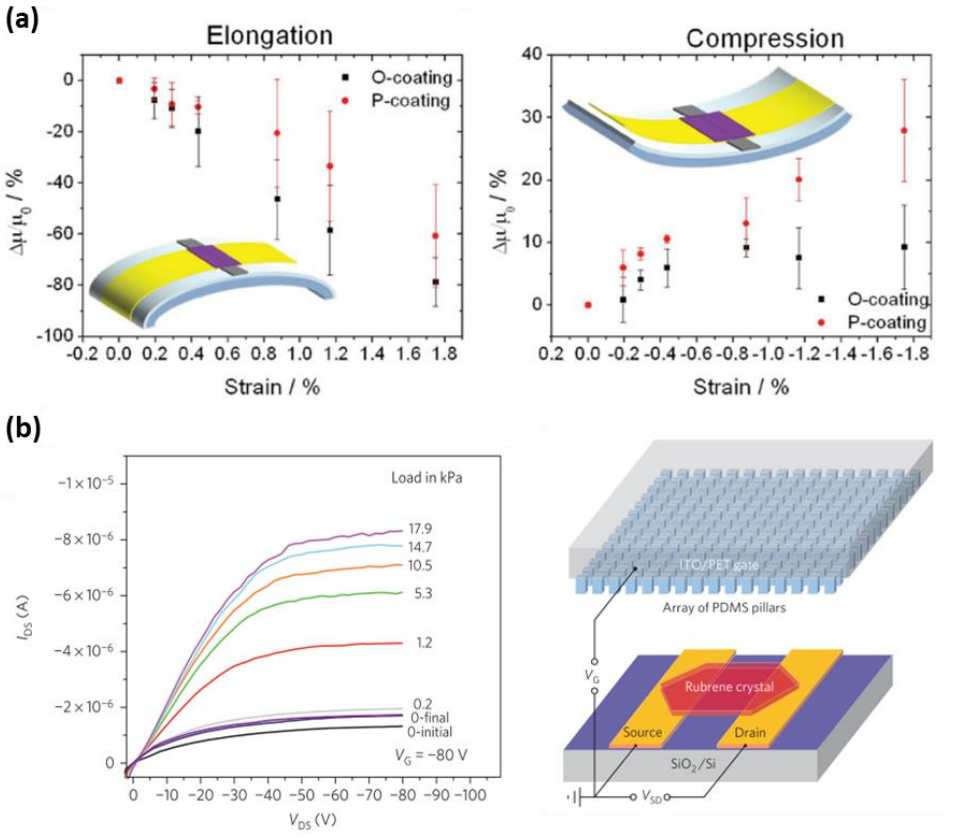

Figure 1.16. **(a)** Average percentage mobility variation ($\Delta\mu/\mu_0$) as a function of the applied strain (elongation and compression) for devices with orthogonal-coated and parallel-coated OSC. Extracted from ref. 136. **(b)** (Right) Layout of a capacitive pressure sensor based on OFETs consisting of rubrene single crystals and microstructured PDMS films. (Left) Electrical characterization of the OFET upon the application of different external pressures. Extracted from ref. 143.

Also, an increased interest in the detection of electromagnetic radiation from visible light to X-rays has been driven by scientific and industrial applications in areas such as defence, security, biomedical imaging/sensing and optical communications. Electromagnetic radiation can photogenerate excitons in the OSC, which dissociate and then mobile charges can be collected at the source/drain electrodes. The electrical properties of the OFET devices under irradiation are dependent on the intensity and the wavelength of the radiation. In the work of Lai *et al*. a novel transistor device on flexible plastic substrate for direct X-ray detection was developed (**Figure 1.17**).[140] The OSC TIPS-pentacene responded directly at real time to different X-ray doses in terms of source-drain current increase. The transistor exhibited excellent reproducibility, stability after the radiation exposition and a remarkably high sensitivity near to 1200 $nC \cdot Gy^{-1}$. In addition, by varying the terminal voltage, the sensitivity of the X-ray detector could be tuned, which was maximised at higher gate voltages.

The photosensitivity of OSCs combined with the possibility of designing customised molecules that can absorb at specific wavelengths is very appealing for the development of a new generation of low-cost flexible photodetectors.

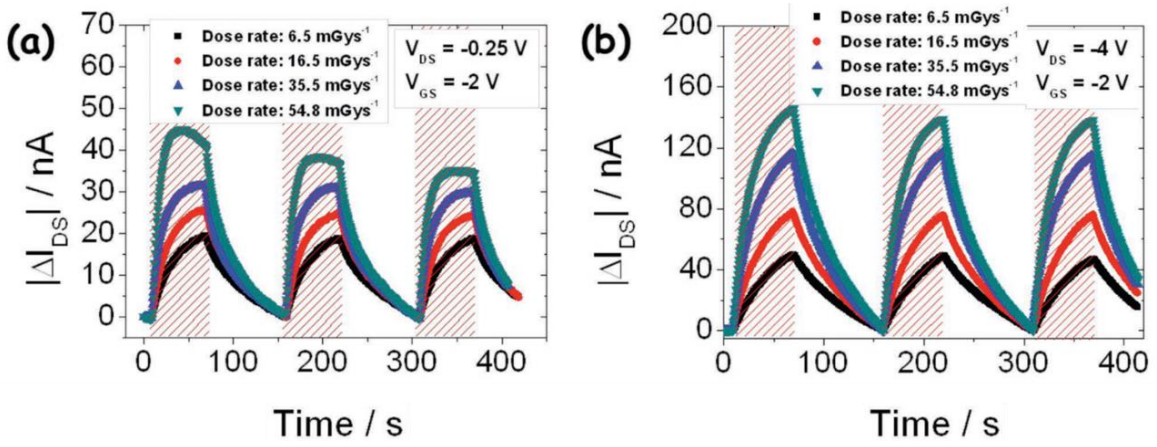

Figure 1.17. Electrical response of a TIPS-pentacene OFET upon the exposition to X-ray radiation at different dose rates in **(a)** linear and **(b)** saturation regimes. Extracted from ref. 140.

1.6.2. BIOSENSORS AND CHEMICAL SENSING

The development of selective low-cost sensors in medicine, food processing, or environmental analysis is of great current interest. OFETs are excellent platforms for this purpose since a chemical event can be converted to an easily read electrical signal.

The detection of gases such as NH_3 or NO_2 was previously reported using an OFET as a transducer. Small gas molecules are capable to penetrate the OSC crystals or to dope defects in the OSC layers, thus the electrical properties of the OFET are altered.[133,144,145] Yangyang Zhu *et al*. explored the effect of the interface layers on the absorption of NO_2 gas on the electrical properties of zinc phthalocyanine (ZnPc)/p-sexiphenyl/α-sexithiophene blend films (Figure 1.18).[146] The ZnPc films grew on top of p-sexiphenyl/α-sexithiophene islands. The stratification of OSCs formed small gaps in the α-sexithiophene films which produced traps and made conduction channels difficult to form, hindering charge transport. Additionally, the gaps facilitate the adsorption and diffusion of gas molecules. It was described that the OFETs performance under NO_2 environment gave rise to an increase in the I_{DS} current. A low limit of detection close to 500 ppb and fast response and recovery time of 1.3 and 4 min, respectively, was reported.

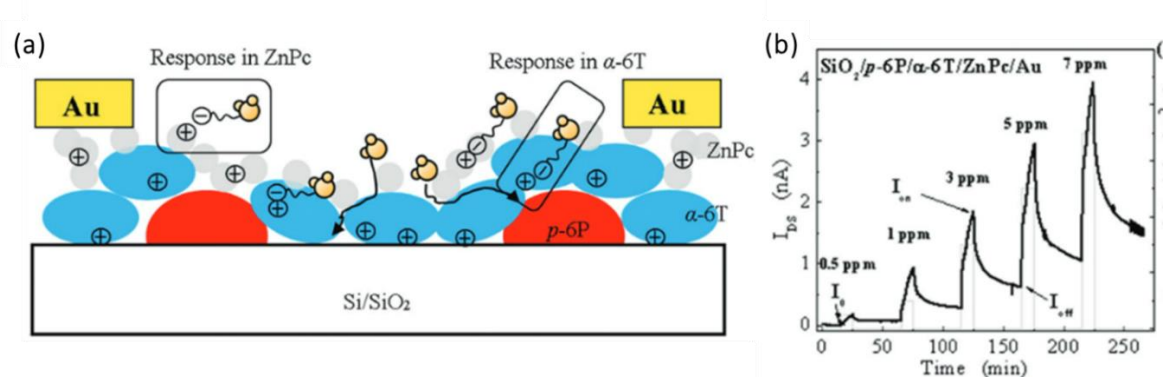

Figure 1.18. (a) Scheme of an OFET based on a ZnPc/p-sexiphenyl/α-sexithiophene blend and principal mechanism that explains the high sensitivity of the device to detect NO_2. (b) I_{DS} current changes of the OFET on the left upon exposure to different NO_2 concentrations. Extracted from ref. 146

In 2010, Kergoat *et al*. developed the first Electrolyte-gated Organic Field-Effect Transistor (EGOFET).[147] EGOFET is a type of transistor that uses an electrolyte as dielectric and the gate electrode is a metal immersed into it. The operation of an EGOFET is based on the capacitive coupling between the gate electrodes and the OSC through the formation of two electrical double layers (EDLs) at the OSC/electrolyte and OSC/gate interfaces. The EDLs produce a high capacitance in the range of 10-40 $\mu F \cdot cm^{-2}$, and hence, the devices operate at very low voltage (below 1 V).[94,111,147–152] Since these devices can work with aqueous electrolytes, they are compatible with biological analytes, becoming an electrical platform highly promising to develop biosensors.

There are different approaches to introduce a receptor group to the EGOFET device to sense a specific analyte. One route is the anchoring of receptors on the surface of the

semiconductor or integrating it in the structure of the organic semiconductor.[153,154] In the work of Magliulo *et al*. the recognition agent (anti-CRP monoclonal antibody) was deposited by physical adsorption onto a poly-3-hexyl thiophene (P3HT) organic semiconductor surface (**Figure 1.19**).[155] Additionally, to prevent non-specific absorption of the analyte (C-reactive protein (CRP)), a non-ionic hydrophilic polymer (pTHMMAA) was employed to cover the surface of P3HT not covered with the anti-CRP monoclonal antibody. The CRP detection was performed by measuring consecutive transfer characteristics after incubation of the CRP protein. A decay in the source-drain current was registered in the range from 4 pM to 2 µM. The adsorption of the molecule on top of the semiconductor produces a change in the response of the transistor due to the accumulation of charge on the surface of the OSC.

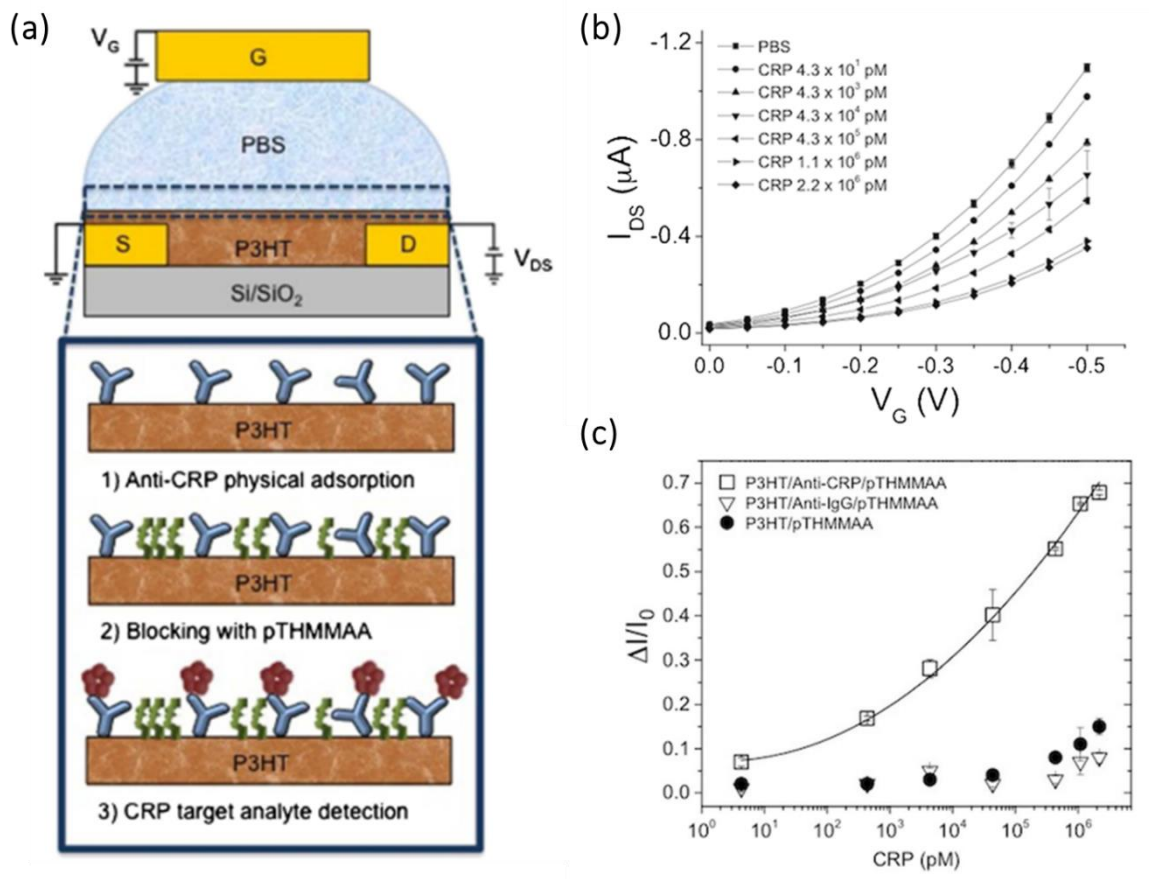

Figure 1.19. **(a)** Schematic structure of the developed EGOFET immunosensor for CRP detection. **(b)** Transfer characteristics (I_{DS} vs. V_G) measured for an EGOFET immunosensor exposed to increasing concentration of CRP (from 4 to $2{\cdot}10^6$ pM). **(c)** Calibration curve obtained for the EGOFET immunosensor. Extracted from ref. 155.

An additional strategy to develop biosensors and chemical sensors is the chemical modification of the gate electrode with specific receptor units. The functionalization of the gate electrode with molecular self-assembled monolayers has provided sensors with unprecedented sensitivity, selectivity and versatility.[148,156–158] Macchia *et al*. explored the capacity to recognize and detect ultra-low concentrations of analyte molecules in solution (**Figure 1.20**).[156] The gate electrode was bio-functionalised with anti-Immunoglobulin-G (anti-IG). The mechanism behind the detection of IG was attributed to the gate work-function change due to the incorporation of the molecule on top of electrode, which disturbed the effective field promoting a variation in the OFET electrical response (i.e., the source drain current of the transistor decreased when the concentration of IG increased).

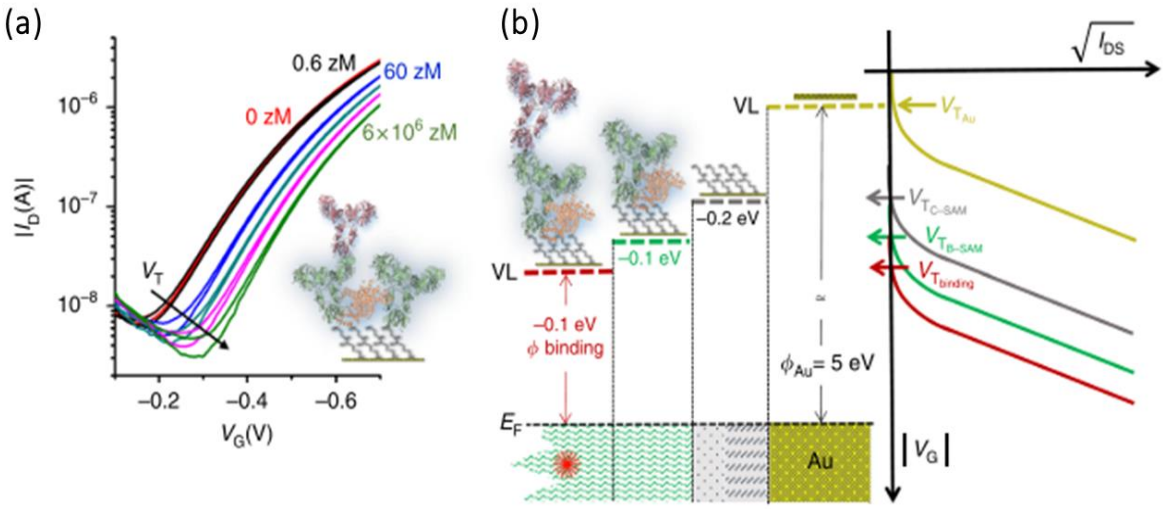

Figure 1.20. **(a)** Transfer characteristics (V_{DS} =−0.4 V) of the OFET device upon the exposition of the gate electrode to Immunoglobulin-G solutions at different concentrations **(b)** Scheme of the decrease of the gate work-function (ϕ) at the different functionalization steps and after the Immunoglobulin-G binding. Extracted from ref. 156.

Sensors based on OFETs are emerging as a next-generation of sensors suitable for the Internet-of-Things (IoT) era because of their various advantages such as low cost, large-area processability, superior mechanical flexibility, tailorable optoelectronic properties and the possibility to combine in a single device the stimuli detection and signal amplification. However, although the progress in OFET-based sensors in the last few years is impressive, their limited stability and reproducibility are still important bottle-necks for their implementation in real devices. Hence, it is crucial to improve the reliability of these devices so they can step into market applications.

1.7. OBJECTIVES

The purpose of this PhD thesis was to investigate the fabrication of high-performance organic field-effect transistors (OFETs) based on blends of small molecule organic semiconductors and polymer binders using a home-made solution shearing deposition technique, namely bar-assisted meniscus shearing or BAMS. Fundamental aspects of these devices have been investigated as well as their implementation into specific sensing applications.

In particular, the general objectives of this thesis are:

1. OFETs fabrication and optimization using as active semiconducting layer thin films of a series of small molecule organic semiconductors blended with polystyrene (PS) and deposited by BAMS. The thin films morphology and crystal structure (i.e., polymorphism) was tuned modifying the coating parameters and formulation, and their effect on the OFET electrical performance was explored.

2. Development of OFET devices based on pentacene derivatives for their application as X-ray photodetector. Study of the impact of the thin film morphology and binding polymer on the X-ray sensitivity.

3. Implementation of non-common gate electrodes based on nanocarbon composite materials in EGOFETs and exploration of their potential and impact on the device properties.

4. Study of the gate gold electrode/electrolyte interface in EGOFET devices. This has been realised by modifying the gold electrode with self-assembled monolayers of molecules with different dipole moments and by studying the interaction of surfactants on the gate electrode.

1.8. REFERENCES

(1) Bardeen, J.; Brattain, W. H. Transistor, a Semiconductor Triode. *Proc. IEEE* 1998, *86* (1), 29–30.

(2) Weimer, P. K. The TFT—A New Thin-Film Transistor. *Proc. IRE* 1962, *50* (6), 1462–1469.

(3) Ryan Smith. NVIDIA Ampere Unleashed: NVIDIA Announces New GPU Architecture, A100 GPU, and Accelerator https://www.anandtech.com/show/15801/nvidia-announces-ampere-architecture-and-a100-products (accessed 2021 -10 -03).

(4) Myny, K. The Development of Flexible Integrated Circuits Based on Thin-Film Transistors. *Nat. Electron.* 2018, *1* (1), 30–39.

(5) Mark Sweney. Global shortage in computer chips "reaches crisis point" https://www.theguardian.com/business/2021/mar/21/global-shortage-in-computer-chips-reaches-crisis-point.

(6) Mas-torrent, M.; Rovira, C. Novel Small Molecules for Organic Field-Effect Transistors: Towards Processability and High Performance. *Chem. Soc. Rev.* 2008, *37* (4), 827–838.

(7) Street, R. A. Thin-Film Transistors. *Adv. Mater.* 2009, *21* (20), 2007–2022.

(8) Heremans, P.; Tripathi, A. K.; de Jamblinne de Meux, A.; Smits, E. C. P.; Hou, B.; Pourtois, G.; Gelinck, G. H. Mechanical and Electronic Properties of Thin-Film Transistors on Plastic, and Their Integration in Flexible Electronic Applications. *Adv. Mater.* 2016, *28* (22), 4266–4282.

(9) Becerril, H. A.; Roberts, M. E.; Liu, Z.; Locklin, J.; Bao, Z. High-Performance Organic Thin-Film Transistors through Solution-Sheared Deposition of Small-Molecule Organic Semiconductors. *Adv. Mater.* 2008, *20* (13), 2588–2594.

(10) Park, S.; Giri, G.; Shaw, L.; Pitner, G.; Ha, J.; Koo, J. H.; Gu, X.; Park, J.; Lee, T. H.; Nam, J. H.; Hong, Y.; Bao, Z. Large-Area Formation of Self-Aligned Crystalline Domains of Organic Semiconductors on Transistor Channels Using CONNECT. *Proc. Natl. Acad. Sci. U. S. A.* 2015, *112* (18), 5561–5566.

(11) Sun, J.; Park, H.; Jung, Y.; Rajbhandari, G.; Maskey, B. B.; Sapkota, A.; Azuma, Y.; Majima, Y.; Cho, G. Proving Scalability of an Organic Semiconductor to Print a TFT-Active Matrix Using a Roll-to-Roll Gravure. *ACS Omega* 2017, *2* (9), 5766–5774.

(12) Köhler, A.; Bässler, H. *Electronic Processes in Organic Semiconductors: An Introduction*; John Wiley & Sons, 2015.

(13) Andersonand, P. W.; Lee, P. A. Remarks on Giant Conductivity in TTF-TCNQ. *Solid State Commun.* 1973, *13* (1), 595–598.

(14) Shirakawa, H.; Louis, E. J.; MacDiarmid, A. G.; Chiang, C. K.; Heeger, A. J. Synthesis of Electrically Conducting Organic Polymers: Halogen Derivatives of Polyacetylene,

(CH)X. *J. Chem. Soc. Chem. Commun.* 1977, *5* (16), 578–580.

(15) Bernius, B. M. T.; Inbasekaran, M.; Brien, J. O.; Wu, W. Progress with Light-Emitting Polymers. *Adv. Mater.* 2000, *12* (23), 1737–1750.

(16) Friend, R. H.; Gymer, R. W.; Holmes, A. B.; Burroughes, J. H.; Marks, R. N.; Taliani, C.; Bradley, D. D. C.; Dos Santos, D. A.; Brédas, J. L.; Logdlum, M.; Salaneck, W. R. Electroluminescence in Conjugated Polymers. *Nature* 1995, *397*, 121–128.

(17) Burroughes, J. H.; Bradley, D. D. C.; Brown, A. R.; Marks, R. N.; Mackay, K.; Friend, R. H.; Burns, P. L.; Holmes, A. B. Light-Emitting Diodes Based on Conjugated Polymers. *Nature* 1990, *347* (6293), 539–541.

(18) Salim, M. B.; Nekovei, R.; Jeyakumar, R. Organic Tandem Solar Cells with 18.6% Efficiency. *Sol. Energy* 2020, *198*, 160–166.

(19) Grätzel, M. Photoelectrochemical Cells. *Nature* 2011, *414*, 338–344.

(20) Ameri, T.; Dennler, G.; Lungenschmied, C.; Brabec, C. J. Organic Tandem Solar Cells: A Review. *Energy Environ. Sci.* 2009, *2* (4), 347–363.

(21) Tang, C. W. Two-Layer Organic Photovoltaic Cell. *Appl. Phys. Lett.* 1986, *48* (2), 183–185.

(22) Peng, W.; Lin, Y.; Jeong, S. Y.; Genene, Z.; Magomedov, A.; Woo, H. Y.; Chen, C.; Wahyudi, W.; Tao, Q.; Deng, J.; Han, Y.; Getautis, V.; Zhu, W.; Anthopoulos, T. D.; Wang, E. Over 18% Ternary Polymer Solar Cells Enabled by a Terpolymer as the Third Component. *Nano Energy* 2022, *92*, 106681.

(23) Braga, D.; Horowitz, G. High-Performance Organic Field-Effect Transistors. *Adv. Mater.* 2009, *21* (14–15), 1473–1486.

(24) Horowitz, G.; Horowitz, B. G. Organic Field-Effect Transistors. *Adv. Mater.* 1998, *10* (5), 365–377.

(25) Horowitz, G.; Fichou, D.; Peng, X.; Xu, Z.; Garnier, F. A Field-Effect Transistor Based on Conjugated Alpha-Sexithienyl. *Solid State Commun.* 1989, *72* (4), 381–384.

(26) Burroughes, J. H.; Jones, C. A.; Friend, R. H. New Semiconductor Device Physics in Polymer Diodes and Transistors. *Nature* 1988, *335*, 137–141.

(27) Chen, Y.; Pistol, M. E.; Anttu, N. Design for Strong Absorption in a Nanowire Array Tandem Solar Cell. *Sci. Rep.* 2016, *6*, 32349.

(28) Riede, M.; Uhrich, C.; Widmer, J.; Timmreck, R.; Wynands, D.; Schwartz, G.; Gnehr, W. M.; Hildebrandt, D.; Weiss, A.; Hwang, J.; Sundarraj, S.; Erk, P.; Pfeiffer, M.; Leo, K. Efficient Organic Tandem Solar Cells Based on Small Molecules. *Adv. Funct. Mater.* 2011, *21* (16), 3019–3028.

(29) Koezuka, H.; Tsumura, A.; Ando, T. Field-Effect Transistor with Polythiophene Thin Film. *Synth. Met.* 1987, *18* (1–3), 699–704.

(30) Tsumura, A.; Koezuka, H.; Ando, T. Macromolecular Electronic Device: Field-Effect Transistor with a Polythiophene Thin Film. *Appl. Phys. Lett.* 1986, *49* (18), 1210–1212.

(31) Iino, H.; Usui, T.; Hanna, J. I. Liquid Crystals for Organic Thin-Film Transistors. *Nat. Commun.* 2015, *6*, 6828.

(32) Chu, M.; Fan, J. X.; Yang, S.; Liu, D.; Ng, C. F.; Dong, H.; Ren, A. M.; Miao, Q. Halogenated Tetraazapentacenes with Electron Mobility as High as 27.8 Cm2 V−1 S−1 in Solution-Processed n-Channel Organic Thin-Film Transistors. *Adv. Mater.* 2018, *30* (38), 1803467.

(33) Haase, K.; Teixeira da Rocha, C.; Hauenstein, C.; Zheng, Y.; Hambsch, M.; Mannsfeld, S. C. B. High-Mobility, Solution-Processed Organic Field-Effect Transistors from C8-BTBT:Polystyrene Blends. *Adv. Electron. Mater.* 2018, *4* (8), 1800076.

(34) Xu, X.; Yao, Y.; Shan, B.; Gu, X.; Liu, D.; Liu, J.; Xu, J.; Zhao, N.; Hu, W.; Miao, Q. Electron Mobility Exceeding 10 Cm2V−1s−1and Band-Like Charge Transport in Solution-Processed n-Channel Organic Thin-Film Transistors. *Adv. Mater.* 2016, *28* (26), 5276–5283.

(35) Dong, H.; Fu, X.; Liu, J.; Wang, Z.; Hu, W. 25th Anniversary Article: Key Points for High-Mobility Organic Field-Effect Transistors. *Adv. Mater.* 2013, *25* (43), 6158–6183.

(36) Sirringhaus, H. 25th Anniversary Article: Organic Field-Effect Transistors: The Path beyond Amorphous Silicon. *Adv. Mater.* 2014, *26* (9), 1319–1335.

(37) De Caro, D.; Jacob, K.; Hahioui, H.; Faulmann, C.; Valade, L.; Kadoya, T.; Mori, T.; Fraxedas, J.; Viau, L. Nanoparticles of Organic Conductors: Synthesis and Application as Electrode Material in Organic Field Effect Transistors. *New J. Chem.* 2011, *35* (6), 1315–1319.

(38) Bao, Z.; Locklin, J. *Organic Field-Effect Transistors*; CRC Press: Boca Raton, 2007.

(39) Iqbal, H. F.; Waldrip, M.; Chen, H.; McCulloch, I.; Jurchescu, O. D. Elucidating the Role of Water-Related Traps in the Operation of Polymer Field-Effect Transistors. *Adv. Electron. Mater.* 2021, *7* (9), 2100393.

(40) De Angelis, F.; Cipolloni, S.; Mariucci, L.; Fortunato, G. Aging Effects in Pentacene Thin-Film Transistors: Analysis of the Density of States Modification. *Appl. Phys. Lett.* 2006, *88* (19), 193508.

(41) Katz, H. E.; Johnson, J.; Kloc, C.; Siegrist, T.; Li, W.; Lin, Y.-Y. A Soluble and Air-Stable Organic Semiconductor with High Electron Mobility. *Nature* 2000, *404*, 478–480.

(42) Lim, B.; Sun, H.; Noh, Y. Y. Highly Soluble Small-Molecule Organic Semiconductor with Trihexylsilyloxy Side Chain for High-Performance Organic Field-Effect Transistors with Mobility of up to 3.10 Cm2 V−1 S−1. *Dye. Pigment.* 2017, *142*, 17–23.

(43) Bi, S.; He, Z.; Chen, J.; Li, D. Solution-Grown Small-Molecule Organic Semiconductor with Enhanced Crystal Alignment and Areal Coverage for Organic Thin Film Transistors. *AIP Adv.* 2015, *5* (7), 077170.

(44) Inoue, S.; Minemawari, H.; Tsutsumi, J.; Chikamatsu, M.; Yamada, T.; Horiuchi, S.; Tanaka, M.; Kumai, R.; Yoneya, M.; Hasegawa, T. Effects of Substituted Alkyl Chain Length on Solution-Processable Layered Organic Semiconductor Crystals. *Chem. Mater.* 2015, *27* (11), 3809–3812.

(45) Gentili, D.; Gazzano, M.; Melucci, M.; Jones, D.; Cavallini, M. Polymorphism as an Additional Functionality of Materials for Technological Applications at Surfaces and Interfaces. *Chem. Soc. Rev.* 2019, *48* (9), 2502–2517.

(46) Reinspach, J. A.; Diao, Y.; Giri, G.; Sachse, T.; England, K.; Zhou, Y.; Tassone, C.; Worfolk, B. J.; Presselt, M.; Toney, M. F.; Mannsfeld, S.; Bao, Z. Tuning the Morphology of Solution-Sheared P3HT:PCBM Films. *ACS Appl. Mater. Interfaces* 2016, *8* (3), 1742–1751.

(47) Giri, G.; Verploegen, E.; Mannsfeld, S. C. B.; Atahan-Evrenk, S.; Kim, D. H.; Lee, S. Y.; Becerril, H. A.; Aspuru-Guzik, A.; Toney, M. F.; Bao, Z. Tuning Charge Transport in Solution-Sheared Organic Semiconductors Using Lattice Strain. *Nature* 2011, *480* (7378), 504–508.

(48) Riera-Galindo, S.; Tamayo, A.; Mas-Torrent, M. Role of Polymorphism and Thin-Film Morphology in Organic Semiconductors Processed by Solution Shearing. *ACS Omega* 2018, *3* (2), 2329–2339.

(49) Diao, Y.; Lenn, K. M.; Lee, W. Y.; Blood-Forsythe, M. A.; Xu, J.; Mao, Y.; Kim, Y.; Reinspach, J. A.; Park, S.; Aspuru-Guzik, A.; Xue, G.; Clancy, P.; Bao, Z.; Mannsfeld, S. C. B. Understanding Polymorphism in Organic Semiconductor Thin Films through Nanoconfinement. *J. Am. Chem. Soc.* 2014, *136* (49), 17046–17057.

(50) Li, M.; Balawi, A. H.; Leenaers, P. J.; Ning, L.; Heintges, G. H. L.; Marszalek, T.; Pisula, W.; Wienk, M. M.; Meskers, S. C. J.; Yi, Y.; Laquai, F.; Janssen, R. A. J. Impact of Polymorphism on the Optoelectronic Properties of a Low-Bandgap Semiconducting Polymer. *Nat. Commun.* 2019, *10*, 2867.

(51) Patel, B. B.; Diao, Y. Multiscale Assembly of Solution-Processed Organic Electronics: The Critical Roles of Confinement, Fluid Flow, and Interfaces. *Nanotechnology* 2018, *29* (4), 044004.

(52) Diao, Y.; Shaw, L.; Bao, Z.; Mannsfeld, S. C. B. Morphology Control Strategies for Solution-Processed Organic Semiconductor Thin Films. *Energy Environ. Sci.* 2014, *7* (7), 2145–2159.

(53) Jurchescu, O. D.; Mourey, D. A.; Subramanian, S.; Parkin, S. R.; Vogel, B. M.; Anthony, J. E.; Jackson, T. N.; Gundlach, D. J. Effects of Polymorphism on Charge Transport in Organic Semiconductors. *Phys. Rev. B* 2009, *80* (8), 085201.

(54) Bhattacharya, P.; Fornari, R.; Kamimura, H. *Comprehensive Semiconductor Science and Technology*; Elsevier: Amsterdam, 2011.

(55) Marcus, R. a. On the Theory of Oxidation-Reduction Reactions Involving Electron Transfer. I. *Phys. Rev.* 1956, *24* (5), 966.

(56) Lu, N.; Li, L.; Banerjee, W.; Sun, P.; Gao, N.; Liu, M. Charge Carrier Hopping Transport Based on Marcus Theory and Variable-Range Hopping Theory in Organic Semiconductors. *J. Appl. Phys.* 2015, *118* (4), 045701.

(57) Abou El Ela, A. H.; Afifi, H. H. Hopping Transport in Organic Semiconductor System. *J. Phys. Chem. Solids* 1979, *40* (4), 257–259.

(58) Geng, H.; Peng, Q.; Wang, L.; Li, H.; Liao, Y.; Ma, Z.; Shuai, Z. Toward Quantitative Prediction of Charge Mobility in Organic Semiconductors: Tunneling Enabled Hopping Model. *Adv. Mater.* 2012, *24* (26), 3568–3572.

(59) Sakanoue, T.; Sirringhaus, H. Band-like Temperature Dependence of Mobility in a Solution-Processed Organic Semiconductor. *Nat. Mater.* 2010, *9* (9), 736–740.

(60) Cho, J. M.; Mori, T. Low-Temperature Band Transport and Impact of Contact Resistance in Organic Field-Effect Transistors Based on Single-Crystal Films of Ph-BTBT-C10. *Phys. Rev. Appl.* 2016, *5* (6), 064017.

(61) Uemura, T.; Nakayama, K.; Hirose, Y.; Soeda, J.; Uno, M.; Li, W.; Yamagishi, M.; Okada, Y.; Takeya, J. Band-like Transport in Solution-Crystallized Organic Transistors. *Curr. Appl. Phys.* 2012, *12* (SUPPL.3), S87–S91.

(62) Coropceanu, V.; Cornil, J.; da Silva Filho, D. A.; Olivier, Y.; Silbey, R.; Brédas, J. L. Charge Transport in Organic Semiconductors. *Chem. Rev.* 2007, *107* (4), 926–952.

(63) Cho, J. M.; Higashino, T.; Mori, T. Band-like Transport down to 20 K in Organic Single-Crystal Transistors Based on Dioctylbenzothienobenzothiophene. *Appl. Phys. Lett.* 2015, *106* (19), 193303.

(64) Galindo, S.; Tamayo, A.; Leonardi, F.; Mas-Torrent, M. Control of Polymorphism and Morphology in Solution Sheared Organic Field-Effect Transistors. *Adv. Funct. Mater.* 2017, *27* (25), 1700526.

(65) Di Maria, F.; Fabiano, E.; Gentili, D.; Biasiucci, M.; Salzillo, T.; Bergamini, G.; Gazzano, M.; Zanelli, A.; Brillante, A.; Cavallini, M.; Della Sala, F.; Gigli, G.; Barbarella, G. Polymorphism in Crystalline Microfibers of Achiral Octithiophene: The Effect on Charge Transport, Supramolecular Chirality and Optical Properties. *Adv. Funct. Mater.* 2014, *24* (31), 4943–4951.

(66) Chen, J.; Shao, M.; Xiao, K.; Rondinone, A. J.; Loo, Y. L.; Kent, P. R. C.; Sumpter, B. G.; Li, D.; Keum, J. K.; Diemer, P. J.; Anthony, J. E.; Jurchescu, O. D.; Huang, J. Solvent-Type-Dependent Polymorphism and Charge Transport in a Long Fused-Ring Organic Semiconductor. *Nanoscale* 2014, *6* (1), 449–456.

(67) Otón, F.; Pfattner, R.; Oxtoby, N. S.; Mas-Torrent, M.; Wurst, K.; Fontrodona, X.; Olivier, Y.; Cornil, J.; Veciana, J.; Rovira, C. Benzodicarbomethoxytetrathiafulvalene Derivatives as Soluble Organic Semiconductors. *J. Org. Chem.* 2011, *76* (1), 154–163.

(68) Inoue, S.; Shinamura, S.; Sadamitsu, Y.; Arai, S.; Horiuchi, S.; Yoneya, M.; Takimiya, K.; Hasegawa, T. Extended and Modulated Thienothiophenes for Thermally Durable and Solution-Processable Organic Semiconductors. *Chem. Mater.* 2018, *30* (15), 5050–5060.

(69) Kim, C. S.; Lee, S.; Gomez, E. D.; Anthony, J. E.; Loo, Y. L. Solvent-Dependent Electrical Characteristics and Stability of Organic Thin-Film Transistors with Drop Cast Bis(Triisopropylsilylethynyl) Pentacene. *Appl. Phys. Lett.* 2008, *93* (10), 103302.

(70) Kim, D. H.; Han, J. T.; Park, Y. D.; Jang, Y.; Cho, J. H.; Hwang, M.; Cho, K. Single-Crystal Polythiophene Microwires Grown by Self-Assembly. *Adv. Mater.* 2006, *18* (6), 719–723.

(71) Yuan, Y.; Giri, G.; Ayzner, A. L.; Zoombelt, A. P.; Mannsfeld, S. C. B.; Chen, J.; Nordlund, D.; Toney, M. F.; Huang, J.; Bao, Z. Ultra-High Mobility Transparent Organic Thin Film Transistors Grown by an off-Centre Spin-Coating Method. *Nat. Commun.* 2014, *5*, 3005.

(72) Chang, J. F.; Sun, B.; Breiby, D. W.; Nielsen, M. M.; Sölling, T. I.; Giles, M.; McCulloch, I.; Sirringhaus, H. Enhanced Mobility of Poly(3-Hexylthiophene) Transistors by Spin-Coating from High-Boiling-Point Solvents. *Chem. Mater.* 2004, *16* (23), 4772–4776.

(73) Huang, Y.; Sun, J.; Zhang, J.; Wang, S.; Huang, H.; Zhang, J.; Yan, D.; Gao, Y.; Yang, J. Controllable Thin-Film Morphology and Structure for 2,7-Dioctyl[1]Benzothieno[3,2-b][1]Benzothiophene (C8BTBT) Based Organic Field-Effect Transistors. *Org. Electron.* 2016, *36*, 73–81.

(74) Ren, H.; Cui, N.; Tang, Q.; Tong, Y.; Zhao, X.; Liu, Y. High-Performance, Ultrathin, Ultraflexible Organic Thin-Film Transistor Array Via Solution Process. *Small* 2018, *14* (33), 1801020.

(75) Georgakopoulos, S.; Pérez-Rodríguez, A.; Campos, A.; Temiño, I.; Galindo, S.; Barrena, E.; Ocal, C.; Mas-Torrent, M. Spray-Coated Contacts from an Organic Charge Transfer Complex Solution for Organic Field-Effect Transistors. *Org. Electron.* 2017, *48*, 365–370.

(76) Treossi, E.; Liscio, A.; Feng, X.; Palermo, V.; Müllen, K.; Samorì, P. Large-Area Bi-Component Processing of Organic Semiconductors by Spray Deposition and Spin Coating with Orthogonal Solvents. *Appl. Phys. A Mater. Sci. Process.* 2009, *95* (1), 15–20.

(77) Kjellander, B. K. C.; Smaal, W. T. T.; Anthony, J. E.; Gelinck, G. H. Inkjet Printing of TIPS-PEN on Soluble Polymer Insulating Films: A Route to High-Performance Thin-Film Transistors. *Adv. Mater.* 2010, *22* (41), 4612–4616.

(78) Mitra, K. Y.; Polomoshnov, M.; Martínez-Domingo, C.; Mitra, D.; Ramon, E.; Baumann, R. R. Fully Inkjet-Printed Thin-Film Transistor Array Manufactured on Paper Substrate for Cheap Electronic Applications. *Adv. Electron. Mater.* 2017, *3* (12), 1700275.

(79) Diao, Y.; Tee, B. C. K.; Giri, G.; Xu, J.; Kim, D. H.; Becerril, H. A.; Stoltenberg, R. M.;

Lee, T. H.; Xue, G.; Mannsfeld, S. C. B.; Bao, Z. Solution Coating of Large-Area Organic Semiconductor Thin Films with Aligned Single-Crystalline Domains. *Nat. Mater.* 2013, *12* (7), 665–671.

(80) Giri, G.; Li, R.; Smilgies, D.-M.; Li, E. Q.; Diao, Y.; Lenn, K. M.; Chiu, M.; Lin, D. W.; Allen, R.; Reinspach, J.; Mannsfeld, S. C. B.; Thoroddsen, S. T.; Clancy, P.; Bao, Z.; Amassian, A. One-Dimensional Self-Confinement Promotes Polymorph Selection in Large-Area Organic Semiconductor Thin Films. *Nat. Commun.* 2014, *5*, 3573.

(81) del Pozo, F. G.; Fabiano, S.; Pfattner, R.; Georgakopoulos, S.; Galindo, S.; Liu, X.; Braun, S.; Fahlman, M.; Veciana, J.; Rovira, C.; Crispin, X.; Berggren, M.; Mas-Torrent, M. Single Crystal-like Performance in Solution-Coated Thin-Film Organic Field-Effect Transistors. *Adv. Funct. Mater.* 2016, *26* (14), 2379–2386.

(82) Niazi, M. R.; Li, R.; Abdelsamie, M.; Zhao, K.; Anjum, D. H.; Payne, M. M.; Anthony, J.; Smilgies, D. M.; Amassian, A. Contact-Induced Nucleation in High-Performance Bottom-Contact Organic Thin Film Transistors Manufactured by Large-Area Compatible Solution Processing. *Adv. Funct. Mater.* 2016, *26* (14), 2371–2378.

(83) Bucella, S. G.; Luzio, A.; Gann, E.; Thomsen, L.; McNeill, C. R.; Pace, G.; Perinot, A.; Chen, Z.; Facchetti, A.; Caironi, M. Macroscopic and High-Throughput Printing of Aligned Nanostructured Polymer Semiconductors for MHz Large-Area Electronics. *Nat. Commun.* 2015, *6*, 8394.

(84) Jang, J.; Nam, S.; Im, K.; Hur, J.; Cha, S. N.; Kim, J.; Son, H. Bin; Suh, H.; Loth, M. A.; Anthony, J. E.; Park, J. J.; Park, C. E.; Kim, J. M.; Kim, K. Highly Crystalline Soluble Acene Crystal Arrays for Organic Transistors: Mechanism of Crystal Growth during Dip-Coating. *Adv. Funct. Mater.* 2012, *22* (5), 1005–1014.

(85) Li, L.; Gao, P.; Schuermann, K. C.; Ostendorp, S.; Wang, W.; Du, C.; Lei, Y.; Fuchs, H.; Cola, L. De; Müllen, K.; Chi, L. Controllable Growth and Field-Effect Property of Monolayer to Multilayer Microstripes of an Organic Semiconductor. *J. Am. Chem. Soc.* 2010, *132* (26), 8807–8809.

(86) Tracz, A.; Jeszka, J. K.; Watson, M. D.; Pisula, W.; Müllen, K.; Pakula, T. Uniaxial Alignment of the Columnar Super-Structure of a Hexa (Alkyl) Hexa-Peri-Hexabenzocoronene on Untreated Glass by Simple Solution Processing. *J. Am. Chem. Soc.* 2003, *125* (7), 1682–1683.

(87) Duffy, C. M.; Andreasen, J. W.; Breiby, D. W.; Nielsen, M. M.; Ando, M.; Minakata, T.; Sirringhaus, H. High-Mobility Aligned Pentacene Films Grown by Zone-Casting. *Chem. Mater.* 2008, *20* (23), 7252–7259.

(88) Janneck, R.; Vercesi, F.; Heremans, P.; Genoe, J.; Rolin, C. Predictive Model for the Meniscus-Guided Coating of High-Quality Organic Single-Crystalline Thin Films. *Adv. Mater.* 2016, *28* (36), 8007–8013.

(89) Janneck, R.; Nowack, T. S.; De Roose, F.; Ali, H.; Dehaene, W.; Heremans, P.; Genoe, J.; Rolin, C. Integration of Highly Crystalline C8-BTBT Thin-Films into Simple Logic Gates and Circuits. *Org. Electron.* 2019, *67*, 64–71.

(90) Yu, L.; Niazi, M. R.; Ngongang Ndjawa, G. O.; Li, R.; Kirmani, A. R.; Munir, R.; Balawi, A. H.; Laquai, F.; Amassian, A. Programmable and Coherent Crystallization of Semiconductors. *Sci. Adv.* 2017, *3* (3), e1602462.

(91) Yuan, J.; Liu, D.; Zhao, H.; Lin, B.; Zhou, X.; Naveed, H. B.; Zhao, C.; Zhou, K.; Tang, Z.; Chen, F.; Ma, W. Patterned Blade Coating Strategy Enables the Enhanced Device Reproducibility and Optimized Morphology of Organic Solar Cells. *Adv. Energy Mater.* 2021, *11* (18), 2100098.

(92) Sugiyama, M.; Jancke, S.; Uemura, T.; Kondo, M.; Inoue, Y.; Namba, N.; Araki, T.; Fukushima, T.; Sekitani, T. Mobility Enhancement of DNTT and BTBT Derivative Organic Thin-Film Transistors by Triptycene Molecule Modification. *Org. Electron.* 2021, *96*, 106219.

(93) Temiño, I.; Del Pozo, F. G.; Ajayakumar, M. R.; Galindo, S.; Puigdollers, J.; Mas-Torrent, M. A Rapid, Low-Cost, and Scalable Technique for Printing State-of-the-Art Organic Field-Effect Transistors. *Adv. Mater. Technol.* 2016, *1* (5), 1600090.

(94) Zhang, Q.; Leonardi, F.; Casalini, S.; Temiño, I.; Mas-Torrent, M. High Performing Solution-Coated Electrolyte-Gated Organic Field-Effect Transistors for Aqueous Media Operation. *Sci. Rep.* 2016, *6*, 39623.

(95) Campos, A.; Riera-Galindo, S.; Puigdollers, J.; Mas-Torrent, M. Reduction of Charge Traps and Stability Enhancement in Solution-Processed Organic Field-Effect Transistors Based on a Blended n-Type Semiconductor. *ACS Appl. Mater. Interfaces* 2018, *10* (18), 15952–15961.

(96) Tamayo, A.; Hofer, S.; Salzillo, T.; Ruzié, C.; Schweicher, G.; Resel, R.; Mas-Torrent, M. Mobility Anisotropy in the Herringbone Structure of Asymmetric Ph-BTBT-10 in Solution Sheared Thin Film Transistors. *J. Mater. Chem. C* 2021, *9* (22), 7186–7193.

(97) Salzillo, T.; Campos, A.; Babuji, A.; Santiago, R.; Bromley, S. T.; Ocal, C.; Barrena, E.; Jouclas, R.; Ruzie, C.; Schweicher, G.; Geerts, Y. H.; Mas-Torrent, M. Enhancing Long-Term Device Stability Using Thin Film Blends of Small Molecule Semiconductors and Insulating Polymers to Trap Surface-Induced Polymorphs. *Adv. Funct. Mater.* 2020, *30* (52), 2006115.

(98) Riera-Galindo, S.; Leonardi, F.; Pfattner, R.; Mas-Torrent, M. Organic Semiconductor/Polymer Blend Films for Organic Field-Effect Transistors. *Adv. Mater. Technol.* 2019, *4* (9), 1900104.

(99) Li, Y.; Sun, H.; Shi, Y.; Tsukagoshi, K. Patterning Technology for Solution-Processed Organic Crystal Field-Effect Transistors. *Sci. Technol. Adv. Mater.* 2014, *15* (2), 024203.

(100) Søndergaard, R. R.; Hösel, M.; Krebs, F. C. Roll-to-Roll Fabrication of Large Area Functional Organic Materials. *J. Polym. Sci. Part B Polym. Phys.* 2013, *51* (1), 16–34.

(101) Abbel, R.; Galagan, Y.; Groen, P. Roll-to-Roll Fabrication of Solution Processed Electronics. *Adv. Eng. Mater.* 2018, *20* (8), 1701190.

(102) Xu, J.; Wu, H. C.; Zhu, C.; Ehrlich, A.; Shaw, L.; Nikolka, M.; Wang, S.; Molina-Lopez, F.; Gu, X.; Luo, S.; Zhou, D.; Kim, Y. H.; Wang, G. J. N.; Gu, K.; Feig, V. R.; Chen, S.; Kim, Y.; Katsumata, T.; Zheng, Y. Q.; Yan, H.; Chung, J. W.; Lopez, J.; Murmann, B.; Bao, Z. Multi-Scale Ordering in Highly Stretchable Polymer Semiconducting Films. *Nat. Mater.* 2019, *18* (6), 594–601.

(103) Le Berre, M.; Chen, Y.; Baigl, D. From Convective Assembly to Landau - Levich Deposition of Multilayered Phospholipid Films of Controlled Thickness. *Langmuir* 2009, *25* (5), 2554–2557.

(104) Faustini, M.; Louis, B.; Albouy, P. A.; Kuemmel, M.; Grosso, D. Preparation of Sol-Gel Films by Dip-Coating in Extreme Conditions. *J. Phys. Chem. C* 2010, *114* (17), 7637–7645.

(105) Smith, J.; Zhang, W.; Sougrat, R.; Zhao, K.; Li, R.; Cha, D.; Amassian, A.; Heeney, M.; McCulloch, I.; Anthopoulos, T. D. Solution-Processed Small Molecule-Polymer Blend Organic Thin-Film Transistors with Hole Mobility Greater than 5 Cm2/Vs. *Adv. Mater.* 2012, *24* (18), 2441–2446.

(106) Paterson, A. F.; Treat, N. D.; Zhang, W.; Fei, Z.; Wyatt-Moon, G.; Faber, H.; Vourlias, G.; Patsalas, P. A.; Solomeshch, O.; Tessler, N.; Heeney, M.; Anthopoulos, T. D. Small Molecule/Polymer Blend Organic Transistors with Hole Mobility Exceeding 13 Cm2V−1s−1. *Adv. Mater.* 2016, *28* (35), 7791–7798.

(107) Smith, J.; Hamilton, R.; Qi, Y.; Kahn, A.; Bradley, D. D. C.; Heeney, M.; McCulloch, I.; Anthopoulos, T. D. The Influence of Film Morphology in High-Mobility Small-Molecule: Polymer Blend Organic Transistors. *Adv. Funct. Mater.* 2010, *20* (14), 2330–2337.

(108) Madec, M. B.; Crouch, D.; Llorente, G. R.; Whittle, T. J.; Geoghegan, M.; Yeates, S. G. Organic Field Effect Transistors from Ambient Solution Processed Low Molar Mass Semiconductor-Insulator Blends. *J. Mater. Chem.* 2008, *18* (27), 3230–3236.

(109) Arias, A. C. Vertically Segregated Polymer Blends: Their Use in Organic Electronics. *Polym. Rev.* 2006, *46* (1), 103–125.

(110) He, Z.; Bi, S.; Asare-Yeboah, K.; Zhang, Z. Phase Segregation Effect on TIPS Pentacene Crystallization and Morphology for Organic Thin Film Transistors. *J. Mater. Sci. Mater. Electron.* 2020, *31* (6), 4503–4510.

(111) Leonardi, F.; Casalini, S.; Zhang, Q.; Galindo, S.; Gutiérrez, D.; Mas-Torrent, M. Electrolyte-Gated Organic Field-Effect Transistor Based on a Solution Sheared Organic Semiconductor Blend. *Adv. Mater.* 2016, *28* (46), 10311–10316.

(112) Zhao, K.; Wodo, O.; Ren, D.; Khan, H. U.; Niazi, M. R.; Hu, H.; Abdelsamie, M.; Li, R.; Li, E. Q.; Yu, L.; Yan, B.; Payne, M. M.; Smith, J.; Anthony, J. E.; Anthopoulos, T. D.; Thoroddsen, S. T.; Ganapathysubramanian, B.; Amassian, A. Vertical Phase Separation in Small Molecule:Polymer Blend Organic Thin Film Transistors Can Be Dynamically Controlled. *Adv. Funct. Mater.* 2016, *26* (11), 1737–1746.

(113) Streetman, B. G.; Banerjee, S. *Solid State Electronic Devices*; Prentice Hall: Upper

Saddle River, 2000.

(114) Kymissis, I. *Organic Field Effect Transistors: Theory, Fabrication and Characterization*; Springer: Boston, 2008.

(115) Shehu, A.; Quiroga, S. D.; D'Angelo, P.; Albonetti, C.; Borgatti, F.; Murgia, M.; Scorzoni, A.; Stoliar, P.; Biscarini, F. Layered Distribution of Charge Carriers in Organic Thin Film Transistors. *Phys. Rev. Lett.* 2010, *104* (24), 246602.

(116) Pérez-Rodríguez, A.; Temiño, I.; Ocal, C.; Mas-Torrent, M.; Barrena, E. Decoding the Vertical Phase Separation and Its Impact on C8-BTBT/PS Transistor Properties. *ACS Appl. Mater. Interfaces* 2018, *10* (8), 7296–7303.

(117) Shim, C.-H.; Maruoka, F.; Hattori, R. Structural Analysis on Organic Thin-Film Transistor With Device Simulation. *IEEE Trans. Electron Devices* 2010, *57* (1), 195–200.

(118) Gundlach, D. J.; Zhou, L.; Nichols, J. A.; Jackson, T. N.; Necliudov, P. V.; Shur, M. S. An Experimental Study of Contact Effects in Organic Thin Film Transistors. *J. Appl. Phys.* 2006, *100* (2), 024509.

(119) Waldrip, M.; Jurchescu, O. D.; Gundlach, D. J.; Bittle, E. G. Contact Resistance in Organic Field-Effect Transistors: Conquering the Barrier. *Adv. Funct. Mater.* 2020, *30* (20), 1904576.

(120) Lüssem, B.; Keum, C. M.; Kasemann, D.; Naab, B.; Bao, Z.; Leo, K. Doped Organic Transistors. *Chem. Rev.* 2016, *116* (22), 13714–13751.

(121) Liu, C.; Xu, Y.; Noh, Y. Contact Engineering in Organic Field-Effect Transistors. *Mater. Today* 2015, *18* (2), 79–96.

(122) Ablat, A.; Kyndiah, A.; Houin, G.; Alic, T. Y.; Hirsch, L. Role of Oxide / Metal Bilayer Electrodes in Solution Processed Organic Field Effect Transistors. *Sci. Rep.* 2019, *9*, 6685.

(123) Kim, Y.; Chung, S.; Cho, K.; Harkin, D.; Hwang, W. T.; Yoo, D.; Kim, J. K.; Lee, W.; Song, Y.; Ahn, H.; Hong, Y.; Sirringhaus, H.; Kang, K.; Lee, T. Enhanced Charge Injection Properties of Organic Field-Effect Transistor by Molecular Implantation Doping. *Adv. Mater.* 2019, *31* (10), 1806697.

(124) Hwang, D. K.; Fuentes-Hernandez, C.; Kim, J.; Potscavage, W. J.; Kim, S. J.; Kippelen, B. Top-Gate Organic Field-Effect Transistors with High Environmental and Operational Stability. *Adv. Mater.* 2011, *23* (10), 1293–1298.

(125) Wang, C. Y.; Fuentes-Hernandez, C.; Chou, W. F.; Kippelen, B. Top-Gate Organic Field-Effect Transistors Fabricated on Paper with High Operational Stability. *Org. Electron.* 2017, *41*, 340–344.

(126) Natali, D.; Caironi, M. Charge Injection in Solution-Processed Organic Field-Effect Transistors : Physics , Models and Characterization Methods. *Adv. Mater.* 2012, *24* (11), 1357.

(127) Choi, S.; Larrain, F. A.; Wang, C. Y.; Fuentes-Hernandez, C.; Chou, W. F.; Kippelen, B. Self-Forming Electrode Modification in Organic Field-Effect Transistors. *J. Mater. Chem. C* 2016, *4* (35), 8297–8303.

(128) Casalini, S.; Bortolotti, C. A.; Leonardi, F.; Biscarini, F. Self-Assembled Monolayers in Organic Electronics. *Chem. Soc. Rev.* 2017, *46* (1), 40–71.

(129) Li, S.; Guérin, D.; Lmimouni, K. Improving Performance of OFET by Tuning Occurrence of Charge Transport Based on Pentacene Interaction with SAM Functionalized Contacts. *Microelectron. Eng.* 2018, *195* (5), 62–67.

(130) Kim, S. H.; Kim, J.; Nam, S.; Lee, H. S.; Lee, S. W.; Jang, J. Tuning the Work Function of Printed Polymer Electrodes by Introducing a Fluorinated Polymer to Enhance the Operational Stability in Bottom-Contact Organic Field-Effect Transistors. *ACS Appl. Mater. Interfaces* 2017, *9* (14), 12637–12646.

(131) Horowitz, G.; Hajlaoui, R.; Bouchriha, H.; Bourguiga, R.; Hajlaoui, M. Concept of `threshold Voltage' in Organic Field-Effect Transistors. *Adv. Mater.* 1998, *10* (12), 923–927.

(132) Torsi, L.; Magliulo, M.; Manoli, K.; Palazzo, G. Organic Field-Effect Transistor Sensors: A Tutorial Review. *Chem. Soc. Rev.* 2013, *42* (22), 8612–8628.

(133) Wang, Y.; Zhang, J.; Zhang, S.; Huang, J. OFET Chemical Sensors : Chemical Sensors Based on Ultrathin Organic Field-Effect Transistors. *Polym. Int.* 2021, *70* (4), 414–425.

(134) Lin, P.; Yan, F. Organic Thin-Film Transistors for Chemical and Biological Sensing. *Adv. Mater.* 2012, *24* (1), 34–51.

(135) Temiño, I.; Basiricò, L.; Fratelli, I.; Tamayo, A.; Ciavatti, A.; Mas-Torrent, M.; Fraboni, B. Morphology and Mobility as Tools to Control and Unprecedentedly Enhance X-Ray Sensitivity in Organic Thin-Films. *Nat. Commun.* 2020, *11* (1), 2136.

(136) Lai, S.; Temiño, I.; Cramer, T.; del Pozo, F. G.; Fraboni, B.; Cosseddu, P.; Bonfiglio, A.; Mas-Torrent, M. Morphology Influence on the Mechanical Stress Response in Bendable Organic Field-Effect Transistors with Solution-Processed Semiconductors. *Adv. Electron. Mater.* 2017, *4* (10), 1700271.

(137) Ogunleye, O. O.; Sakai, H.; Ishii, Y.; Murata, H. Investigation of the Sensing Mechanism of Dual-Gate Low-Voltage Organic Transistor Based Pressure Sensor. *Org. Electron.* 2019, *75*, 105431.

(138) Wang, Z.; Guo, S.; Li, H.; Wang, B.; Sun, Y.; Xu, Z.; Chen, X.; Wu, K.; Zhang, X.; Xing, F.; Li, L.; Hu, W. The Semiconductor/Conductor Interface Piezoresistive Effect in an Organic Transistor for Highly Sensitive Pressure Sensors. *Adv. Mater.* 2019, *31* (6), 1805630.

(139) Zeidell, A. M.; Ren, T.; Filston, D. S.; Iqbal, H. F.; Holland, E.; Bourland, J. D.; Anthony, J. E.; Jurchescu, O. D. Organic Field-Effect Transistors as Flexible, Tissue-Equivalent Radiation Dosimeters in Medical Applications. *Adv. Sci.* 2020, *7* (18), 2001522.

(140) Lai, S.; Cosseddu, P.; Basiricò, L.; Ciavatti, A.; Fraboni, B.; Bonfiglio, A. A Highly Sensitive, Direct X-Ray Detector Based on a Low-Voltage Organic Field-Effect Transistor. *Adv. Electron. Mater.* 2017, *3* (8), 1600409.

(141) Kaltenbrunner, M.; Sekitani, T.; Reeder, J.; Yokota, T.; Kuribara, K.; Tokuhara, T.; Drack, M.; Schwödiauer, R.; Graz, I.; Bauer-Gogonea, S.; Bauer, S.; Someya, T. An Ultra-Lightweight Design for Imperceptible Plastic Electronics. *Nature* 2013, *499* (7459), 458–463.

(142) Lee, H.; Chang, S.; Yoon, E. A Flexible Polymer Tactile Sensor : Fabrication and Modular Expandability for Large Area Deployment. *J. Microelectromechanical Syst.* 2006, *15* (6), 1681–1686.

(143) Mannsfeld, S. C. B.; Tee, B. C. K.; Stoltenberg, R. M.; Chen, C. V. H. H.; Barman, S.; Muir, B. V. O.; Sokolov, A. N.; Reese, C.; Bao, Z. Highly Sensitive Flexible Pressure Sensors with Microstructured Rubber Dielectric Layers. *Nat. Mater.* 2010, *9* (10), 859–864.

(144) Han, S.; Zhuang, X.; Shi, W.; Yang, X.; Li, L.; Yu, J. Poly(3-Hexylthiophene)/Polystyrene (P3HT/PS) Blends Based Organic Field-Effect Transistor Ammonia Gas Sensor. *Sensors Actuators, B Chem.* 2016, *225*, 10–15.

(145) Wang, Z.; Huang, L.; Zhu, X.; Zhou, X.; Chi, L. An Ultrasensitive Organic Semiconductor NO2 Sensor Based on Crystalline TIPS-Pentacene Films. *Adv. Mater.* 2017, *29* (38), 1703192.

(146) Zhu, Y.; Xie, Q.; Sun, Y.; Wang, L.; Sun, Q.; Wang, L. High-Performance NO2 Sensors Based on Ultrathin Heterogeneous Interface Layers. *Adv. Mater. Interfaces* 2020, *7* (2), 1901579.

(147) Kergoat, L.; Herlogsson, L.; Braga, D.; Piro, B.; Pham, M. C.; Crispin, X.; Berggren, M.; Horowitz, G. A Water-Gate Organic Field-Effect Transistor. *Adv. Mater.* 2010, *22* (23), 2565–2569.

(148) Ricci, S.; Casalini, S.; Parkula, V.; Selvaraj, M.; Saygin, G. D.; Greco, P.; Biscarini, F.; Mas-Torrent, M. Label-Free Immunodetection of α-Synuclein by Using a Microfluidics Coplanar Electrolyte-Gated Organic Field-Effect Transistor. *Biosens. Bioelectron.* 2020, *167*, 112433.

(149) Herlogsson, L.; Crispin, X.; Robinson, N. D.; Sandberg, M.; Hagel, O. J.; Gustafsson, G.; Berggren, M. Low-Voltage Polymer Field-Effect Transistors Gated via a Proton Conductor. *Adv. Mater.* 2007, *19* (1), 97–101.

(150) Magliulo, M.; Mallardi, A.; Mulla, M. Y.; Cotrone, S.; Pistillo, B. R.; Favia, P.; Vikholm-Lundin, I.; Palazzo, G.; Torsi, L. Electrolyte-Gated Organic Field-Effect Transistor Sensors Based on Supported Biotinylated Phospholipid Bilayer. *Adv. Mater.* 2013, *25* (14), 2090–2094.

(151) Casalini, S.; Dumitru, A. C.; Leonardi, F.; Bortolotti, C. A.; Herruzo, E. T.; Campana, A.; Oliveira, R. F. De; Cramer, T.; Garcia, R.; Biscarini, F. Multiscale Sensing of Antibody À Antigen Interactions by Organic Transistors and Single-Molecule Force

Spectroscopy. *ACS Nano* 2015, *9* (5), 5051–5062.

(152) Mulla, M. Y.; Tuccori, E.; Magliulo, M.; Lattanzi, G.; Palazzo, G.; Persaud, K.; Torsi, L. Capacitance-Modulated Transistor Detects Odorant Binding Protein Chiral Interactions. *Nat. Commun.* 2015, *6*, 6010.

(153) Mulla, M. Y.; Seshadri, P.; Torsi, L.; Manoli, K.; Mallardi, A.; Ditaranto, N.; Santacroce, M. V.; Di Franco, C.; Scamarcio, G.; Magliulo, M. UV Crosslinked Poly(Acrylic Acid): A Simple Method to Bio-Functionalize Electrolyte-Gated OFET Biosensors. *J. Mater. Chem. B* 2015, *3* (25), 5049–5057.

(154) Pfattner, R.; Foudeh, A. M.; Chen, S.; Niu, W.; Matthews, J. R.; He, M.; Bao, Z. Dual-Gate Organic Field-Effect Transistor for PH Sensors with Tunable Sensitivity. *Adv. Electron. Mater.* 2019, *5* (1), 1800381.

(155) Magliulo, M.; De Tullio, D.; Vikholm-Lundin, I.; Albers, W. M.; Munter, T.; Manoli, K.; Palazzo, G.; Torsi, L. Label-Free C-Reactive Protein Electronic Detection with an Electrolyte-Gated Organic Field-Effect Transistor-Based Immunosensor. *Anal. Bioanal. Chem.* 2016, *408* (15), 3943–3952.

(156) Macchia, E.; Manoli, K.; Holzer, B.; Di Franco, C.; Ghittorelli, M.; Torricelli, F.; Alberga, D.; Mangiatordi, G. F.; Palazzo, G.; Scamarcio, G.; Torsi, L. Single-Molecule Detection with a Millimetre-Sized Transistor. *Nat. Commun.* 2018, *9* (1), 3223.

(157) Casalini, S.; Leonardi, F.; Cramer, T.; Biscarini, F. Organic Field-Effect Transistor for Label-Free Dopamine Sensing. *Org. Electron.* 2013, *14* (1), 156–163.

(158) Nguyen, T. T. K.; Tran, H. V.; Vu, T. T.; Reisberg, S.; Noël, V.; Mattana, G.; Pham, M. C.; Piro, B. Peptide-Modified Electrolyte-Gated Organic Field Effect Transistor. Application to Cu 2+ Detection. *Biosens. Bioelectron.* 2019, *127*, 118–125.

CHAPTER II

THIN FILM OPTIMIZATION FOR ACHIEVING HIGH OFET PERFORMANCE

This chapter is composed of 7 scientific articles related to the study of the morphology and crystal structure of organic semiconductor (OSC) thin films and their electrical characteristics when implemented in organic field-effect transistors (OFETs).

Article 1: Role of polymorphism and thin-film morphology in organic semiconductors processed by solution shearing.

Article 2: Control of polymorphism and morphology in solution sheared organic field-effect transistors.

Article 3: Impact of the ink formulation and coating speed on the polymorphism and morphology of a solution-sheared thin film of a blended organic semiconductor.

Article 4: Mobility anisotropy in the herringbone structure of asymmetric Ph-BTBT-10 in solution sheared thin film transistors.

Article 5: Molecular disorder in crystalline thin films of an asymmetric BTBT derivative.

Article 6: Low activation energy field-effect transistors fabricated by bar-assisted meniscus shearing.

Article 7: Organic field-effect transistors based on ternary blends including a fluorinated polymer for achieving enhanced device stability.

2.1. Influence of polymorphism and morphology in films based on blends of small molecule semiconductors and insulating polymers on device performance

***Article 1**: Role of polymorphism and thin-film morphology in organic semiconductors processed by solution shearing*.

The thin film morphology and polymorphism have a profound impact on their resultant optoelectronic properties.[1–7] As previously mentioned in the introduction, the charge carrier mobility in organic field-effect transistors (OFETs) is highly dependent on the molecular packing and direction along the crystal structure.[8–11] The control of polymorphism, especially in thin films, is challenging but crucial to achieve reproducible devices. Metastable or surface confined polymorphs have been reported in organic semiconductor (OSC) thin films (10 to 50 nm thick) deposited by chemical vapour deposition or solution-based techniques.[12–15] The identification and characterization of such polymorphs is complex, although their impact on the device performance can be very significant. A slight change in the π-orbital overlap between the OSC molecules can lead to a large difference in the charge carrier mobility.[12]

Additionally, considering the thin films morphology, the crystal size and orientation, and the subsequent density of grain boundaries, are parameters that affect the electrical properties of the thin films.[16–18] These features can be tuned with the deposition parameters (shearing speed and temperature) and the solution formulation employed (concentration, solvent, binder polymers, doping, etc.).[18–22]

In this Review paper (***Article 1***), we describe the importance of controlling morphology and polymorphism in small molecule organic semiconductor thin films deposited by solution shearing techniques. In particular, we focus on how the different deposition parameters and formulation of the OSC inks are impacting the thin film characteristics and, in turn, the OFET electrical performance. Additionally, an exhaustive description of a variety of techniques commonly employed for the structural characterization of OSC thin films (X-ray, microscopy, IR/Raman spectroscopies, etc.) is carried out, highlighting the *in situ* characterization tools that can provide essential insights into the crystallization mechanisms.

The main objective of this part of the Thesis is to fabricate optimised OFETs based on thin films of blends of three different OSCs (i.e., DB-TTF, TIPS-pentacene and Ph-BTBT-C_{10}) with insulating polymers deposited by BAMS. The thin films are prepared using different formulations and deposition conditions and their crystal structure and morphology are investigated and correlated with the device performance (Scheme 2.1).

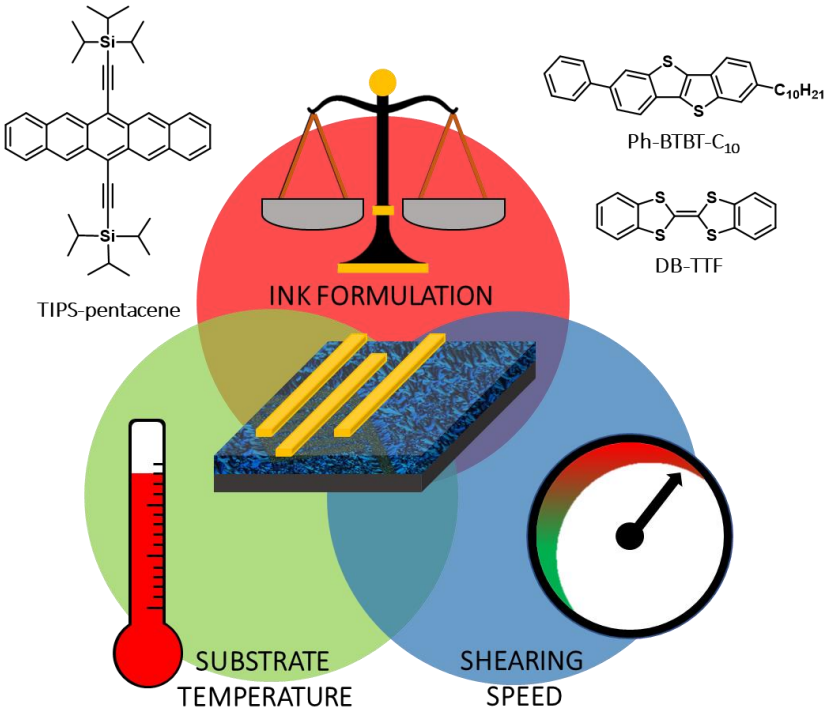

Scheme 2.1. The ink formulation and the solution shearing deposition parameters are key tools to control the OSC thin film structure and morphology and to optimise the OFET performance.

2.2. Organic field-effect transistors based on dibenzotetrathiafulvalene thin films prepared by solution shearing technique

Article 2: Control of polymorphism and morphology in solution sheared organic field-effect transistors.

Article 3: Impact of the ink formulation and coating speed on the polymorphism and morphology of a solution-sheared thin film of a blended organic semiconductor.

In these papers we deeply investigated the influence of the deposition parameters and formulation in the crystal structure and morphology of thin films of dibenzotetrathiafulvalene (DB-TTF) blended with polystyrene (PS), and their impact on the OFET properties. It is known that DB-TTF presents at least four polymorphic forms at ambient conditions, namely the α, β, γ and δ polymorphs.[23,24] By drop casting, crystals of the monoclinic thermodynamically more stable α form are formed (**Figure 2.1a**).[25] On the other hand, the γ phase is obtained in solution processed or evaporated thin films (**Figure**

2.1b),[26–28] being a kinetic polymorph induced on surfaces. The γ crystallises following a herringbone structure, while α-phase displays a parallel stacked structure.

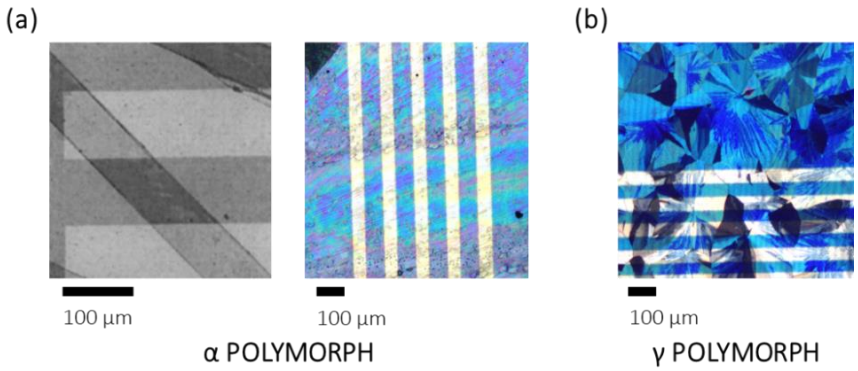

Figure 2.1. Polarized optical microscope images for bottom contact OFET devices based on DB-TTF (a) single crystal and thin films of α polymorph and (b) thin film of γ polymorph. Extracted from ref. 25.

The effect of the substrate temperature was investigated in films coated at 10 mm·s^{-1} and at temperature ranging from 25 to 120 ºC employing an ink composed of DB-TTF:PS in a ratio 1:2 and using a PS of 3000 g·mol^{-1}. We found that the substrate temperature affected the evaporation of the solvent. Below 100 ºC, the solvent evaporation was slow leading to the formation of mixtures of the thermodynamic and kinetic polymorphs. On the other hand, at higher temperature, the evaporation of the solvent was faster and only the kinetic phase was found. Additionally, the deposition at 120ºC caused the boiling of the solvent, which produced defects on the thin films. Accordingly, in terms of electrical performance, the devices prepared in the temperature range from 90 to 110 ºC gave the highest mobility (> 0.1 cm^2·V^{-1}·s^{-1}). The best electrical performance was found in devices prepared at 105 ºC, which resulted in highly homogenous and crystalline films composed of only the γ phase.

The shearing speed was the parameter which had the greatest impact on the film polymorphism. At low shearing speed (1 mm·s^{-1}), the films showed ribbon-shaped crystals that corresponded to the α DB-TTF phase. In fact, this was the first time that this phase was obtained as thin film (Figure 2.1). On the other hand, plate-like crystalline domains were observed at middle and high speed (from 2 to 100 mm·s^{-1}), corresponding to the pure γ phase. In fact, three different deposition regimes depending on the shearing speed were distinguished. In the region from 1 to 5 mm·s^{-1}, the thickness decreased when increasing the shearing speed, while in the range 20 to 100 mm·s^{-1}, the opposite behaviour was encountered. Both regimes are associated to the evaporation and Landau regime, respectively.[29–31] In addition, an intermediate regime was observed at intermediate speeds (from 5 to 20 mm·s^{-1}) that gave the thinnest films without dependency on the coating speed. In this intermediate regime, an equilibrium between the evaporation and viscous

force was taking place,[31] which produced the smoothest films with large crystal domains and a low density of grain boundaries. The devices deposited in this intermediate regime exhibited the highest mobility of 0.25 $cm^2 \cdot V^{-1} \cdot s^{-1}$ and a threshold voltage close to 0 V. In contrast, the devices deposited in both the evaporation and Landau regimes displayed mobility values five times lower. The device mobility of the thin films based on the α polymorph obtained at 1 $mm \cdot s^{-1}$ was 0.05 $cm^2 \cdot V^{-1} \cdot s^{-1}$, lower than the γ polymorph.

Furthermore, the effect of the formulation was also explored. Films with different PS ratio and different PS molecular weight were prepared at 105 ºC and at a coating speed of 1, 10 and 100 $mm \cdot s^{-1}$. The formulation directly impacted the solution viscosity affecting the growth of the OSC crystals and the thin film morphology. It was found that the films with more than 50 % wt. of DB-TTF consisted in oriented crystals belonging to a mixture of the α and γ forms. In terms of electrical performance, the OFETs exhibited a high degree of doping (with high threshold voltage and high off current) and low mobilities (< 0.05 $cm^2 \cdot V^{-1} \cdot s^{-1}$). On the contrary, the films with 50 % wt. or less of DB-TTF were more homogeneous with crystals that corresponded to the γ polymorph when deposited above 1 $mm \cdot s^{-1}$. As previously mentioned, at 1 $mm \cdot s^{-1}$ the α polymorph was obtained solely, but only for specific DB-TTF:PS ratios and PS molecular weights.

Importantly to note is the fact that depending on the conditions of preparation, the γ polymorph provided films with different morphology, namely striped, plate-like and spherulitic crystalline domains. The striped morphologies displayed a high degree of electrical anisotropy, while the films based on plate-like and spherulitic crystals were completely isotropic. The best electrical performance was found for films with a plate-like crystal morphology, which exhibited mobilities higher than 0.1 $cm^2 \cdot V^{-1} \cdot s^{-1}$ and threshold voltage close to 0 V.

Finally, to visualise this high complex scenario, a phase diagram for DB-TTF thin films was elaborated. This work unambiguously elucidated the importance of controlling polymorphism and thin film morphology to fabricate devices with an enhanced OFET performance and high device-to-device reproducibility.

2.3. Organic field-effect transistors based on 7-phenyl[1]benzothieno[3,2-b][1]benzothiophene thin films

Article 4: Mobility anisotropy in the herringbone structure of asymmetric Ph-BTBT-10 in solution sheared thin film transistors.

Article 5: Molecular disorder in crystalline thin films of an asymmetric BTBT derivative.

The OSC 7-phenyl[1]benzothieno[3,2-b][1]benzothiophene (Ph-BTBT-C_{10}) is a soluble asymmetric molecule with high potential for OFET applications.[32–34] The crystal structure of Ph-BTBT-C_{10} is characterized by a strong and sharp segregation into π-conjugated and alkyl layers, which alternate along the *c* axis. Previously, it was reported that spin coated films of Ph-BTBT-C_{10} crystallise forming a herringbone structure in a monolayer (head-to-tail) structure (**Figure 2.2**). However, such Ph-BTBT-C_{10} films show a phase transition from the monolayer to a bilayer crystal structure (head-to-head) after annealing at 120ºC, which leads to a dramatic enhancement of the OFET mobility from 0.8 $cm^2 \cdot V^{-1} \cdot s^{-1}$ to 13.9 $cm^2 \cdot V^{-1} \cdot s^{-1}$.[32,35]

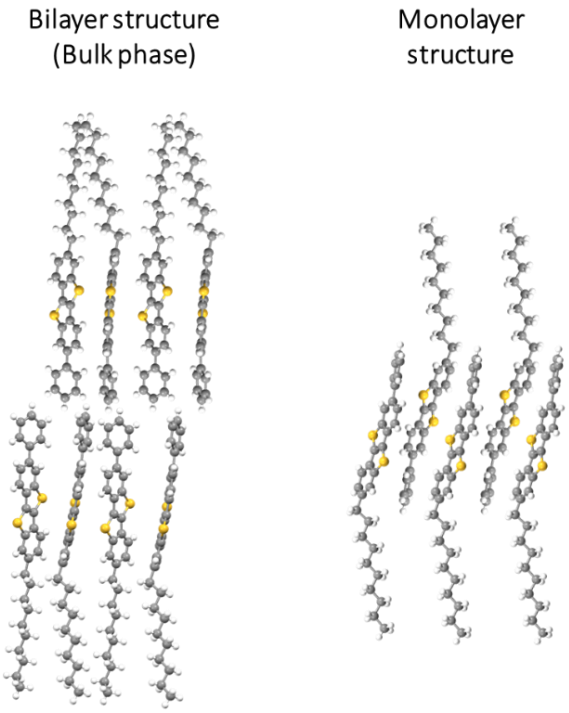

Figure 2.2. Schematic illustration of the bilayer and monolayer structures of Ph-BTBT-C_{10}.

Our work consisted in the fabrication of bottom-gate bottom-contact OFETs devices based on thin films of Ph-BTBT-C_{10} and Ph-BTBT-C_{10}:PS deposited by BAMS. The goal was to fabricate high performance OFET devices employing a high-throughput technique avoiding the thermal annealing step and gain insights into the crystal order in the thin film.

We investigated the thin film anisotropy in films deposited at 1 and 10 $mm \cdot s^{-1}$. The films based on Ph-BTBT-C_{10} and Ph-BTBT-C_{10}:PS deposited at 1 $mm \cdot s^{-1}$ exhibited long crystals along the shearing direction. In contrast, the films based on Ph-BTBT-C_{10} and Ph-BTBT-C_{10}:PS deposited at 10 $mm \cdot s^{-1}$ showed smaller crystal domains with plate-like morphology without a strong preferential orientation. In both cases, the films showed step edges with heights of 2.6 and 5.2 nm, which corresponded to monolayer and bilayer structures, respectively.

Additionally, XRD measurements were carried out to investigate the crystal structure and orientation in the Ph-BTBT-C_{10} films. The XRD measurements showed that the films deposited at low speed were oriented along the *(010)* direction. Remarkably, all the films belonged to the bilayer structure, so the bulk structure was obtained without performing the annealing process (Figure 2.2). However, the XRD data revealed that the peak width of the specular diffractions showed an unusual different peak- broadening behaviour for the odd-numbered and even-numbered 00L peaks. This experimental evidence was explained by the presence of certain disorder within the crystal bilayer structure caused by the asymmetry of the molecule. The known head-to-head stacking within the crystalline phase was disturbed by the statistic integration of reversed (or flipped) molecules. Such molecular disorder breaks the crystallographic long-range order, which can negatively impact the device mobility.

The Ph-BTBT-C_{10} and Ph-BTBT-C_{10}:PS films deposited at 1 $mm \cdot s^{-1}$ exhibited p-type behaviour with mobility values of 0.48 and 0.43 $cm^2 \cdot V^{-1} \cdot s^{-1}$ along the coating direction respectively. However, in the parallel direction the mobilities measured were 3 times lower. On the contrary, the OFET devices deposited at 10 $mm \cdot s^{-1}$ did not exhibit a significant anisotropy and mobility values of 1.3 $cm^2 \cdot V^{-1} \cdot s^{-1}$ and 0.16 $cm^2 \cdot V^{-1} \cdot s^{-1}$ were found for the for Ph-BTBT-C_{10}:PS and Ph-BTBT-C_{10} films, respectively. This result proves again that the use PS improves the device electrical properties. Future work will be devoted to improving the thin films crystallinity order modifying the coating conditions in order to improve the device mobility.

2.4. Thin films of 6,13-Bis(triisopropylsilylethynyl)pentacene blends prepared by solution shearing technique

Article 6: Low activation energy field-effect transistors fabricated by bar-assisted meniscus shearing.

Article 7: Organic field-effect transistors based on ternary blends including a fluorinated polymer for achieving enhanced device stability.

6,13-Bis(triisopropylsilylethynyl)pentacene (TIPS-pentacene) is an organic semiconductor that shows good solubility and high p-type mobility.[8,36–40] TIPS-pentacene crystallises in a brickwork packing motif with a preferential 1D charge carrier transport, which causes that thin films of this material can be highly sensible to the presence of defects or misaligned crystals.[20,36,39,41–44]

Previously, it was shown that OFETs based on thin films of TIPS-pentacene:PS blends deposited by BAMS exhibited mobilities in the range from 0.4 to 0.9 $cm^2 \cdot V^{-1} \cdot s^{-1}$ and threshold voltage close to 0 V, while the pristine TIPS-pentacene films exhibited mobilities of 0.04 $cm^2\ V^{-1}\ s^{-1}$ and threshold voltage +10 V.[20] Thus, also in this case, the devices with PS showed a marked improvement over devices based on only the OSC. However, the main limitation of these devices for the practical implementation is their limited stability over time and under continuous operation. In this part of the thesis, we deeply investigated the impact of the binder polymers in the electrical performance and stability of polycrystalline thin films based on TIPS-pentacene deposited by BAMS.

The prepared devices based on TIPS-pentacene:PS (4:1) blends exhibited mobilities of 0.4 $cm^2 \cdot V^{-1} \cdot s^{-1}$ in the OFETs with short channel lengths (i.e., 50 μm) and 0.9 $cm^2 \cdot V^{-1} \cdot s^{-1}$ in the OFETs with long channel length (i.e., 200 μm). Such clear mobility dependence with the channel length is an unquestionable sign of contact resistance problems. To extract the contact resistance, the transfer-length method (TLM) was employed, which provided an estimated contact resistance of 85±6 kΩ·cm. Taking into account this contact resistance, a corrected mobility of 1.2 $cm^2 \cdot V^{-1} \cdot s^{-1}$ was estimated, which was independent of the length of the channel.

Next step to evaluate the mobility of the TIPS-pentacene blends was to estimate the effect of the binder polymer (i.e., polystyrene) on the device capacitance since it is known that a vertical stratification of the OSC and PS occurs on the surface (**Figure 2.3**).[41,45–49] Considering this, PS acts as an additional dielectric layer on top of the SiO_2. It was found that PS produces a reduction of the global capacitance from 17.24 to 14.09 $nF \cdot cm^{-2}$, meaning that the real mobility value was 1.4 $cm^2 \cdot V^{-1} \cdot s^{-1}$. Additionally, the activation energy of the TIPS-pentacene blended films was extracted performing temperature dependence measurements. It was found that the films revealed a thermally activated charge transport and showed the lowest activation energy (15 meV) reported for thin films of this material.

Long term environmental stability of OFETs due to the high susceptibility of OSCs to interact with water and oxygen molecules is one of the main bottlenecks hindering their practical implementation. To circumvent this problem, here, we developed a new approach based on employing blends composed of TIPS-pentacene with mixtures of PS and poly(pentafluorostyrene) (PFS) as binder polymers. PFS is a highly hydrophobic polymer which can confer more environmental stability to the device. However, the main disadvantages of the fluorinated polystyrene is its low solubility in common organic solvents.

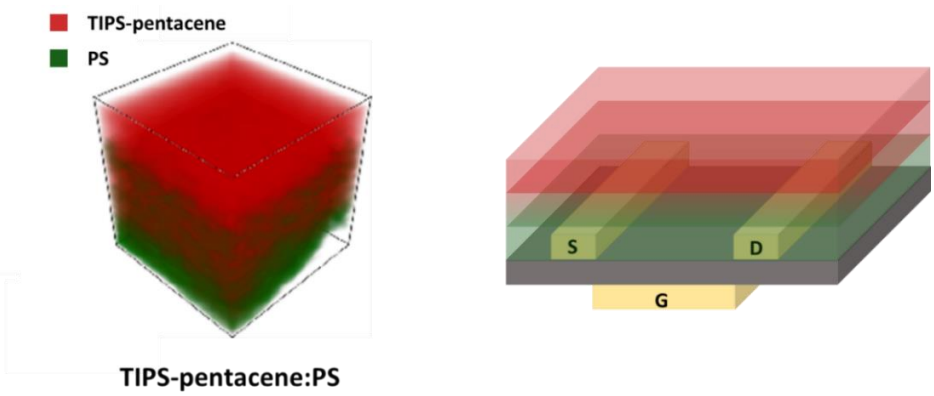

Figure 2.3 Left. PS and TIPS-pentacene distribution in TIPS-pentacene:PS (4:1) films extracted from Time-of-Flight Secondary Ion Mass Spectrometry (ToF-SIMS) measurements. 3D rendering TIPS-pentacene (red) and PS (green) secondary ions signals. **Right.** Scheme of the stratification of PS and TIPS-pentacene on the device configuration.

The inks based on TIPS-pentacene blended with PFS and PS provided crystalline films with good coverage. The addition of PFS did not affect critically the morphology of the crystals, but caused a reduction of the crystal size. By AFM measurements, a horizontal phase separation was observed when the percentage of PFS was high and small nanoagglomerates were observed due to the low miscibility of the two binding polymers.

The OFETs based on TIPS-pentacene:PS:PFS exhibited a good electrical performance. However, the presence of PFS affected negatively the charge carrier mobility and threshold voltage. The threshold voltage shifted to positive voltage values, which was attributed to a certain chemical doping produced by the high electron affinity of PFS. In addition, the mobility drop was attributed to a reduction of the crystal domains as observed by optical microscopy. Despite this negative impact on these electrical parameters, PFS promoted a significant increase in the stability of the OFET devices. The half-life time of the OFETs devices based on the ternary blends was 5 times higher than that of the OFETs based on TIPS-pentacene:PS blends. Additionally, PFS improved the bias stability of the devices. By balancing the PS:PFS ratio, it was found that films containing only 20 % of PFS led to devices with and enhanced shelf and bias stress stability without critically affecting the charge transport.

Hence, here we demonstrated that the addition of a certain percentage of a fluorinated polymer in the blend was an excellent strategy to improve devices stability, which is crucial for their practical implementation.

2.5. SUMMARY

In summary, thin-films based on blends of DB-TTF, Ph-BTBT-C10 and TIPS-pentacene with insulating polymers have been successfully deposited by a solution shearing technique (i.e., BAMS). The effect of the temperature, shearing speed, shearing direction, molecular weight of the insulator polymer, OSC:PS ratio and chemical characteristics of the insulator polymer on the morphology, polymorphism, and electrical performance of the organic semiconductor was in depth investigated.

The films deposited at evaporation conditions (low speed) displayed aligned films with high anisotropic charge transport properties, while at high speed, the films exhibited an isotropic charge transport. In general, BAMS leads to kinetic polymorphs, although at low speed it is also possible to form thermodynamic forms.

It was also found that the use of blends of OSCs and PS is a very promising strategy to improve the device performance. This methodology results in more homogenous and crystalline films with an enhanced electrical performance. The latter is also thanks to the passivation of the dielectric with PS, which reduces the interfacial charge traps. Furthermore, it was also found that adding a proportion of fluorinated PS as binder polymer provided devices that exhibited a higher bias stress and shelf-stability. This was ascribed to the hydrophobic character of the fluorinated PS that hampers the water penetration into the OSC.

2.6. REFERENCES

(1) Chung, H.; Diao, Y. Polymorphism as an Emerging Design Strategy for High Performance Organic Electronics. *J. Mater. Chem. C* 2016, *4* (18), 3915–3933.

(2) Lu, J.; Rohani, S. Polymorphism and Crystallization of Active Pharmaceutical Ingredients (APIs). *Curr. Med. Chem.* 2009, *16* (7), 884–905.

(3) Li, M.; Balawi, A. H.; Leenaers, P. J.; Ning, L.; Heintges, G. H. L.; Marszalek, T.; Pisula, W.; Wienk, M. M.; Meskers, S. C. J.; Yi, Y.; Laquai, F.; Janssen, R. A. J. Impact of Polymorphism on the Optoelectronic Properties of a Low-Bandgap Semiconducting Polymer. *Nat. Commun.* 2019, *10*, 2867.

(4) Jurchescu, O. D.; Mourey, D. A.; Subramanian, S.; Parkin, S. R.; Vogel, B. M.; Anthony, J. E.; Jackson, T. N.; Gundlach, D. J. Effects of Polymorphism on Charge Transport in Organic Semiconductors. *Phys. Rev. B* 2009, *80* (8), 085201.

(5) Diao, Y.; Shaw, L.; Bao, Z.; Mannsfeld, S. C. B. Morphology Control Strategies for Solution-Processed Organic Semiconductor Thin Films. *Energy Environ. Sci.* 2014, *7* (7), 2145–2159.

(6) Steyrleuthner, R.; Schubert, M.; Howard, I.; Klaumünzer, B.; Schilling, K.; Chen, Z.; Saalfrank, P.; Laquai, F.; Facchetti, A.; Neher, D. Aggregation in a High-Mobility n-Type Low-Bandgap Copolymer with Implications on Semicrystalline Morphology. *J. Am. Chem. Soc.* 2012, *134* (44), 18303–18317.

(7) He, Z.; Bi, S.; Asare-Yeboah, K.; Zhang, Z. Phase Segregation Effect on TIPS Pentacene Crystallization and Morphology for Organic Thin Film Transistors. *J. Mater. Sci. Mater. Electron.* 2020, *31* (6), 4503–4510.

(8) Giri, G.; Verploegen, E.; Mannsfeld, S. C. B.; Atahan-Evrenk, S.; Kim, D. H.; Lee, S. Y.; Becerril, H. A.; Aspuru-Guzik, A.; Toney, M. F.; Bao, Z. Tuning Charge Transport in Solution-Sheared Organic Semiconductors Using Lattice Strain. *Nature* 2011, *480* (7378), 504–508.

(9) Molina-Lopez, F.; Yan, H.; Gu, X.; Kim, Y.; Toney, M. F.; Bao, Z. Electric Field Tuning Molecular Packing and Electrical Properties of Solution-Shearing Coated Organic Semiconducting Thin Films. *Adv. Funct. Mater.* 2017, *27* (8), 1605503.

(10) Wang, X.; Garcia, T.; Monaco, S.; Schatschneider, B.; Marom, N. Effect of Crystal Packing on the Excitonic Properties of Rubrene Polymorphs. *CrystEngComm* 2016, *18* (38), 7353–7362.

(11) Chang, J.; Chi, C.; Zhang, J.; Wu, J. Controlled Growth of Large-Area High-Performance Small-Molecule Organic Single-Crystalline Transistors by Slot-Die Coating Using a Mixed Solvent System. *Adv. Mater.* 2013, *25* (44), 6442–6447.

(12) Diao, Y.; Lenn, K. M.; Lee, W. Y.; Blood-Forsythe, M. A.; Xu, J.; Mao, Y.; Kim, Y.; Reinspach, J. A.; Park, S.; Aspuru-Guzik, A.; Xue, G.; Clancy, P.; Bao, Z.; Mannsfeld, S. C. B. Understanding Polymorphism in Organic Semiconductor Thin Films through Nanoconfinement. *J. Am. Chem. Soc.* 2014, *136* (49), 17046–17057.

(13) Patel, B. B.; Diao, Y. Multiscale Assembly of Solution-Processed Organic Electronics: The Critical Roles of Confinement, Fluid Flow, and Interfaces. *Nanotechnology* 2018, *29* (4), 044004.

(14) Salzillo, T.; Campos, A.; Babuji, A.; Santiago, R.; Bromley, S. T.; Ocal, C.; Barrena, E.; Jouclas, R.; Ruzie, C.; Schweicher, G.; Geerts, Y. H.; Mas-Torrent, M. Enhancing Long-Term Device Stability Using Thin Film Blends of Small Molecule Semiconductors and Insulating Polymers to Trap Surface-Induced Polymorphs. *Adv. Funct. Mater.* 2020, *30* (52), 2006115.

(15) Kim, M. W.; Kwon, S.; Kim, J.; Lee, C.; Park, I.; Shim, J. H.; Jeong, I. S.; Jo, Y. R.; Park, B.; Lee, J. H.; Lee, K.; Kim, B. J. Reversible Polymorphic Transition and Hysteresis-Driven Phase Selectivity in Single-Crystalline C8-BTBT Rods. *Small* 2020, *16* (3), 1906109.

(16) Vladimirov, I.; Kühn, M.; Geßner, T.; May, F.; Weitz, R. T. Energy Barriers at Grain Boundaries Dominate Charge Carrier Transport in an Electron-Conductive Organic Semiconductor. *Sci. Rep.* 2018, *8* (1), 14868.

(17) Headrick, R. L.; Wo, S.; Sansoz, F.; Anthony, J. E. Anisotropic Mobility in Large Grain Size Solution Processed Organic Semiconductor Thin Films. *Appl. Phys. Lett.* 2008, *92* (6), 063302.

(18) Weitz, R. T.; Amsharov, K.; Zschieschang, U.; Burghard, M.; Jansen, M.; Kelsch, M.; Rhamati, B.; Van Aken, P. A.; Kern, K.; Klauk, H. The Importance of Grain Boundaries for the Time-Dependent Mobility Degradation in Organic Thin-Film Transistors. *Chem. Mater.* 2009, *21* (20), 4949–4954.

(19) Lai, S.; Temiño, I.; Cramer, T.; del Pozo, F. G.; Fraboni, B.; Cosseddu, P.; Bonfiglio, A.; Mas-Torrent, M. Morphology Influence on the Mechanical Stress Response in Bendable Organic Field-Effect Transistors with Solution-Processed Semiconductors. *Adv. Electron. Mater.* 2017, *4* (10), 1700271.

(20) Temiño, I.; Basiricò, L.; Fratelli, I.; Tamayo, A.; Ciavatti, A.; Mas-Torrent, M.; Fraboni, B. Morphology and Mobility as Tools to Control and Unprecedentedly Enhance X-Ray Sensitivity in Organic Thin-Films. *Nat. Commun.* 2020, *11* (1), 2136.

(21) Chang, M.; Lim, G. T.; Park, B.; Reichmanis, E. Control of Molecular Ordering, Alignment, and Charge Transport in Solution-Processed Conjugated Polymer Thin Films. *Polymers (Basel).* 2017, *9* (6), 212.

(22) Rubinger, C. P. L.; Haneef, H. F.; Hewitt, C.; Carroll, D.; Anthony, J. E.; Jurchescu, O. D. Influence of Solvent Additives on the Morphology and Electrical Properties of DiF-TES ADT Organic Field-Effect Transistors. *Org. Electron.* 2019, *68*, 205–211.

(23) Brillante, A.; Bilotti, I.; Della Valle, R. G.; Venuti, E.; Milita, S.; Dionigi, C.; Borgatti, F.; Lazar, A. N.; Biscarini, F.; Mas-Torrent, M.; Oxtoby, N. S.; Crivillers, N.; Veciana, J.; Rovira, C.; Leufgen, M.; Schmidt, G.; Molenkamp, L. W. The Four Polymorphic Modifications of the Semiconductor Dibenzo-Tetrathiafulvalene. *CrystEngComm* 2008, *10* (12), 1899–1909.

(24) Brillante, A.; Bilotti, I.; Della Valle, R. G.; Venuti, E.; Girlando, A. Probing Polymorphs of Organic Semiconductors by Lattice Phonon Raman Microscopy. *CrystEngComm* 2008, *10* (8), 937–946.

(25) Mas-Torrent, M.; Hadley, P.; Bromley, S. T.; Crivillers, N.; Veciana, J.; Rovira, C. Single-Crystal Organic Field-Effect Transistors Based on Dibenzo-Tetrathiafulvalene. *Appl. Phys. Lett.* 2005, *86* (1), 012110.

(26) del Pozo, F. G.; Fabiano, S.; Pfattner, R.; Georgakopoulos, S.; Galindo, S.; Liu, X.; Braun, S.; Fahlman, M.; Veciana, J.; Rovira, C.; Crispin, X.; Berggren, M.; Mas-Torrent, M. Single Crystal-like Performance in Solution-Coated Thin-Film Organic Field-Effect Transistors. *Adv. Funct. Mater.* 2016, *26* (14), 2379–2386.

(27) Galindo, S.; Tamayo, A.; Leonardi, F.; Mas-Torrent, M. Control of Polymorphism and Morphology in Solution Sheared Organic Field-Effect Transistors. *Adv. Funct. Mater.* 2017, *27* (25), 1700526.

(28) Tamayo, A.; Riera-Galindo, S.; Jones, A. O. F.; Resel, R.; Mas-Torrent, M. Impact of the Ink Formulation and Coating Speed on the Polymorphism and Morphology of a Solution-Sheared Thin Film of a Blended Organic Semiconductor. *Adv. Mater. Interfaces* 2019, *6* (22), 1900950.

(29) Le Berre, M.; Chen, Y.; Baigl, D. From Convective Assembly to Landau - Levich Deposition of Multilayered Phospholipid Films of Controlled Thickness. *Langmuir* 2009, *25* (5), 2554–2557.

(30) Faustini, M.; Louis, B.; Albouy, P. A.; Kuemmel, M.; Grosso, D. Preparation of Sol-Gel Films by Dip-Coating in Extreme Conditions. *J. Phys. Chem. C* 2010, *114* (17), 7637–7645.

(31) Grosso, D. How to Exploit the Full Potential of the Dip-Coating Process to Better Control Film Formation. *J. Mater. Chem.* 2011, *21* (43), 17033–17038.

(32) Iino, H.; Usui, T.; Hanna, J. I. Liquid Crystals for Organic Thin-Film Transistors. *Nat. Commun.* 2015, *6*, 6828.

(33) Wu, H.; Iino, H.; Hanna, J. I. Scalable Ultrahigh-Speed Fabrication of Uniform Polycrystalline Thin Films for Organic Transistors. *ACS Appl. Mater. Interfaces* 2020, *12* (26), 29497–29504.

(34) Cho, J. M.; Mori, T. Low-Temperature Band Transport and Impact of Contact Resistance in Organic Field-Effect Transistors Based on Single-Crystal Films of Ph-BTBT-C10. *Phys. Rev. Appl.* 2016, *5* (6), 064017.

(35) Iino, H.; Hanna, J. I. Liquid Crystalline Organic Semiconductors for Organic Transistor Applications. *Polym. J.* 2017, *49* (1), 23–30.

(36) Temiño, I.; Del Pozo, F. G.; Ajayakumar, M. R.; Galindo, S.; Puigdollers, J.; Mas-Torrent, M. A Rapid, Low-Cost, and Scalable Technique for Printing State-of-the-Art Organic Field-Effect Transistors. *Adv. Mater. Technol.* 2016, *1* (5), 1600090.

(37) Giri, G.; Li, R.; Smilgies, D.-M.; Li, E. Q.; Diao, Y.; Lenn, K. M.; Chiu, M.; Lin, D. W.; Allen, R.; Reinspach, J.; Mannsfeld, S. C. B.; Thoroddsen, S. T.; Clancy, P.; Bao, Z.; Amassian, A. One-Dimensional Self-Confinement Promotes Polymorph Selection in Large-Area Organic Semiconductor Thin Films. *Nat. Commun.* 2014, *5*, 3573.

(38) Teixeira da Rocha, C.; Haase, K.; Zheng, Y.; Löffler, M.; Hambsch, M.; Mannsfeld, S. C. B. Solution Coating of Small Molecule/Polymer Blends Enabling Ultralow Voltage and High-Mobility Organic Transistors. *Adv. Electron. Mater.* 2018, *4* (8), 1800141.

(39) Giri, G.; Park, S.; Vosgueritchian, M.; Shulaker, M. M.; Bao, Z. High-Mobility, Aligned Crystalline Domains of TIPS-Pentacene with Metastable Polymorphs Through Lateral Confinement of Crystal Growth. *Adv. Mater.* 2014, *26* (3), 487–493.

(40) Kjellander, B. K. C.; Smaal, W. T. T.; Anthony, J. E.; Gelinck, G. H. Inkjet Printing of TIPS-PEN on Soluble Polymer Insulating Films: A Route to High-Performance Thin-Film Transistors. *Adv. Mater.* 2010, *22* (41), 4612–4616.

(41) Lee, J. H.; Seo, Y.; Park, Y. D.; Anthony, J. E.; Kwak, D. H.; Lim, J. A.; Ko, S.; Jang, H. W.; Cho, K.; Lee, W. H. Effect of Crystallization Modes in TIPS-Pentacene/Insulating Polymer Blends on the Gas Sensing Properties of Organic Field-Effect Transistors. *Sci. Rep.* 2019, *9* (1), 21.

(42) Wang, Z.; Huang, L.; Zhu, X.; Zhou, X.; Chi, L. An Ultrasensitive Organic Semiconductor NO2 Sensor Based on Crystalline TIPS-Pentacene Films. *Adv. Mater.* 2017, *29* (38), 1703192.

(43) Bae, J. H.; Park, J.; Keum, C. M.; Kim, W. H.; Kim, M. H.; Kim, S. O.; Kwon, S. K.; Lee, S. D. Thermal Annealing Effect on the Crack Development and the Stability of 6,13-Bis(Triisopropylsilylethynyl)-Pentacene Field-Effect Transistors with a Solution-Processed Polymer Insulator. *Org. Electron.* 2010, *11* (5), 784–788.

(44) Sorli, J. C.; Ai, Q.; Granger, D. B.; Gu, K.; Parkin, S.; Jarolimek, K.; Telesz, N.; Anthony, J. E.; Risko, C.; Loo, Y. L. Impact of Atomistic Substitution on Thin-Film Structure and Charge Transport in a Germanyl-Ethynyl Functionalized Pentacene. *Chem. Mater.* 2019, *31* (17), 6615–6623.

(45) Smith, J.; Hamilton, R.; Qi, Y.; Kahn, A.; Bradley, D. D. C.; Heeney, M.; McCulloch, I.; Anthopoulos, T. D. The Influence of Film Morphology in High-Mobility Small-Molecule: Polymer Blend Organic Transistors. *Adv. Funct. Mater.* 2010, *20* (14), 2330–2337.

(46) Zhao, K.; Wodo, O.; Ren, D.; Khan, H. U.; Niazi, M. R.; Hu, H.; Abdelsamie, M.; Li, R.; Li, E. Q.; Yu, L.; Yan, B.; Payne, M. M.; Smith, J.; Anthony, J. E.; Anthopoulos, T. D.; Thoroddsen, S. T.; Ganapathysubramanian, B.; Amassian, A. Vertical Phase Separation in Small Molecule:Polymer Blend Organic Thin Film Transistors Can Be Dynamically Controlled. *Adv. Funct. Mater.* 2016, *26* (11), 1737–1746.

(47) Smith, J.; Hamilton, R.; McCulloch, I.; Stingelin-Stutzmann, N.; Heeney, M.; Bradley, D. D. C.; Anthopoulos, T. D. Solution-Processed Organic Transistors Based on Semiconducting Blends. *J. Mater. Chem.* 2010, *20* (13), 2562–2574.

(48) Leonardi, F.; Casalini, S.; Zhang, Q.; Galindo, S.; Gutiérrez, D.; Mas-Torrent, M. Electrolyte-Gated Organic Field-Effect Transistor Based on a Solution Sheared Organic Semiconductor Blend. *Adv. Mater.* 2016, *28* (46), 10311–10316.

(49) Yuan, Y.; Giri, G.; Ayzner, A. L.; Zoombelt, A. P.; Mannsfeld, S. C. B.; Chen, J.; Nordlund, D.; Toney, M. F.; Huang, J.; Bao, Z. Ultra-High Mobility Transparent Organic Thin Film Transistors Grown by an off-Centre Spin-Coating Method. *Nat. Commun.* 2014, *5*, 3005.

ARTICLE 1: ROLE OF POLYMORPHISM AND THIN-FILM MORPHOLOGY IN ORGANIC SEMICONDUCTORS PROCESSED BY SOLUTION SHEARING

AUTHORS: Sergi Riera Galindo, Adrián Tamayo and Marta Mas-Torrent

PUBLICATION: ACS omega 3 (2), 2329 (2018)

ARTICLE 2: CONTROL OF POLYMORPHISM AND MORPHOLOGY IN SOLUTION SHEARED ORGANIC FIELD-EFFECT TRANSISTORS

AUTHORS: Sergi Galindo, Adrián Tamayo, Francesca Leonardi and Marta Mas-Torrent

PUBLICATION: Advanced Functional Materials 27 (25), 1700526 (2017)

ARTICLE 3: IMPACT OF THE INK FORMULATION AND COATING SPEED ON THE POLYMORPHISM AND MORPHOLOGY OF A SOLUTION-SHEARED THIN FILM OF A BLENDED ORGANIC SEMICONDUCTOR

AUTHORS: Adrián Tamayo, Sergi Riera Galindo, Andrew OF Jones, Roland Resel and Marta Mas-Torrent

PUBLICATION: Advanced Materials Interfaces 6 (22), 1900950 (2019)

ARTICLE 4: MOBILITY ANISOTROPY IN THE HERRINGBONE STRUCTURE OF ASYMMETRIC PH-BTBT-10 IN SOLUTION SHEARED THIN FILM TRANSISTORS

AUTHORS: Adrián Tamayo, Sebastian Hofer, Tommaso Salzillo, Christian Ruzié, Guillaume Schweicher, Roland Resel, Marta Mas-Torrent

PUBLICATION: Journal of Materials Chemistry C 9, 7186 (2021)

ARTICLE 5: Molecular Disorder in Crystalline Thin Films of an Asymmetric BTBT Derivative

AUTHORS: Sebastian Hofer, Johanna Unterkofler, Martin Kaltenegger, Guillaume Schweicher, Christian Ruzié, Adrián Tamayo, Tommaso Salzillo, Marta Mas-Torrent, Alessandro Sanzone, Luca Beverina, Yves Henry Geerts, Roland Resel

PUBLICATION: Chemistry of Materials 33 (4), 1455 (2021)

ARTICLE 6: LOW ACTIVATION ENERGY FIELD-EFFECT TRANSISTORS FABRICATED BY BAR-ASSISTED MENISCUS SHEARING

AUTHORS: Michael Berteau-Rainville, Adrián Tamayo, Tim Leydecker, Atiye Pezeshki, Ingo Salzmann, Marta Mas-Torrent, Emanuele Orgiu

PUBLICATION: Applied Physics Letters 119 (10), 103301 (2021)

ARTICLE 7: ORGANIC FIELD EFFECT TRANSISTORS BASED ON TERNARY BLENDS INCLUDING A FLUORINATED POLYMER FOR ACHIEVING ENHANCED DEVICE STABILITY

AUTHORS: Adrián Tamayo, Tommaso Salzillo, and Marta Mas-Torrent

PUBLICATION: Advanced Materials Interfaces 9 (6), 2101679 (2022)

CHAPTER III

ORGANIC FIELD-EFFECT TRANSISTORS AS X-RAY DETECTORS

3.1. TRANSISTORS AS X-RAY PHOTODETECTORS

One possible niche of applications for large area flexible organic electronic devices is in the field of X-ray detection. Nowadays, there is a high demand on photosensors for high-energy photons with applications in medical, security, energy, and nuclear research.[1] The mainstream awareness of minimizing the X-ray dose and reducing the cost while keeping the sensitivity of the X-ray detectors, has led to the development of responsive low-cost photodetectors.[2–7]

X-ray photodetectors can be classified into direct and indirect detectors. Indirect detectors transform the high energy radiation into UV-Vis radiation through a scintillator, and then, a photodiode converts this signal into an electrical one. On the other hand, in the direct detection, the high energy radiation generates directly electron-hole pairs in a semiconductor material, which is transduced into an electrical signal within the same device.[8]

Current direct X-ray detectors are based on inorganic semiconductors (amorphous silicon (a-Si), amorphous selenium (a-Se), and polycrystalline cadmium zinc telluride (poly-CZT)). However, the fabrication of these materials is expensive and they are not compatible with flexible substrates. To overcome these technological issues, the use of X-ray detectors based on organic semiconductors (OSCs), which are compatible with solution-processing techniques, represents a promising alternative and, hence, these devices are raising a lot of interest in the scientific community.[8–12]

The first reports on the use of OSCs to detect in real-time high energy consisted in a photodiode with a conjugated polymer,[13] which showed moderate sensitivity values. The first use of two-terminal devices based on thin films of TIPS-pentacene to detect X-ray radiation was reported by B. Fraboni *et al.*[8] The change in the thin film resistance upon X-ray exposure led to sensitivity values of 200 $nC \cdot Gy^{-1}$. Later on, with the use of TIPS-pentacene OFETs higher sensitivities up to 1200 $nC \cdot Gy^{-1}$ were achieved,[10] and a flexible OFET detector was also demonstrated.[14] The OFET architecture allows to monitor the changes of multiple parameters during the irradiation.

The parameters that influence the X-ray sensitivity are: i) the transport characteristics of the semiconductor material (i.e., high charge carrier mobility is desirable in order to reduce recombination of electron-hole pairs), and ii) the absorption spectra of the OSC in order to maximize the absorption of the radiation. The latter is achieved adding high-Z atoms

directly into the OSC molecule structure.[15] However, other approaches have been employed, such as the introduction in the active layer of additives with high-Z number[16–19] (i.e., nanoparticles or quantum dots) or carbon nanotubes.[20]

L. Basiricò *et al*. reported that the photocurrent observed by X-ray photons in a polycrystalline TIPS-pentacene thin film was higher than the estimated by a simple model based on the electron-hole photogeneration. The signal was two orders of magnitude higher than the expected for the simple model of charges photogeneration.[10] They explained the gain in the photodetected signal based on the trapping of electrons in the bulk of the semiconductor material and dielectric surface. According to this model, the X-ray generates the electron-hole pair in the semiconductor material and holes (in a p-type transistor) drift along the electric field until the corresponding electrode (**Figure 3.1a**). However, the electrons are trapped in deep electron traps in the semiconductor material, causing the injection of more holes into the OSC to keep the electroneutrality of the system. When the radiation source disappears, the electrons return to the ground state, and the charges are recombined. Therefore, in addition to the parameters mentioned above, the electron trap density can also impact on the sensitivity of the OFET photodetectors.[21]

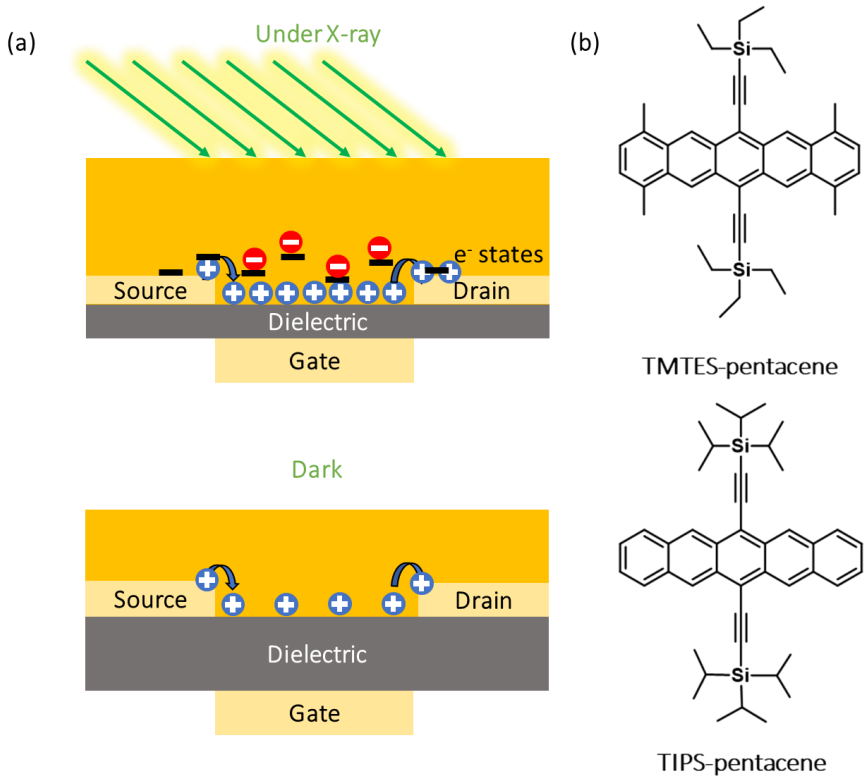

Figure 3.1. (a) Schematic of the photoconductive gain mechanism that modulates the photocurrent induced by X-rays. Adapted from ref. 10. **(b)** Molecular structures of TMTES-pentacene and TIPS-pentacene.

The carrier mobility-lifetime product ($\mu \cdot \boldsymbol{\tau}$) is a key parameter to describe the ability to generate and maintain the electron-hole pair inside the semiconductor without recombination. The probability of a carrier to be captured and recombined at the traps either within the OSC or at the channel interface can be dramatically reduced by achieving large $\mu \cdot \boldsymbol{\tau}$, which would enable highly efficient detectors due to the longer carrier diffusion lengths, increasing hence the amount of charge carriers collected by the electrodes.[22]

The development of flexible X-ray detectors with high sensitivity and fast response is very appealing for medical diagnosis. The objective of this Chapter is to explore the potential of OFETs fabricated by bar-assisted meniscus shearing (BAMS) as X-ray detectors. In addition, we focused on the understanding of the mechanisms behind detection to establish guidelines to improve the device performance.

3.2. ORGANIC PHOTODETECTORS BASED ON THIN FILM OF SOLUBLE PENTACENE DERIVATES

Article 8: Morphology and mobility as tools to control and unprecedentedly enhance X-ray sensitivity in organic thin-films.

Article 9: Ultrahigh sensitive X-ray detectors employing high performance organic transistors based on a small molecule semiconductor/polymer blend.

In these papers, we report the production of highly sensitive direct X-ray detectors based on thin films of the small molecule semiconductors 6,13-Bis(triisopropylsilylethynyl)pentacene (TIPS-pentacene) and 1,4,8,11-tetramethyl-6,13-triethylsilylethynylpentacene (TMTES-pentacene) (Figure 3.1b) deposited by BAMS, a high throughput and scalable deposition technique. Both OSCs were selected due to the presence of a high Z-atom (i.e., Si) in their molecular structure and their high charge carrier mobility.

With the aim at understanding the parameters playing a role on the photoresponse, we fabricated films of TIPS-pentacene by BAMS employing different coating speeds, which led to films exhibiting similar mobility but differing on the crystalline domain sizes. We found that the thin films with smaller grain size exhibited a higher sensitivity, which was attributed to a higher number of electron traps at the grain boundaries.[23,24] In fact, the presence of a high density of electron traps increased the recombination time of the electron-hole pair, which is proportional to the photodetected signal. Thus, we showed that the control of the

morphology to increase the density of electron traps was an excellent tool to improve the gain in the OFETs photodetectors.

Secondly, the photoresponse of OFETs based on blends of TIPS-pentacene and polystyrene (PS) were explored. As mentioned before, the use of binder polymers such as PS boosted the carrier mobility due to an improvement of the OSC crystallization and the reduction of the hole traps at the OSC/dielectric interface.[25–27] After testing blends based on TIPS-pentacene and PS with different ratios, it was possible to correlate that the films showing the lowest hole trap density, showed an enhanced field-effect mobility and X-ray photoresponse. Remarkably the best devices showed an X-ray sensitivity of ($3 \cdot 10^9$ $\mu C \cdot Gy^{-1} \cdot cm^{-3}$), which was about three orders of magnitude higher than the previous reported X-ray detectors based on spin-coated TIPS-pentacene OFETs and of the same order as commercial inorganic detectors.[6,9,10,15]

Considering these results, we investigated the photoresponse of a similar blend based on TMTES-pentacene and PS. The films prepared by BAMS exhibited a higher hole mobility (<2.6 $cm^2 \cdot V^{-1} \cdot s^{-1}$) than the TIPS-pentacene films (0.7 $cm^2 \cdot V^{-1} \cdot s^{-1}$) and a lower density of hole traps. Noticeably, it was found that this molecule crystallises in a more favourable 2-dimensional herringbone packing,[28] instead of following a slipped-stacking motif as most pentacene derivatives do, including TIPS-Pentacene.[29] Additionally, a careful investigation of the TMTES-pentacene:PS blend films by time-of-flight secondary ion mass spectrometry (ToF-SIMS) clearly demonstrated that a vertical stratification of the two materials takes place, in which PS stays in the bottom passivating the dielectric layer.

The photodetectors based on TMTES-pentacene:PS OFETs gave rise to a record X-ray photosensitivity of $4 \cdot 10^{10}$ $\mu C \cdot Gy^{-1} \cdot cm^{-3}$, one order of magnitude higher than that found for blends based on TIPS-pentacene and PS. This sensitivity value is the highest reported so far for a direct X-ray detector based on a tissue equivalent full organic active layer.[30–38]

To demonstrate the excellent properties of these sensors, a 4-pixel array was designed as a proof of concept of the reliability of our devices as large area X-ray detectors for medical applications in the energy range of (8.5 - 35 keV) and dose rates (0.05 - 35 mGy s^{-1}). The X-ray projection image of a metal object exhibited an excellent contrast with a lateral resolution of 250 µm. Further, the image was acquired over a total of 3,600 expositions at the same experimental conditions, elucidating the high reproducibility of the devices.

3.3. SUMMARY

We showed that the use of blends of OSCs with PS combined with the BAMS deposition technique brings great opportunities to develop a new generation of low-cost organic photodetectors, especially appealing for medical imaging. We demonstrated that the photo- response can be optimised by: 1) increasing the device mobility, 2) increasing the density of traps of the minority carriers (i.e., electrons in p-type OFETs), or 3) decreasing the density of traps of the majority carriers (i.e., holes in p-type OFETs). The latter can be realised using blends of OSCs with binding polymers such as PS thanks to the vertical phase separation that takes place, in which the PS rests in contact with the dielectric passivating the charge traps. We achieved a sensitivity to X-rays up to $4 \cdot 10^{10}$ $\mu C \cdot Gy^{-1} \cdot cm^{-3}$, which represents the highest value reported for organic semiconductors. It is noteworthy that with the high X-ray sensitivity of TMTES-pentacene based OFETs, a photodetector for imaging with sub-millimetre resolution was developed.

3.4. REFERENCES

(1) Chung, F. H.; Smith, D. K. *Industrial Applications of X-Ray Diffraction*; CRC press, 1999.

(2) Clairand, I.; Bordy, J. M.; Carinou, E.; Daures, J.; Debroas, J.; Denozire, M.; Donadille, L.; Ginjaume, M.; Itié, C.; Koukorava, C.; Krim, S.; Lebacq, A. L.; Martin, P.; Struelens, L.; Sans-Merce, M.; Vanhavere, F. Use of Active Personal Dosemeters in Interventional Radiology and Cardiology: Tests in Laboratory Conditions and Recommendations - ORAMED Project. *Radiat. Meas.* 2011, *46* (11), 1252–1257.

(3) Zeidell, A. M.; Ren, T.; Filston, D. S.; Iqbal, H. F.; Holland, E.; Bourland, J. D.; Anthony, J. E.; Jurchescu, O. D. Organic Field-Effect Transistors as Flexible, Tissue-Equivalent Radiation Dosimeters in Medical Applications. *Adv. Sci.* 2020, *7* (18), 2001522.

(4) Demchyshyn, S.; Verdi, M.; Basiricò, L.; Ciavatti, A.; Hailegnaw, B.; Cavalcoli, D.; Scharber, M. C.; Sariciftci, N. S.; Kaltenbrunner, M.; Fraboni, B. Designing Ultraflexible Perovskite X-Ray Detectors through Interface Engineering. *Adv. Sci.* 2020, *7* (24), 2002586.

(5) Kim, Y. C.; Kim, K. H.; Son, D. Y.; Jeong, D. N.; Seo, J. Y.; Choi, Y. S.; Han, I. T.; Lee, S. Y.; Park, N. G. Printable Organometallic Perovskite Enables Large-Area, Low-Dose X-Ray Imaging. *Nature* 2017, *550* (7674), 87–91.

(6) Zygmanski, P.; Abkai, C.; Han, Z.; Shulevich, Y.; Menichelli, D.; Hesser, J. Low-Cost Flexible Thin-Film Detector for Medical Dosimetry Applications. *J. Appl. Clin. Med. Phys.* 2014, *15* (2), 311–326.

(7) Owens, A.; Peacock, A. Compound Semiconductor Radiation Detectors. *Nucl. Instruments Methods Phys. Res. Sect. A Accel. Spectrometers, Detect. Assoc. Equip.* 2004, *531* (1–2), 18–37.

(8) Fraboni, B.; Fraleoni-Morgera, A.; Zaitseva, N. Ionizing Radiation Detectors Based on Solution-Grown Organic Single Crystals. *Adv. Funct. Mater.* 2016, *26* (14), 2276–2291.

(9) Lai, S.; Cosseddu, P.; Basiricò, L.; Ciavatti, A.; Fraboni, B.; Bonfiglio, A. A Highly Sensitive, Direct X-Ray Detector Based on a Low-Voltage Organic Field-Effect Transistor. *Adv. Electron. Mater.* 2017, *3* (8), 1600409.

(10) Basiricò, L.; Ciavatti, A.; Cramer, T.; Cosseddu, P.; Bonfiglio, A.; Fraboni, B. Direct X-Ray Photoconversion in Flexible Organic Thin Film Devices Operated below 1 V. *Nat. Commun.* 2016, *7*, 13063.

(11) Kaltenbrunner, M.; Sekitani, T.; Reeder, J.; Yokota, T.; Kuribara, K.; Tokuhara, T.; Drack, M.; Schwödiauer, R.; Graz, I.; Bauer-Gogonea, S.; Bauer, S.; Someya, T. An Ultra-Lightweight Design for Imperceptible Plastic Electronics. *Nature* 2013, *499* (7459), 458–463.

(12) Blom, P. W. M. Polymer Electronics: To Be or Not to Be? *Adv. Mater. Technol.* 2020, *5* (6), 2000144.

(13) Boroumand, F. A.; Zhu, M.; Dalton, A. B.; Keddie, J. L.; Sellin, P. J.; Gutierrez, J. J. Direct X-Ray Detection with Conjugated Polymer Devices. *Appl. Phys. Lett.* 2007, *91* (3), 033509.

(14) Lai, S.; Casula, G.; Cosseddu, P.; Basiricò, L.; Ciavatti, A.; D'Annunzio, F.; Loussert, C.; Fischer, V.; Fraboni, B.; Barbaro, M.; Bonfiglio, A. A Plastic Electronic Circuit Based on Low Voltage, Organic Thin-Film Transistors for Monitoring the X-Ray Checking History of Luggage in Airports. *Org. Electron.* 2018, *58*, 263–269.

(15) Ciavatti, A.; Basiricò, L.; Fratelli, I.; Lai, S.; Cosseddu, P.; Bonfiglio, A.; Anthony, J. E.; Fraboni, B. Boosting Direct X-Ray Detection in Organic Thin Films by Small Molecules Tailoring. *Adv. Funct. Mater.* 2019, *29* (21), 1806119.

(16) Intaniwet, A.; Mills, C. A.; Shkunov, M.; Sellin, P. J.; Keddie, J. L. Heavy Metallic Oxide Nanoparticles for Enhanced Sensitivity in Semiconducting Polymer X-Ray Detectors. *Nanotechnology* 2012, *23* (23), 235502.

(17) Ankah, G. N.; Büchele, P.; Poulsen, K.; Rauch, T.; Tedde, S. F.; Gimmler, C.; Schmidt, O.; Kraus, T. PbS Quantum Dot Based Hybrid-Organic Photodetectors for X-Ray Sensing. *Org. Electron.* 2016, *33*, 201–206.

(18) Thirimanne, H. M.; Jayawardena, K. D. G. I.; Parnell, A. J.; Bandara, R. M. I.; Karalasingam, A.; Pani, S.; Huerdler, J. E.; Lidzey, D. G.; Tedde, S. F.; Nisbet, A.; Mills, C. A.; Silva, S. R. P. High Sensitivity Organic Inorganic Hybrid X-Ray Detectors with Direct Transduction and Broadband Response. *Nat. Commun.* 2018, *9*, 2926.

(19) Li, Y.; Adeagbo, E.; Koughia, C.; Simonson, B.; Pettipas, R.; Mishchenko, A.; Arnab, S.; Laperrière, L.; Belev, G.; Stevens, A.; Kasap, S.; Kelly, T. L. Direct Conversion X-Ray Detectors with 70 PA/Cm2 Dark Currents Coated from an Alcohol-Based Perovskite Ink. *J. Mater. Chem. C* 2022, *10* (4), 1228–1235.

(20) Han, H.; Lee, S.; Seo, J.; Mahata, C.; Cho, S.; Han, A.-R.; Hong, K.-S.; Park, J.-H.; Soh, M.-J.; Park, C.; Lee, T. Enhancement of X-Ray Detection by Single-Walled Carbon Nanotube Enriched Flexible Polymer Composite. *Nanoscale Res. Lett.* 2014, *9*, 610.

(21) Kasap, S.; Frey, J. B.; Belev, G.; Tousignant, O.; Mani, H.; Greenspan, J.; Laperriere, L.; Bubon, O.; Reznik, A.; DeCrescenzo, G.; Karim, K. S.; Rowlands, J. A. Amorphous and Polycrystalline Photoconductors for Direct Conversion Flat Panel X-Ray Image Sensors. *Sensors* 2011, *11* (5), 5112–5157.

(22) Yang, T.; Li, F.; Zheng, R. Recent Advances in Radiation Detection Technologies Enabled by Metal-Halide Perovskites. *Mater. Adv.* 2021, *2* (21), 6744–6767.

(23) Kobayashi, H.; Tokita, Y. Modeling of Hole Transport across Grain Boundaries in Organic Semiconductors for Mesoscale Simulations. *Appl. Phys. Express* 2015, *8* (5), 051602.

(24) Vladimirov, I.; Kühn, M.; Geßner, T.; May, F.; Weitz, R. T. Energy Barriers at Grain Boundaries Dominate Charge Carrier Transport in an Electron-Conductive Organic Semiconductor. *Sci. Rep.* 2018, *8* (1), 14868.

(25) Zhao, K.; Wodo, O.; Ren, D.; Khan, H. U.; Niazi, M. R.; Hu, H.; Abdelsamie, M.; Li, R.; Li, E. Q.; Yu, L.; Yan, B.; Payne, M. M.; Smith, J.; Anthony, J. E.; Anthopoulos, T. D.; Thoroddsen, S. T.; Ganapathysubramanian, B.; Amassian, A. Vertical Phase Separation in Small Molecule:Polymer Blend Organic Thin Film Transistors Can Be Dynamically Controlled. *Adv. Funct. Mater.* 2016, *26* (11), 1737–1746.

(26) Paterson, A. F.; Treat, N. D.; Zhang, W.; Fei, Z.; Wyatt-Moon, G.; Faber, H.; Vourlias, G.; Patsalas, P. A.; Solomeshch, O.; Tessler, N.; Heeney, M.; Anthopoulos, T. D. Small Molecule/Polymer Blend Organic Transistors with Hole Mobility Exceeding 13 Cm2V−1s−1. *Adv. Mater.* 2016, *28* (35), 7791–7798.

(27) Niazi, M. R.; Li, R.; Abdelsamie, M.; Zhao, K.; Anjum, D. H.; Payne, M. M.; Anthony, J.; Smilgies, D. M.; Amassian, A. Contact-Induced Nucleation in High-Performance Bottom-Contact Organic Thin Film Transistors Manufactured by Large-Area Compatible Solution Processing. *Adv. Funct. Mater.* 2016, *26* (14), 2371–2378.

(28) Illig, S.; Eggeman, A. S.; Troisi, A.; Jiang, L.; Warwick, C.; Nikolka, M.; Schweicher, G.; Yeates, S. G.; Henri Geerts, Y.; Anthony, J. E.; Sirringhaus, H. Reducing Dynamic Disorder in Small-Molecule Organic Semiconductors by Suppressing Large-Amplitude Thermal Motions. *Nat. Commun.* 2016, *7*, 10736.

(29) Sorli, J. C.; Ai, Q.; Granger, D. B.; Gu, K.; Parkin, S.; Jarolimek, K.; Telesz, N.; Anthony, J. E.; Risko, C.; Loo, Y. L. Impact of Atomistic Substitution on Thin-Film Structure and Charge Transport in a Germanyl-Ethynyl Functionalized Pentacene. *Chem. Mater.* 2019, *31* (17), 6615–6623.

(30) Mao, L.; Li, Y.; Chen, H.; Yu, L.; Zhang, J. A High-Sensitivity Flexible Direct X-Ray Detector Based on Bi2O3/PDMS Nanocomposite Thin Film. *Nanomaterials* 2021, *11* (7), 1832.

(31) Gao, Y.; Ge, Y.; Wang, X.; Liu, J.; Liu, W.; Cao, Y.; Gu, K.; Guo, Z.; Wei, Y. M.; Zhou, N.; Yu, D.; Meng, H.; Yu, X. F.; Zheng, H.; Huang, W.; Li, J. Ultrathin and Ultrasensitive Direct X-Ray Detector Based on Heterojunction Phototransistors. *Adv. Mater.* 2021, *33* (32), 2101717.

(32) Ciavatti, A.; Sorrentino, R.; Basiricò, L.; Passarella, B.; Caironi, M.; Petrozza, A.; Fraboni, B. High-Sensitivity Flexible X-Ray Detectors Based on Printed Perovskite Inks. *Adv. Funct. Mater.* 2021, *31* (11), 2009072.

(33) Nanayakkara, M. P. A.; Matjačić, L.; Wood, S.; Richheimer, F.; Castro, F. A.; Jenatsch, S.; Züfle, S.; Kilbride, R.; Parnell, A. J.; Masteghin, M. G.; Thirimanne, H. M.; Nisbet, A.; Jayawardena, K. D. G. I.; Silva, S. R. P. Ultra-Low Dark Current Organic–Inorganic Hybrid X-Ray Detectors. *Adv. Funct. Mater.* 2021, *31* (8), 2008482.

(34) Thirimanne, H. M.; Jayawardena, K. D. G. I.; Nisbet, A.; Shen, Y.; Bandara, R. M. I.; Mills, C. A.; Shao, G.; Silva, S. R. P. Hybrid Multipixel Array X-Ray Detectors for Real-Time Direct Detection of Hard X-Rays. *IEEE Trans. Nucl. Sci.* 2020, *67* (10), 2238–2245.

(35) Peng, J.; Ye, K.; Xu, Y.; Cui, L.; Li, R.; Peng, H.; Lin, Q. X-Ray Detection Based on

Crushed Perovskite Crystal/Polymer Composites. *Sensors Actuators, A Phys.* 2020, *312*, 112132.

(36) Zhao, J.; Zhao, L.; Deng, Y.; Xiao, X.; Ni, Z.; Xu, S.; Huang, J. Perovskite-Filled Membranes for Flexible and Large-Area Direct-Conversion X-Ray Detector Arrays. *Nat. Photonics* 2020, *14* (10), 612–617.

(37) Mescher, H.; Schackmar, F.; Eggers, H.; Abzieher, T.; Zuber, M.; Hamann, E.; Baumbach, T.; Richards, B. S.; Hernandez-Sosa, G.; Paetzold, U. W.; Lemmer, U. Flexible Inkjet-Printed Triple Cation Perovskite X-Ray Detectors. *ACS Appl. Mater. Interfaces* 2020, *12* (13), 15774–15784.

(38) Guo, J.; Xu, Y.; Yang, W.; Xiao, B.; Sun, Q.; Zhang, X.; Zhang, B.; Zhu, M.; Jie, W. High-Stability Flexible X-Ray Detectors Based on Lead-Free Halide Perovskite Cs2TeI6Films. *ACS Appl. Mater. Interfaces* 2021, *13* (20), 23928–23935.

ARTICLE 8: MORPHOLOGY AND MOBILITY AS TOOLS TO CONTROL AND UNPRECEDENTEDLY ENHANCE X-RAY SENSITIVITY IN ORGANIC THIN-FILM

AUTHORS: Inés Temiño, Laura Basiricò, Ilaria Fratelli, Adrián Tamayo, Andrea Ciavatti, Marta Mas-Torrent & Beatrice Fraboni

PUBLICATION: Nature Communications 11, 2136 (2020)

ARTICLE 9: X-RAY DETECTORS WITH ULTRAHIGH SENSITIVITY EMPLOYING HIGH PERFORMANCE TRANSISTORS BASED ON A FULLY ORGANIC SMALL MOLECULE SEMICONDUCTOR/POLYMER BLEND ACTIVE LAYER

AUTHORS: Adrián Tamayo, Ilaria Fratelli, Andrea Ciavatti, Carme Martínez-Domingo, Paolo Branchini, Elisabetta Colantoni, Stefania De Rosa, Luca Tortora, Adriano Contillo, Raul Santiago, Stefan T. Bromley, Beatrice Fraboni, Marta Mas-Torrent, Laura Basiricò

PUBLICATION: Adv. Electron. Mater., Submitted (2022)

X-ray detectors with ultrahigh sensitivity employing high performance transistors based on a fully organic small molecule semiconductor/polymer blend active layer

Adrián Tamayo,[1] Ilaria Fratelli,[2] Andrea Ciavatti,[2] Carme Martínez-Domingo,[1] Paolo Branchini,[3,4] Elisabetta Colantoni,[3,4,5] Stefania De Rosa,[3,4] Luca Tortora,[3,4,6] Adriano Contillo,[7] Raul Santiago,[8] Stefan T. Bromley,[8,9] Beatrice Fraboni,[2,] Marta Mas-Torrent,[1,*] Laura Basiricò[2]*

[1] Institut de Ciència de Materials de Barcelona (ICMAB-CSIC) and Networking Research Center on Bioengineering, Biomaterials and Nanomedicine (CIBER-BBN), Campus de la Universitat Autònoma de Barcelona, Cerdanyola, E-08193 Barcelona, Spain.

[2] Department of Physics and Astronomy, University of Bologna and National Institute for Nuclear Physics - INFN section of Bologna, Viale Berti Pichat 6/2, 40127 Bologna, Italy.

[3] Surface Analysis Laboratory INFN Roma Tre, Via della Vasca Navale 84, 00146 Rome, Italy.

[4] INFN, Roma Tre, via della Vasca Navale 84, Rome, Italy.

[5] Department of Mathematics and Physics, Roma Tre University, via della Vasca Navale 84, Rome, Italy.

[6] Department of Sciences, Roma Tre University, Via della Vasca Navale 84, Rome, Italy.

[7] Elettra-Sincrotrone Trieste, Area Science Park Strada Statale 14, km 163.5, 34149 Basovizza, Trieste , Italy

[8] Departament de Ciència de Materials i Química Física & Institut de Química Teòrica i Computacional (IQTCUB), Universitat de Barcelona, Barcelona, Spain.

[9] Institució Catalana de Recerca i Estudis Avançats (ICREA), Barcelona, Spain.

E-mail: mmas@icmab.es; beatrice.fraboni@unibo.it

Keywords: organic field-effect transistor, X-ray detector, organic semiconductor blends, X-ray image, high performance

Abstract

The implementation of organic semiconductor (OSC) materials in X-ray detectors provides exciting new opportunities towards a new generation of biocompatible devices with high potential for the fabrication of sensitive and low-cost X-ray imaging systems. Here, we report the fabrication of highly performing organic field-effect transistors (OFETs) based on blends of 1,4,8,11-tetramethyl-6,13-triethylsilylethynyl pentacene (TMTES) with polystyrene. The films are printed employing a low cost and high-throughput deposition technique. The devices exhibit a very high electrical performance with a high mobility and low density of hole traps, which is ascribed to the favorable herringbone packing (different from most pentacene derivatives) and the vertical phase separation taking place in the blend films. As a consequence, an exceptional high sensitivity of (4.10±0.05) 10^{10} μC Gy^{-1} cm^{-3} for X-ray detection is achieved, which is the highest reported so far for a direct X-ray detector based on a tissue equivalent full organic active layer, and is higher than most perovskite film-based X-ray detectors. As a proof of concept to demonstrate the high potential of these devices, an X-ray image with sub-millimeter pixel size is recorded employing a 4-pixel array. This work highlights the potential exploitation of high performing OFETs for future innovative large-area and highly sensitive X-ray detectors for medical dosimetry and diagnostic applications.

1. Introduction

The capacity of X-rays to traverse optically opaque substances with little absorption has led to their widespread use in modern society. X-ray detectors are key to high-resolution imaging systems employed in many fields such as diagnostic healthcare, astrophysics, industrial inspection, security, and cultural heritage preservation.[1] The demand for low X-ray dose detection, high sensitivity and cost-efficient devices has led to the development of new X-ray detectors based on responsive semiconductors. Such detectors rely on the generation of electron-hole pairs from incoming radiation, which can be measured by an electrical readout.[2] The main virtue of these detectors is their outstanding combination of high speed, spatial resolution, and sensitivity.

Current X-ray detectors use inorganic semiconductors (e.g. amorphous-Se, amorphous-Si, poly-CdZnTe (CZT), diamond). However, these materials present severe limitations for the growing need for curved and large area image detectors with reduced image distortion and vignetting. To overcome these technological issues, the use of organic semiconductors (OSCs) in X-ray detectors has several advantages, such as light weight, compatibility with flexible substrates and low-cost solution processability (e.g. by roll-to-roll production).

The inherent low atomic number (Z) of OSCs mimicking human tissue meets the requirements for medical dosimetry applications. These materials are suitable for detectors with wide dynamic range and low energy and, hence, are highly promising for medical applications in the so-called “mammography energy range”, <40 KeV.[3] For applications requiring high attenuation

for hard X-rays (>40 KeV), composite films have also been introduced comprising high-Z elements integrated into an OSC such as lead-halide perovskites, nanoparticles or quantum dots containing heavy elements.[4–11] However, the manufacturing of these materials requires complicated processes and still remains a challenge. Moreover, the introduction of high absorbing elements limits the tissue equivalence peculiar of OSCs, also introducing a higher toxicity level, e. g. due to the presence of lead in the most commonly used perovskites. Therefore, the implementation of novel OSC materials in X-ray detectors provides exciting new opportunities towards a new generation of biocompatible devices with high potential for the fabrication of sensitive and low-cost X-ray imaging systems.

Recently, organic X-ray detectors based on organic field-effect transistors (OFETs) have successfully been reported.[12,13] High-energy photon absorption is challenging in organic materials since they are constituted of atoms with low Z atomic numbers. Hence, semiconductors with high-Z atoms included into their basic molecular structure, such as the benchmark OSC bis-(triisopropylsilylethynyl) pentacene (TIPS-pentacene), have been used as active materials to increase radiation capture, while preserving tissue equivalence.[14] In our previous work, p-type OFETs using blends of TIPS-pentacene with polystyrene (PS) were reported to exhibit an unprecedented X-ray sensitivity for organic-based direct detectors, and matching that of perovskite thick films.[13] The OSC films were prepared by a high throughput solution shearing technique (i.e., bar-assisted meniscus shearing, BAMS)[15–18] which gives rise to large area crystalline films. Our findings concluded that the detector performance is strongly affected by both i) the grain size and boundaries and ii) the device mobility. Regarding the former, films with lower crystal domains revealed a higher performance due to an increase in the density of traps for minority charge carriers (i.e., electrons in TIPS-pentacene) that assist the photoconductive gain effect. On the other hand, the device mobility can be optimised by using OSCs thin films crystallising in structures exhibiting high intermolecular electronic coupling and by minimising the trap density for majority charge carriers (i.e., holes in TIPS-pentacene). The latter is strongly reduced by using OSC:PS blends since during the thin film deposition a vertical phase separation takes place resulting in a bottom PS layer that passivates the interfacial charge traps.[19]

With the aim at further improving the X-ray detector performance, we searched for the fabrication of OFETs showing an enhanced hole transport. Specifically, in this work, blends of PS with the OSC 1,4,8,11-tetramethyl-6,13-triethylsilylethynyl pentacene (TMTES) were investigated. The molecular structure of this material is very similar to TIPS-pentacene, however, the BAMS deposited thin films crystallise in a totally different crystal packing (i.e., herringbone packing motif). This resulted in OFETs that reached very high mobilities of up to 2.5 $cm^2 \cdot V^{-1} \cdot s^{-1}$ and showed a reduced density of interfacial hole traps thanks to the previously mentioned phase separation of

the blend. As a consequence, an exceptional high sensitivity of (4.10±0.05) 10^{10} µC Gy^{-1} cm^{-3} for X-ray detection was achieved, surpassing by one order of magnitude TIPS-pentacene detectors. This sensitivity value is the highest reported so far for a direct X-ray detector based on a tissue equivalent full organic active layer. As a proof of concept to demonstrate the high potential of these devices and thanks to the outstanding X-ray sensitivity of TMTES, an X-ray image with sub-millimeter pixel size was recorded employing a 4-pixel array.

2. Results

Thin films of TMTES and blends of TMTES:PS were prepared using Bar-Assisted Meniscus Shearing (BAMS) technique in ambient conditions (**Figure 1a**). The use of blends of small molecule semiconductors with insulating polymers has shown to facilitate the semiconductor processability and to lead to thin films with an enhanced crystallinity, electrical performance and device stability.[20–24] Solutions of 2.0% w/w in chlorobenzene were employed. In the case of blends, the best thin film characteristics were achieved using a TMTES:PS (PS of 280 KDa) with a ratio 2:1 and a coating speed of 10 mm s^{-1} (**Table S1**). All the inks were deposited at 105 °C (a temperature compatible with flexible electronic applications) on Si/SiO_2 substrates with interdigitated gold electrodes treated with a self-assembled monolayer of 2,3,4,5,6-pentafluorobenzenethiol (PFBT) (see experimental section). The films prepared were isotropic, highly homogenous, and crystalline and exhibited an excellent device-to-device reproducibility with almost 100% yield.

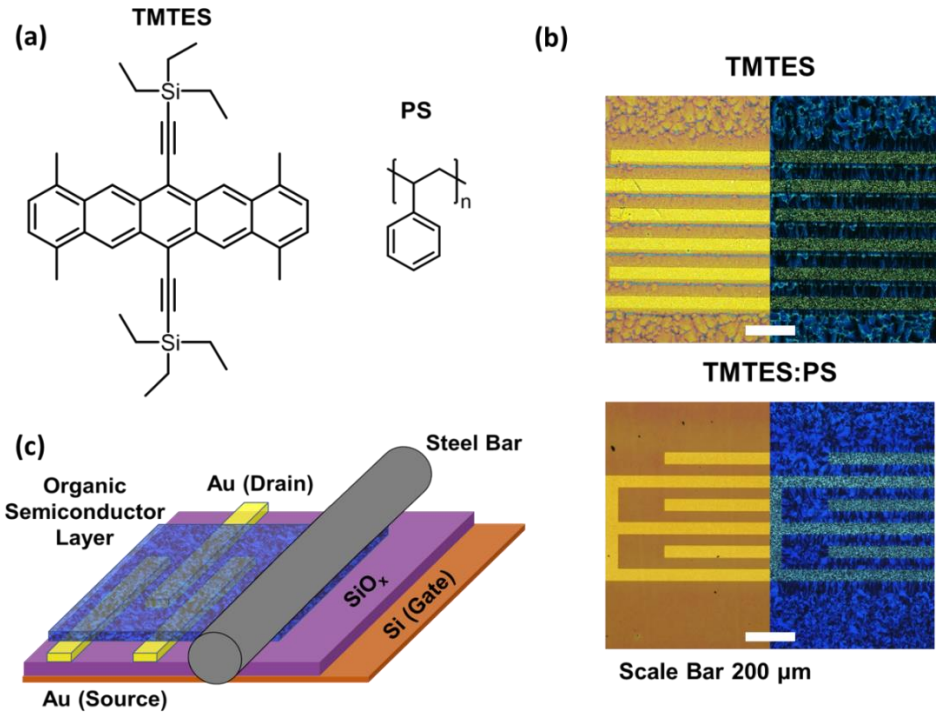

Figure 1. BAMS deposition of TMTES and TMTES:PS thin films. a) Molecular structures of TMTES and PS. b) Optical microscope images (left) and cross-polarized optical microscope images (right)

of TMTES and TMTES:PS thin films deposited by BAMS on a Si/SiO_2 substrate with pre-patterned interdigitated gold electrodes. c) Scheme of the BAMS technique for the deposition of the active layer.

The polarized optical microscopy (POM) images of the films are shown in **Figure 1b**. All the films show polycrystalline spherulitic domains without a clear preferential orientation of the crystals. This morphology is similar to the one previously observed in TIPS-pentacene films.[13,16,25,26] It can be noticed that the grains are smaller in the channel area than on the SiO_2 regions far from the electrodes, which can be ascribed to the gold PBFT treatment that promotes nucleation.[27–29]

TMTES and TMTES:PS thin films were further characterized by Atomic Force Microscopy (AFM), as shown in **Figure 2a-b**. All the films showed step edges of around 1.7 ± 0.1 nm, which is in agreement with the length of an extended molecule (inset **Figure 2a**). A low roughness of 6.5 ± 1.2 nm and 7.0 ± 3.8 nm for TMTES and TMTES:PS, respectively, were observed. Further, the thicknesses of TMTES and TMTES:PS films were found to be 22 ± 6 nm and 32 ± 7 nm, respectively (**Figure S1**).

The chemical maps of TMTES and TMTES:PS films obtained by Time-of-Flight Secondary Ion Mass Spectrometry (ToF-SIMS) are reported in **Figure S2a-b**. The characteristic molecular ion fragment originating from TMTES ($SiC_3H_9^+$ m/z = 73.05) was used to monitor the distribution of the semiconductor over an area of 500 µm × 500 µm. The ion signal of TMTES appears uniformly distributed all over the surface for the blended TMTES:PS film, indicating that there is not horizontal phase segregation. The different surface morphology of the two films is visible in the 3D surface height profiles maps, obtained by the stylus profilometer (**Figure S2c-d**). In order to study the vertical distribution of the insulating polymer, ToF-SIMS depth profiling of TMTES:PS film was investigated (**Figure 2c**). The four representative profiles of TMTES, PS, PBFT, and the SiO_2 substrate were obtained averaging the signal intensities of the characteristic secondary ions. These ions are generated from the different stratified materials constituting the OFET channel area. The behaviour of characteristic fragments from TMTES and PS confirm the co-presence of the organic semiconductor and the insulator. As we inspect deeper in the film towards the substrate, the PS ion signals evolve separately from the ones of the organic semiconductor appreciating a well-defined TMTES-PS transition region. At this point, the signal coming from TMTES decreases significantly, while PS signal increases. Further, the signal shape of PFBT shows an additional layer between the PS and the Si/SiO_2 substrate, that represents the experimental evidence of the effective electrode functionalization carried out to improve charge injection and the semiconductor crystallisation.[30–32] In **Figure 2d**, the three-dimensional (3D) ToF-SIMS map reconstruction of the overlayed signals from thin film profile are reported. These measurements are in agreement with previous results[16,22,33–35] and demonstrate that PS is acting as a dielectric passivating layer.

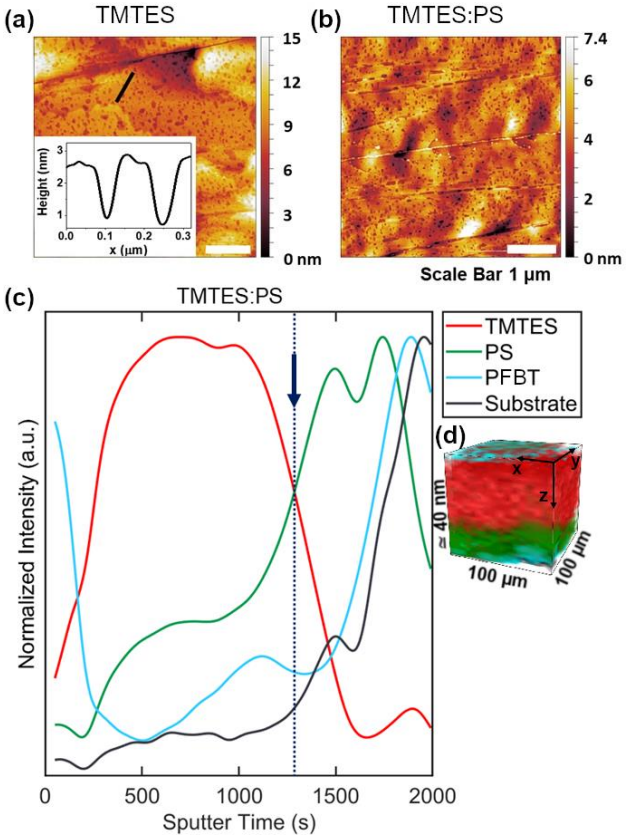

Figure 2. AFM topography images of TMTES (a) and TMTES:PS (b) thin films. The inset in (a) corresponds to the height profile along the black line in the figure. c) ToF-SIMS study of the TMTES:PS thin films. Normalized (to maximum) ToF-SIMS depth profile acquired in the channel area of the OFET starting from the surface and reaching the SiO_2 substrate (black curve). The TMTES signal (red curve) includes the SiC^-, $SiCH^-$, SiC_2H^-, $SiC_5H_2^-$, $SiC_7H_2^-$ species; the PS signal (green curve) includes the $C_3H_3^-$, $C_4H_3^-$, $C_5H_3^-$, $C_6H_3^-$, $C_7H_3^-$ species; the PBFT signal (light blue curve) includes the F^- and S^- species. d) 3D rendering of the same species of the (c) panel, as the sputter time is proportional to Z-profiling of the layers. The analysed thickness (40 ± 12 nm) was multiplied by a factor 2.5 10^4 to better appreciate the multilayer architecture in the 3D rendering. Dashed line and arrow indicate the TMTES-PS transition region.

Two different TMTES polymorphs are reported in the literature. TMTES films deposited from solution (i.e., drop casting, spin coating) have been described to crystallise into the same phase as the previously resolved single crystal structure, here-after named Polymorph I (PI).[36,37] This polymorph crystallises forming a slip-stack structure. On the other hand, more recently, TMTES microcrystals grown from solution and analysed by transmission electron microscopy were found to exhibit a new structure (i.e., Polymorph II or PII), in which the molecules stack in a herringbone motif.[38] X-ray diffraction measurements performed in the here-prepared films reveal that, in all the cases explored, TMTES crystallises in the PII phase (**Figure 3a** and **Figure S3**). Additionally, the

observation of only the (*00l*) reflection peaks confirms that the crystals are oriented with the *ab* plane parallel to the substrate, which is the most favourable scenario for charge transport, as detailed below.

Polymorphism is known to have a strong impact on device performance.[39–42] In order to compare the hole transport tendencies of the two TMTES polymorphs, we analysed all independent pairwise HOMO-HOMO (Highest Occupied Molecular Orbital) intermolecular electronic couplings (J_{HOMO}) in the two crystal structures using Density Functional Theory (DFT) based calculations (**Figure 3b** and **Table 1**). For polymorph TMTES-PI, we find a highly anisotropic one dimensional (1D) electronic structure with only a single dominant J_{HOMO} value of 105 meV along the *a*-axis. On the other hand, TMTES-PII exhibits stronger intermolecular intra-stack couplings (J_{HOMO} = 172 meV) with also significant inter-stack electronic couplings. The electronic interactions span hence in PII along the whole *ab* plane, indicative of a 2D electronic isotropy, which is more desirable for charge transport.[43–45]

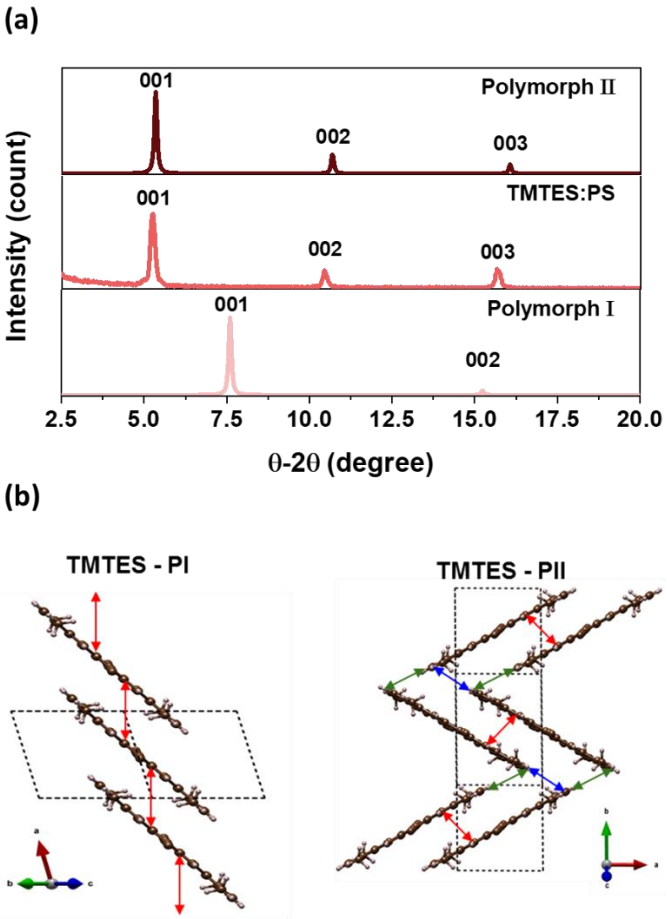

Figure 3. a) X-ray diffractogram of a representative TMTES:PS film together with the simulated diffractograms of the reported polymorphs in the (*00l*) plane. b) Crystal packing of TMTES polymorphs PI and PII. The arrows indicate pair of dimers.

Table 1: Transfers integrals calculated for each pair of dimers of the two polymorphs TMTES-PI and TMTES-PII.

	Dimer	J_{HOMO} (meV)
TMTES PI	1	105
TMTES PII	1	172
	2	17
	3	17

All the films were electrically characterized as active layers in OFETs under ambient conditions. **Table S1** collect the electrical parameters extracted for all the devices and **Figure 4** shows the transfer and output characteristics of representative OFETs based on the two formulations. All the OFETs based on TMTES (i.e., without PS binding polymer) exhibit an average mobility of 0.10 ± 0.03 $cm^2 V^{-1} s^{-1}$ and a high positive threshold voltage (V_{TH}) of 27 ± 9 V. The latter is indicative of some unintentional doping of the semiconductor, which might be ascribed to the penetration of water towards the dielectric interface. In contrast, OFETs based on TMTES:PS as active layer show an improved device performance. The devices operate with a much lower voltage window (5 V) and exhibit excellent electrical characteristics with lower hysteresis and a much lower mobility dependence with the gate voltage (**Figure S4**). The V_{TH} of these devices are closer to 0 V (in the range -0.5 to -1 V), further proving that the use of PS is beneficial for the processing of the organic semiconductor in environmental conditions.[15,20,22,23] Also, a low density of traps for majority charge carriers (i.e., holes) of (3.9 ± 0.9) 10^{11} $eV^{-1} cm^{-2}$ was estimated from the sub-threshold slope, which is one order of magnitude lower than the value found for the films without PS ((6.3 ± 1.1) 10^{12} $eV^{-1} cm^{-2}$). This finding is in agreement with previous results and advocates that the passivation of the dielectric with PS is responsible for the reduction of interfacial traps. Additionally, the shelf-stability of the TMTES:PS devices showed a mobility decay less than 50% after 90 days. On the contrary, TMTES OFETs reveal poor time stability, as reflected mainly by a very high positive threshold voltage shift after the same period of time (**Figure S5**).

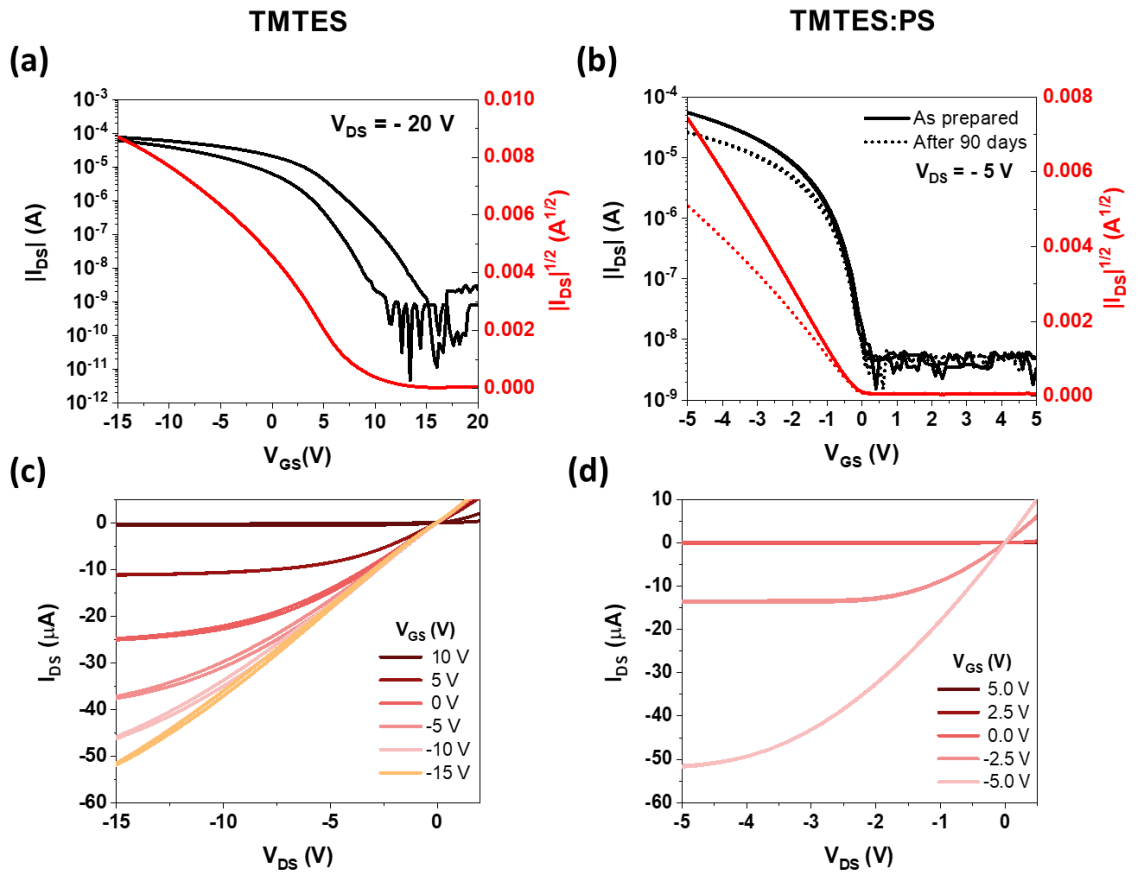

Figure 4. Electrical performance of the OFET devices. Transfer characteristics in saturation regime of representative (a) TMTES and (b) TMTES:PS based OFETs. For the blended films, the device characteristics after 90 days are shown (dashed lines). Output characteristics of representative (c) TMTES and (d) TMTES:PS based OFETs.

The TMTES:PS based devices showed a high average mobility of 2.6 ± 0.6 $cm^2 V^{-1} s^{-1}$ (maximum mobility found: 3.1 $cm^2 V^{-1} s^{-1}$). Further, the measured anisotropy ratio, that is the ratio between the mobility of the films with channel length parallel and perpendicular to the coating directions (∥/⊥), was estimated to be in the range 1.4–1.2 for TMTES films and 1.1–1.3 for the TMTES:PS ones (**Table S1**). Such mobility values and electrical characteristics found for the TMTES:PS films are among the best values reported for this semiconductor (see **Table S2**).[36,37,46–48] It should be also highlighted that the films previously reported were fabricated by means of lab-scaled solution deposition techniques (such as spin-coating and drop casting), while in this work the films are fabricated employing a low-cost high throughput technique compatible with roll-to-roll processes, a strong added-value forward mass customization.

OFETs based on the parent compound TIPS-pentacene fabricated following the same methodology (i.e., blended with PS and deposited by BAMS, hereafter TIPS:PS) led to device mobilities in the range 0.5-1 $cm^2 V^{-1} s^{-1}$ and a density of traps of (9.2 ± 2.8) 10^{11} $eV^{-1} cm^{-2}$.[13,16,26,49] In

comparison, TMTES films show a field-effect mobility between 2 and 4 times higher, that we ascribe to the more favourable 2D herringbone crystal packing and also to the lower presence of interfacial hole-traps.

The superior transport properties of TMTES:PS films deposited by BAMS have been exploited to realize organic thin film direct X-ray detectors exhibiting ultrahigh sensitivity to the radiation. During irradiation the devices have been biased to work in saturation regime (V_{DS}=-15 V and V_{GS}=-20 V) and the current flowing between the source and drain electrodes have been measured upon multiple on/off beam switching cycles. The real-time current response to irradiation at different dose rates showed the typical photoconversion dynamic processes found in organic microcrystalline thin films (see **Figure S6**). These are ruled by a photoconductive gain effect, assisted by traps for minority carriers present in the organic semiconducting layer, that allows effective and highly sensitive detection of high energy photons in tissue equivalent, low absorbing material systems such as full-organic thin films.[12] According to this detection mechanism, the photocurrent gain is defined as the ratio between two characteristic times: the lifetime of the minority charge carriers (i.e., electrons in our case) trapped in the material (τ_r) and the transit time of the majority charge carriers (i.e., holes in our case) along the channel (τ_t). The transit time is affected by the efficacy to the charge transport within the channel since it is inversely dependent from the mobility of majority charge carriers ($\tau_t = L^2/\mu V$, where L is the channel length and V is the applied bias). The sensitivity of the detector depends linearly on the gain and can be thus boosted by acting both on the electron trap density (e. g. by tuning the grain boundary density) and on the optimization of the hole transport in the active layer (e. g. by optimising the OSC structure/crystallinity and the OSC/dielectric interface by passivating the holes traps).[13] The X-ray sensitivity value has been calculated as the slope of the X-ray induced photocurrent in function of the impinging dose rate, as reported in **Figure 5a**. We achieved sensitivity to X-rays up to (4.10 ± 0.05) 10^{10} µC Gy^{-1} cm^{-3}, which represents not only the highest value reported so far for a full-organic tissue equivalent active layer, but it is also higher than most perovskite film-based X-ray detectors, as shown in **Figure 5b**. Considering that our active layer is composed of very thin films (i.e., a few tens of nm), we also plotted the corresponding graph of the sensitivity values per unit area in **Figure S7**. Further, the here-reported sensitivity value is only slightly lower than that recently reported for similar photon energies for hybrid organic-perovskite thin film X-ray detectors[50] deposited by spin coating, i.e., not a scalable process. Noteworthy, the employment of lead-halide perovskite in the active layer limits the tissue-equivalence of the sensing material. Having a human tissue equivalence absorbance of the ionizing radiation represents a strong added value of the here reported device, allowing unique perspectives in medical dosimetry application. We ascribe the accomplishment of such outstanding detection performance of TMTES:PS thin film to their

excellent transport properties, achieved thanks to the fabrication of highly crystalline thin films combined with their high electrical stability due the passivation role of PS.

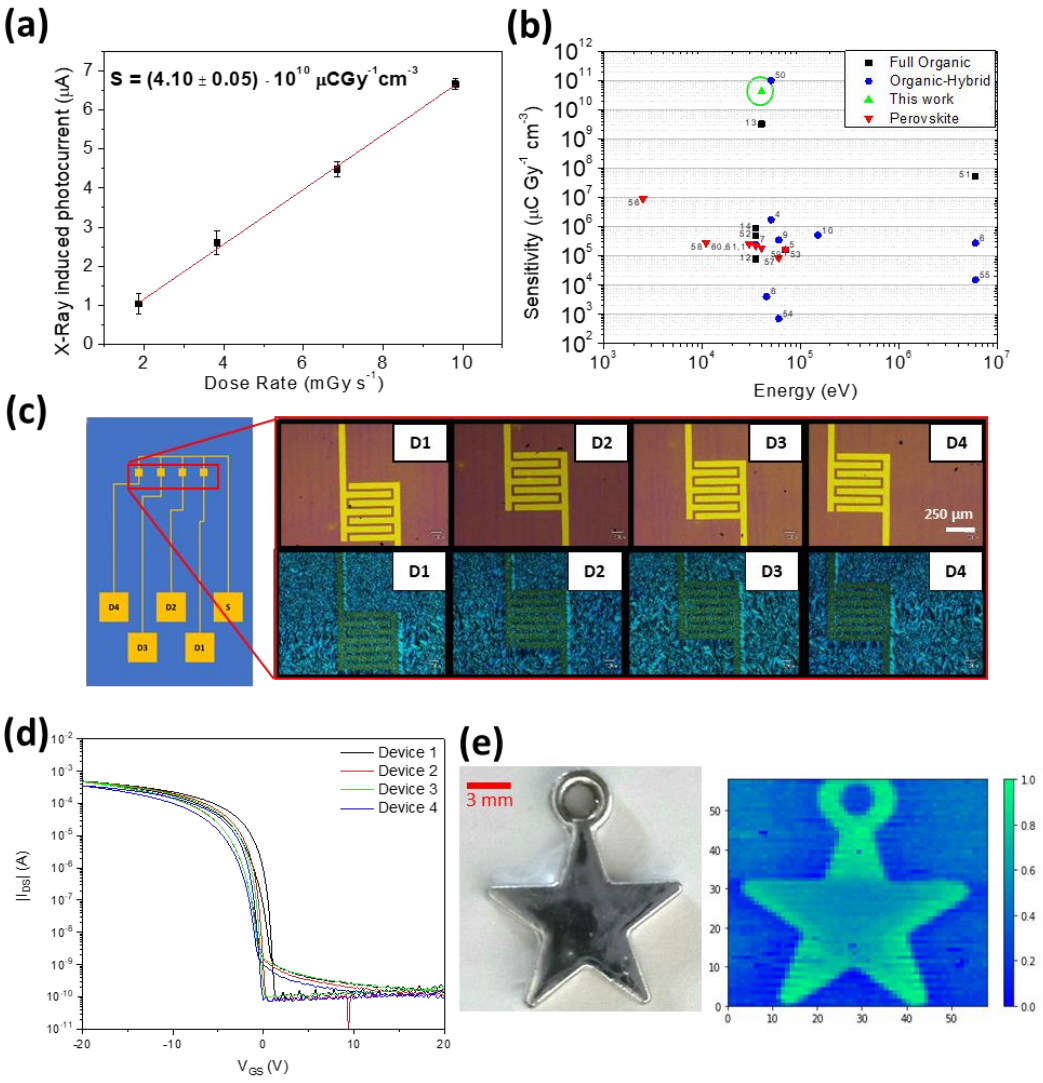

Figure 5. X-ray detection of TMTES:PS film-based devices. a) X-ray induced photocurrent as a function of the dose rate. The sensitivity is estimated as the slope of the linear fit of the experimental points and resulted in the top value reported in inset. b) Comparison of the sensitivity values per unit volume achieved in this work (green triangle), with those reported at the state of the art for thin-film detectors based on perovskite (red triangles), organic-hybrid (blue circles), and full-organic (black squares) active layers.[1,4–10,12-14,50–61] c) Layout and POM images of the 4 pixels array BAMS printed TMTES:PS detector. d) OFET transfer characteristics of the 4 pixels of the array. e) Photograph (right) and corresponding X-ray image by a single pixel device (left) of an aluminium object.

As a proof of concept of the reliability of our devices as large area detectors for medical application we realized an array of 4 pixels and tested them at the SYRMEP (Synchrotron Radiation for Medical Physics) beamline of the ELETTRA light source (Trieste, Italy). SYRMEP was chosen since

it is designed for research in biomedical imaging with X-ray energy range (8.5 – 35 keV) and dose rates (0.05 – 35 mGy s^{-1}), well suited for diagnostic mammography. The homogeneous coating achieved by means of BAMS technique is testified by similar morphologies shown by POM images, and overlapping OFETs transfer characteristics of the 4 pixels, reported in **Figure 5c-d** and **5d**, respectively. The X-ray projection image of a star-shaped metal object (**Figure 5d**) shows high contrast and assesses the good reproducibility of the detector performance over a total of 3,600 expositions at the same experimental conditions, with a lateral resolution of 250 µm, limited by the device dimension and the X-ray beam collimation. It is noteworthy that thanks to the very high X-ray sensitivity of TMTES, it was possible to employ a sub-millimetre pixel size, in a range very appealing for large-area portable X-ray panels.[62]

Conclusion

Thin films of the OSC TMTES and TMTES blended with PS were prepared employing a high throughput printing technique. The thin films crystallise in a herringbone motif that exhibit 2D electronic interactions. The OFETs fabricated with the blended films exhibited excellent device performance and stability compared to the OFETs based on the pristine OSC. Accordingly, TMTES:PS based OFETs exhibited a threshold voltage close to zero, low operation voltage and an average mobility of 2.6 $cm^2 V^{-1} s^{-1}$. Further, the density of hole traps was significantly reduced when using the PS due to the vertical phase separation taking place during the crystallisation, that leads to the passivation of the dielectric.

The OFET devices were then investigated as X-ray detectors. An unprecedented X-ray sensitivity was achieved for an organic electronic device (up to $(4.10 \pm 0.05)\, 10^{10}$ µC $Gy^{-1} cm^{-3}$), which was even higher than most perovskite film-based X-ray detectors. As a proof of concept, an array of four pixels was employed for imaging a metallic object in an X-ray beamline designed for medical radiographies. In conclusion, this work highlights the potential exploitation of high performing OFETs, fabricated by high throughput solution-based technique and employing human-tissue equivalent organic materials as active layers, for future innovative large-area and highly sensitive X-ray detectors for medical dosimetry and diagnostic applications.

Experimental Section

Materials and device fabrication

1,4,8,11-tetramethyl-6,13-triethylsilylethynyl pentacene (TMTES) and polystyrene (PS) of 10000 and 280000 g·mol^{-1} were purchased from Ossila and Sigma-Aldrich, respectively, and used without further purification. The TMTES and PS solutions were prepared in anhydrous chlorobenzene with a final concentration of 2.0 % w/w: For the blend solutions, the TMTES and PS solutions were mixed

in a TMTES:PS volume ratio of 2:1. Before deposition, the solutions were heated at the substrate temperature used for the coating process.

Interdigitated gold electrodes were patterned by photolithography on heavily n-doped Si wafer (Si-Mat) with a 200 nm thick layer of SiO_2. 5 nm of Cr (acting as adhesion layer) followed by 40 nm of Au were thermally evaporated on the Si wafer. The channel lengths (L) varied from 25 to 200 µm and the channel width/length ratio were always set constant to 100 (W/L). The substrates were then cleaned by sonication with acetone and isopropanol in HPLC grade and then dried under nitrogen flow.

The surface of the source and drain electrodes were chemically modified with a self-assembled monolayer of 2,3,4,5,6-pentafluorothiophenol (PFBT, from Sigma-Aldrich). The gold surfaces were exposed to an ultraviolet ozone cleaner for 25 min and then immersed in a 15 mM solution of PFBT in isopropanol for 15 min. Finally, the substrates were washed with pure isopropanol to remove the PFBT excess and dried under nitrogen flow.

The TMTES solutions were then deposited by Bar- Assisted Meniscus Shearing (BAMS) following the previously reported methodology.[15–17] The BAMS deposition was carried out at a substrate temperature of 105 ºC and with a coating speed of 1 and 10 $mm \cdot s^{-1}$. Note that all the fabrication process was carried out under ambient conditions and no post-thermal treatments were required.

Thin film characterization

The optical microscopy images were taken using an Olympus BX51 equipped with polarizer and analyser. Surface topographies of the thin films were examined by a 5500LS Scanning Probe Microscopy system from Agilent Technologies and subsequent data analysis was performed by using Gwyddion 2.56 software.

X-ray diffraction measurements were carried out with a PANalytical X'Pert Pro MRD (Materials Research Diffractometer) diffractometer. The Cu K-alpha radiation 1.54187 Å was used.

Time-of-flight secondary ion mass spectrometry (ToF-SIMS) measurements were performed using a TOF SIMS V instrument (ION-TOF GmbH, Muenster, Germany). The base pressure of the analysis chamber during the ToF-SIMS data acquisition was ~ $1.3\ 10^{-9}$ mbar. Bi_3^{++} primary ions at 30 keV provided by a liquid metal ion gun (LMIG) were used for surface analysis. For depth profiling in dual-beam mode, the analysis beam was combined with a sputter ion gun producing Cs^+ ions at 500 eV. The analysis area of the surface chemical maps was 500 µm × 500 µm. Sputtering was carried out over 300 µm × 300 µm areas inside the OFET active layer. Depth profiles were acquired over 100 µm × 100 µm areas within the centre of the sputter crater. The analysis beam (pulse width: 18.4 ns, current: ~ 0.3 pA) and the sputtering beam (current: ~ 6 nA) were employed in non-interlaced mode (1 analysis frame, 1 s sputter and 1 s pause per cycle) for sample charge compensation. Secondary ions were extracted at 2 kV and detected with a time-of-flight mass analyzer. A cycle time of 100

μs allowed to obtain a mass range from 1 m/z to 900 m/z. The detected secondary ions had negative and positive polarity. Negative and positive mass spectra were calibrated using CH^-, Si^-, C_5^-, and $C_{42}H_{50}Si_2^-$, and H^+, CH^+, CH_3^+, and $C_{42}H_{50}Si_2^+$ signal peaks, respectively. The mass resolution ($m \cdot \Delta m^{-1}$) achieved is better of 6000 for all analysed masses. Mass spectra and depth profile signals were exported for further analysis by SurfaceLab v6.5 software. A list of characteristic secondary ions was obtained for TMTES, TIPS and PS mass spectra through a multivariate analysis approach.

Device characterization

The OFETs were characterised by measuring their transfer and output characteristics, using an Agilent B1500A semiconductor device analyser connected to the samples with a Karl SÜSS probe station, at ambient conditions.

The characteristic field-effect mobility (μ) and threshold voltage (V_{TH}) parameters were extracted in saturation regime using the following classic MOSFET equation:

$$\mu = \frac{2L}{WC}\left(\frac{\partial\sqrt{|I_{DS}|}}{\partial V_{GS}}\right)^2$$

where C is insulator capacitance per unit area (C = 17.26 nF cm^{-2}), and W and L are the width and length of the channel, respectively. For each ink formulation, the devices parameters were extracted from at least 30 devices from 2 substrates to ensure thin film homogeneity and reproducibility.

The interfacial trap density for the majority charge carriers (i.e., holes) per unit area (N_T) was extracted directly to subthreshold swing (SS), and has been estimated using the following equations:

$$S = \left(\frac{\partial(\log I_{DS})}{\partial V_{GS}}\right)^{-1}$$

$$N_T \approx \frac{C}{q^2}\left[\frac{q\,SS}{k_B\,T\ln(10)} - 1\right]$$

where q is the electronic charge, k_B is the Boltzmann constant, and T is the absolute temperature.

During X-ray irradiation tests, the electrical photoresponse of the devices was measured by using a Keithley 2614 Source Meter, controlled by a customised Labview software. All measurements were carried out keeping the device in dark, in a Faraday cage, to reduce electrical noise and avoid light-induced photogeneration in the organic semiconductor.

X-ray irradiation

Two different X-ray beam sources are employed for the characterization of the detectors: a) Hamamatsu L12161 X-ray tube with tungsten target was used at fixed 40 kV operating voltage the filament current was changed between 100 and 500 μA leading to an incident dose rate on the samples between 318 and 1665 μGy s^{-1}. The dose rate calibrations were previously performed employing the Barracuda radiation detector (RTI Group). The modulation of the beam was obtained with a mechanical lead shutter placed close to the X-ray tube window. Keithley SMU 2614 was used in combination with a LabVIEW program for electrical signal acquisition. b) A monochromatic and aligned synchrotron X-ray beam with energy of 12 keV and dose rate in the range 0.05 – 35 mGy s^{-1}. Synchrotron measurements are carried out at ELETTRA - Trieste, in the SYRMEP beamline that is equipped with an ionization chamber for real-time dose rate monitoring. In addition, precision slits and a CCD camera allow to focus the beam and to control the irradiated area of the samples.

Theoretical calculations

The electronic couplings (i.e. transfer integrals) between all crystallographically independent pairs of nearby molecules in both TMTES polymorphs were calculated using DFT based calculations employing the Gaussian code[63] employing a 6-31(d,p) double zeta polarized basis set and the B3YLP hybrid functional[64]. The possible effects of differences in on-site energy for each molecule in a pair[65,66] was taken into account using the fragment charge difference approach as implemented in the e-coupling server.[67]

Supporting Information

Supporting Information is available from the Wiley Online Library or from the author.

Acknowledgements

This work was funded by the Spanish Government within: research projects GENESIS PID2019-111682RB-I00 and RTI2018-095460-B-I00, the “Severo Ochoa” Programme for Centers of Excellence in R&D (FUNFUTURE CEX2019-000917-S) and the “María de Maeztu” program for Spanish Structures of Excellence (MDM-2017-0767). Funding was also provided by the Generalitat de Catalunya (2017-SGR-918, 2017-SGR13). A.T. acknowledges his FPU fellowship and is enrolled in the UAB Materials Science PhD program. C.M-D acknowledges her Juan de la Cierva grant (ref. FJC2019-042161-I) from Ministerio de Ciencia e Innovación. I.F., A.C., B.F. and L.B acknowledge funding from INFN through the CSN5 FIRE project. All the authors acknowledge Giuliana Tromba and Diego Dreossi at ELETTRA synchrotron in Trieste for hardware and software technical support during the experiments, in particular for the acquisition of X-ray image.

Received: ((will be filled in by the editorial staff))
Revised: ((will be filled in by the editorial staff))
Published online: ((will be filled in by the editorial staff))

References

[1] S. Demchyshyn, M. Verdi, L. Basiricò, A. Ciavatti, B. Hailegnaw, D. Cavalcoli, M. C. Scharber, N. S. Sariciftci, M. Kaltenbrunner, B. Fraboni, *Adv. Sci.* 2020, *7*, 2002586.

[2] G. Lutz, *Semiconductor Radiation Detectors - Device Physics*, Springer-Verlag Berlin and Heidelberg GmbH & Co. KG, Heidelberg, Germany, 2007.

[3] A. Sultana, A. Reznik, K. S. Karim, J. A. Rowlands, *Med. Phys.* 2008, *35*, 4324.

[4] H. M. Thirimanne, K. D. G. I. Jayawardena, A. J. Parnell, R. M. I. Bandara, A. Karalasingam, S. Pani, J. E. Huerdler, D. G. Lidzey, S. F. Tedde, A. Nisbet, C. A. Mills, S. R. P. Silva, *Nat. Commun.* 2018, *9*, 2926.

[5] K. D. G. I. Jayawardena, H. M. Thirimanne, S. F. Tedde, J. E. Huerdler, A. J. Parnell, R. M. I. Bandara, C. A. Mills, S. R. P. Silva, *ACS Nano* 2019, *13*, 6973.

[6] M. P. A. Nanayakkara, L. Matjačić, S. Wood, F. Richheimer, F. A. Castro, S. Jenatsch, S. Züfle, R. Kilbride, A. J. Parnell, M. G. Masteghin, H. M. Thirimanne, A. Nisbet, K. D. G. I. Jayawardena, S. R. P. Silva, *Adv. Funct. Mater.* 2021, *31*, 2008482.

[7] A. Ciavatti, T. Cramer, M. Carroli, L. Basiricò, R. Fuhrer, D. M. De Leeuw, B. Fraboni, *Appl. Phys. Lett.* 2017, *111*, 183301.

[8] H. Li, X. Shan, J. N. Neu, T. Geske, M. Davis, P. Mao, K. Xiao, T. Siegrist, Z. Yu, *J. Mater. Chem. C* 2018, *6*, 11961.

[9] J. Peng, K. Ye, Y. Xu, L. Cui, R. Li, H. Peng, Q. Lin, *Sensors Actuators, A Phys.* 2020, *312*, 112132.

[10] A. Ciavatti, R. Sorrentino, L. Basiricò, B. Passarella, M. Caironi, A. Petrozza, B. Fraboni, *Adv. Funct. Mater.* 2021, *31*, 2009072.

[11] G. N. Ankah, P. Büchele, K. Poulsen, T. Rauch, S. F. Tedde, C. Gimmler, O. Schmidt, T. Kraus, *Org. Electron.* 2016, *33*, 201.

[12] L. Basiricò, A. Ciavatti, T. Cramer, P. Cosseddu, A. Bonfiglio, B. Fraboni, *Nat. Commun.* 2016, *7*, 13063.

[13] I. Temiño, L. Basiricò, I. Fratelli, A. Tamayo, A. Ciavatti, M. Mas-Torrent, B. Fraboni, *Nat. Commun.* 2020, *11*, 2136.

[14] A. Ciavatti, L. Basiricò, I. Fratelli, S. Lai, P. Cosseddu, A. Bonfiglio, J. E. Anthony, B. Fraboni, *Adv. Funct. Mater.* 2019, *29*, 1806119.

[15] F. G. del Pozo, S. Fabiano, R. Pfattner, S. Georgakopoulos, S. Galindo, X. Liu, S. Braun, M.

Fahlman, J. Veciana, C. Rovira, X. Crispin, M. Berggren, M. Mas-Torrent, *Adv. Funct. Mater.* 2016, *26*, 2379.

[16] I. Temiño, F. G. Del Pozo, M. R. Ajayakumar, S. Galindo, J. Puigdollers, M. Mas-Torrent, *Adv. Mater. Technol.* 2016, *1*, 1600090.

[17] A. Tamayo, S. Hofer, T. Salzillo, C. Ruzié, G. Schweicher, R. Resel, M. Mas-Torrent, *J. Mater. Chem. C* 2021, *9*, 7186.

[18] T. Salzillo, A. Campos, A. Babuji, R. Santiago, S. T. Bromley, C. Ocal, E. Barrena, R. Jouclas, C. Ruzie, G. Schweicher, Y. H. Geerts, M. Mas-Torrent, *Adv. Funct. Mater.* 2020, *30*, 2006115.

[19] A. Campos, S. Riera-Galindo, J. Puigdollers, M. Mas-Torrent, *ACS Appl. Mater. Interfaces* 2018, *10*, 15952.

[20] K. Zhang, T. Marszalek, P. Wucher, Z. Wang, L. Veith, H. Lu, H. J. Räder, P. M. Beaujuge, P. W. M. Blom, W. Pisula, *Adv. Funct. Mater.* 2018, *28*, 1805594.

[21] J. Panidi, A. F. Paterson, D. Khim, Z. Fei, Y. Han, L. Tsetseris, G. Vourlias, P. A. Patsalas, M. Heeney, T. D. Anthopoulos, *Adv. Sci.* 2018, *5*, 1700290.

[22] K. Zhao, O. Wodo, D. Ren, H. U. Khan, M. R. Niazi, H. Hu, M. Abdelsamie, R. Li, E. Q. Li, L. Yu, B. Yan, M. M. Payne, J. Smith, J. E. Anthony, T. D. Anthopoulos, S. T. Thoroddsen, B. Ganapathysubramanian, A. Amassian, *Adv. Funct. Mater.* 2016, *26*, 1737.

[23] M. R. Niazi, R. Li, E. Qiang Li, A. R. Kirmani, M. Abdelsamie, Q. Wang, W. Pan, M. M. Payne, J. E. Anthony, D. M. Smilgies, S. T. Thoroddsen, E. P. Giannelis, A. Amassian, *Nat. Commun.* 2015, *6*, 8598.

[24] M. B. Madec, J. J. Morrison, V. Sanchez-Romaguera, M. L. Turner, S. G. Yeates, *J. Mater. Chem.* 2009, *19*, 6750.

[25] J. H. Lee, Y. Seo, Y. D. Park, J. E. Anthony, D. H. Kwak, J. A. Lim, S. Ko, H. W. Jang, K. Cho, W. H. Lee, *Sci. Rep.* 2019, *9*, 21.

[26] M. Berteau-rainville, A. Tamayo, T. Leydecker, A. Pezeshki, E. Orgiu, M. Mas-torrent, *Appl. Phys. Express* 2021, *119*, 103301.

[27] D. J. Gundlach, J. E. Royer, S. K. Park, S. Subramanian, O. D. Jurchescu, B. H. Hamadani, A. J. Moad, R. J. Kline, L. C. Teague, O. Kirillov, C. A. Richter, J. G. Kushmerick, L. J. Richter, S. R. Parkin, T. N. Jackson, J. E. Anthony, *Nat. Mater.* 2008, *7*, 216.

[28] T. Salzillo, N. Montes, R. Pfattner, M. Mas-Torrent, *J. Mater. Chem. C* 2020, *8*, 15361.

[29] M. R. Niazi, R. Li, M. Abdelsamie, K. Zhao, D. H. Anjum, M. M. Payne, J. Anthony, D. M. Smilgies, A. Amassian, *Adv. Funct. Mater.* 2016, *26*, 2371.

[30] S. Choi, F. A. Larrain, C. Y. Wang, C. Fuentes-Hernandez, W. F. Chou, B. Kippelen, *J. Mater. Chem. C* 2016, *4*, 8297.

[31] S. Li, D. Guérin, K. Lmimouni, *Microelectron. Eng.* 2018, *195*, 62.

[32] Z. A. Lamport, K. J. Barth, H. Lee, E. Gann, S. Engmann, H. Chen, M. Guthold, I. McCulloch, J. E. Anthony, L. J. Richter, D. M. DeLongchamp, O. D. Jurchescu, *Nat. Commun.* 2018, *9*, 5130.

[33] A. Pérez-Rodríguez, I. Temiño, C. Ocal, M. Mas-Torrent, E. Barrena, *ACS Appl. Mater. Interfaces* 2018, *10*, 7296.

[34] F. Leonardi, S. Casalini, Q. Zhang, S. Galindo, D. Gutiérrez, M. Mas-Torrent, *Adv. Mater.* 2016, *28*, 10311.

[35] R. Hamilton, J. Smith, S. Ogier, M. Heeney, J. E. Anthony, I. McCulloch, J. Veres, D. D. C. Bradley, T. D. Anthopoulos, *Adv. Mater.* 2009, *21*, 1166.

[36] G. R. Llorente, M. B. Dufourg-Madec, D. J. Crouch, R. G. Pritchard, S. Ogier, S. G. Yeates, *Chem. Commun.* 2009, 3059.

[37] J. F. Chang, T. Sakanoue, Y. Olivier, T. Uemura, M. B. Dufourg-Madec, S. G. Yeates, J. Cornil, J. Takeya, A. Troisi, H. Sirringhaus, *Phys. Rev. Lett.* 2011, *107*, 066601.

[38] S. Illig, A. S. Eggeman, A. Troisi, L. Jiang, C. Warwick, M. Nikolka, G. Schweicher, S. G. Yeates, Y. Henri Geerts, J. E. Anthony, H. Sirringhaus, *Nat. Commun.* 2016, *7*, 10736.

[39] S. Riera-Galindo, A. Tamayo, M. Mas-Torrent, *ACS Omega* 2018, *3*, 2329.

[40] H. Chung, Y. Diao, *J. Mater. Chem. C* 2016, *4*, 3915.

[41] V. Coropceanu, J. Cornil, D. A. da Silva Filho, Y. Olivier, R. Silbey, J. L. Brédas, *Chem. Rev.* 2007, *107*, 926.

[42] R. Pfattner, S. T. Bromley, C. Rovira, M. Mas-Torrent, *Adv. Funct. Mater.* 2016, *26*, 2256.

[43] G. Schweicher, V. Lemaur, C. Niebel, C. Ruzié, Y. Diao, O. Goto, W. Y. Lee, Y. Kim, J. B. Arlin, J. Karpinska, A. R. Kennedy, S. R. Parkin, Y. Olivier, S. C. B. Mannsfeld, J. Cornil, Y. H. Geerts, Z. Bao, *Adv. Mater.* 2015, *27*, 3066.

[44] P. J. Skabara, J. B. Arlin, Y. H. Geerts, *Adv. Mater.* 2013, *25*, 1948.

[45] A. Campos, N. Oxtoby, S. Galindo, R. Pfattner, J. Veciana, S. T. Bromley, C. Rovira, M. Mas-Torrent, *CrystEngComm* 2016, *18*, 6149.

[46] K. L. Mccall, S. R. Rutter, E. L. Bone, N. D. Forrest, J. S. Bissett, J. D. E. Jones, M. J. Simms, A. J. Page, R. Fisher, B. A. Brown, S. D. Ogier, *Adv. Funct. Mater.* 2014, *24*, 3067.

[47] M. M. Ibrahim, A. C. MacIel, C. P. Watson, M. B. Madec, S. G. Yeates, D. M. Taylor, *Org. Electron.* 2010, *11*, 1234.

[48] A. Y. B. Meneau, Y. Olivier, T. Backlund, M. James, D. W. Breiby, J. W. Andreasen, H. Sirringhaus, *Adv. Funct. Mater.* 2016, *26*, 2326.

[49] A. Tamayo, T. Salzillo, M. Mas-torrent, *Adv. Mater. Interfaces* 2022, *9*, 2101679.

[50] Y. Gao, Y. Ge, X. Wang, J. Liu, W. Liu, Y. Cao, K. Gu, Z. Guo, Y. M. Wei, N. Zhou, D. Yu, H. Meng, X. F. Yu, H. Zheng, W. Huang, J. Li, *Adv. Mater.* 2021, *33*, 2101717.

[51] A. M. Zeidell, T. Ren, D. S. Filston, H. F. Iqbal, E. Holland, J. D. Bourland, J. E. Anthony, O. D. Jurchescu, *Adv. Sci.* 2020, *7*, 2001522.

[52] S. Lai, P. Cosseddu, L. Basiricò, A. Ciavatti, B. Fraboni, A. Bonfiglio, *Adv. Electron. Mater.* 2017, *3*, 1600409.

[53] L. Basiricò, A. Ciavatti, I. Fratelli, D. Dreossi, G. Tromba, S. Lai, P. Cosseddu, A. Bonfiglio, F. Mariotti, C. Dalla Val, V. Bellucci, J. E. Anthony, B. Fraboni, *Front. Phys.* 2020, *8*, 10.3389/fphy.2020.00013.

[54] L. Mao, Y. Li, H. Chen, L. Yu, J. Zhang, *Nanomaterials* 2021, *11*, 1832.

[55] H. M. Thirimanne, K. D. G. I. Jayawardena, A. Nisbet, Y. Shen, R. M. I. Bandara, C. A. Mills, G. Shao, S. R. P. Silva, *IEEE Trans. Nucl. Sci.* 2020, *67*, 2238.

[56] J. Liu, B. Shabbir, C. Wang, T. Wan, Q. Ou, P. Yu, A. Tadich, X. Jiao, D. Chu, D. Qi, D. Li, R. Kan, Y. Huang, Y. Dong, J. Jasieniak, Y. Zhang, Q. Bao, *Adv. Mater.* 2019, *31*, 1901644.

[57] J. Zhao, L. Zhao, Y. Deng, X. Xiao, Z. Ni, S. Xu, J. Huang, *Nat. Photonics* 2020, *14*, 612.

[58] H. Tsai, F. Liu, S. Shrestha, K. Fernando, S. Tretiak, B. Scott, D. T. Vo, J. Strzalka, W. Nie, *Sci. Adv.* 2020, *6*, eaay0815.

[59] H. Mescher, F. Schackmar, H. Eggers, T. Abzieher, M. Zuber, E. Hamann, T. Baumbach, B. S. Richards, G. Hernandez-Sosa, U. W. Paetzold, U. Lemmer, *ACS Appl. Mater. Interfaces* 2020, *12*, 15774.

[60] J. Guo, Y. Xu, W. Yang, B. Xiao, Q. Sun, X. Zhang, B. Zhang, M. Zhu, W. Jie, *ACS Appl. Mater. Interfaces* 2021, *13*, 23928.

[61] L. Basiricò, S. P. Senanayak, A. Ciavatti, M. Abdi-Jalebi, B. Fraboni, H. Sirringhaus, *Adv. Funct. Mater.* 2019, *29*, 1902346.

[62] Pexraytech, Portable X-Ray Systems, Security Systems, Https://pexraytech.com/security-systems/ 26th Febrary, 2022.

[63] M. Frisch, G. Trucks, H. Schlegel, G. Scuseria, M. Robb, J. Cheeseman, G. Scalmani, V. Barone, G. Petersson, H. Nakatsuji, *Gaussian09, Revis. D 1*.

[64] P. J. Stephen, F. J. Devlin, C. F. Chabalowski, M. J. Frisch, *J. Phys. Chem.* 1994, *98*, 11623.

[65] K. Senthilkumar, F. C. Grozema, F. M. Bickelhaupt, L. D. A. Siebbeles, *J. Chem. Phys.* 2003, *119*, 9809.

[66] E. F. Valeev, V. Coropceanu, D. A. Da Silva Filho, S. Salman, J. L. Brédas, *J. Am. Chem. Soc.* 2006, *128*, 9882.

[67] I. Cabeza de Vaca, S. Acebes, V. Guallar, *J. Comput. Chem.* 2016, *37*, 1740.

Supporting Information

X-ray detectors with ultrahigh sensitivity employing high performance transistors based on a fully organic small molecule semiconductor/polymer blend active layer

Adrián Tamayo,[1] Ilaria Fratelli,[2] Andrea Ciavatti,[2] Carme Martínez-Domingo,[1] Paolo Branchini,[3,4] Elisabetta Colantoni,[3,4,5] Stefania De Rosa,[3,4] Luca Tortora,[3,4,6] Adriano Contillo,[7] Raul Santiago,[8] Stefan T. Bromley,[8,9] Beatrice Fraboni,[2,] Marta Mas-Torrent,[1,*] Laura Basiricò[2]*

[1] Institut de Ciència de Materials de Barcelona (ICMAB-CSIC) and Networking Research Center on Bioengineering, Biomaterials and Nanomedicine (CIBER-BBN), Campus de la Universitat Autònoma de Barcelona, Cerdanyola, E-08193 Barcelona, Spain.

[2] Department of Physics and Astronomy, University of Bologna and National Institute for Nuclear Physics - INFN section of Bologna, Viale Berti Pichat 6/2, 40127 Bologna, Italy.

[3] Surface Analysis Laboratory INFN Roma Tre, Via della Vasca Navale 84, 00146 Rome, Italy.

[4] INFN, Roma Tre, via della Vasca Navale 84, Rome, Italy.

[5] Department of Mathematics and Physics, Roma Tre University, via della Vasca Navale 84, Rome, Italy.

[6] Department of Sciences, Roma Tre University, Via della Vasca Navale 84, Rome, Italy.

[7] Elettra-Sincrotrone Trieste, Area Science Park Strada Statale 14, km 163.5, 34149 Basovizza, Trieste , Italy

[8] Departament de Ciència de Materials i Química Física & Institut de Química Teòrica i Computacional (IQTCUB), Universitat de Barcelona, Barcelona, Spain.

[9] Institució Catalana de Recerca i Estudis Avançats (ICREA), Barcelona, Spain.

Table S1. Electrical parameters of OFETs based on films of TMTES and TMTES:PS deposited by BAMS. The parameters are calculated for OFETs with the conducting channel parallel (∥) and perpendicular (⊥) to the coating direction.

Ink formulation	**Speed (mm s^{-1})**		**Mobility ($cm^2 V^{-1} s^{-1}$)**	**V_{TH} (V)**	**On/Off**	**μ^{max} ($cm^2 V^{-1} s^{-1}$)**
TMTES	1	∥	$(1.1 \pm 0.3)\cdot10^{-1}$	(30 ± 10)	10^3	0.19 ± 0.2
		⊥	$(9 \pm 4)\cdot10^{-2}$	(40 ± 10)	10^3	0.11 ± 0.2
	10	∥	$(1.0 \pm 0.3)\cdot10^{-1}$	(27 ± 9)	10^3	0.22 ± 0.3
		⊥	$(7.4 \pm 1.9)\cdot10^{-2}$	(34 ± 9)	10^3	0.10 ± 0.2
TMTES:PS (4:1) PS_{10K}	1	∥	1.2 ± 0.2	2 ± 2	10^4	1.4 ± 0.2
		⊥	0.2 ± 0.1	4 ± 3	10^4	0.4 ± 0.2
	10	∥	1.3 ± 0.3	1 ± 1	10^4	1.6 ± 0.2
		⊥	0.7 ± 0.3	-0.1 ± 0.3	10^4	0.9 ± 0.2
TMTES:PS (4:1) PS_{280K}	1	∥	0.7 ± 0.1	-(2 ± 1)	10^4	0.9 ± 0.2
		⊥	0.4 ± 0.3	-(2.6 ± 0.7)	10^4	0.7 ± 0.2
	10	∥	1.7 ± 0.4	-(0.7 ± 0.2)	10^4	2.3 ± 0.3
		⊥	1.0 ± 0.2	-(0.2 ± 0.6)	10^4	1.5 ± 0.2
TMTES:PS (2:1) PS_{280K}	1	∥	2.4 ± 0.4	-(0.53 ± 0.17)	10^5	3.6 ± 0.4
		⊥	2.0 ± 0.4	-(0.45 ± 0.15)	10^5	2.5 ± 0.3
	10	∥	**2.6 ± 0.6**	**-(1.1 ± 0.2)**	**10^5**	**3.1 ± 0.2**
		⊥	**2.1 ± 0.6**	**-(1.00±0.11)**	**10^5**	**2.8 ± 0.3**
TMTES:PS (1:2) PS_{280K}	1	∥	1.1±0.2	-(0.4 ± 0.8)	10^4	1.6 ± 0.2
		⊥	1.0±0.3	-(0.4 ± 0.3)	10^4	1.4 ± 0.3
	10	∥	0.9±0.2	-(1.0 ± 0.2)	10^4	1.4 ± 0.2
		⊥	0.7±0.3	-(0.9 ± 0.3)	10^4	1.0 ± 0.2

Table S2. Comparison of our results with the electrical transport parameters of solution processed OFETs based on TMTES reported in literature.

OSC Formulation	Scalable to Roll-to-Roll (Deposition Technique)	Binder	μ ($cm^2 \cdot V^{-1} \cdot s^{-1}$)	V_{TH} (V)	Ref
2.0 wt % CB (2:1) PS	YES (Solution Shearing)	YES	2.6±0.6	-1	This work
2.0 wt % CB	YES (Solution Shearing)	NO	0.10±0.03	~30	This work
0.5 wt % TL	NO (Drop casting)	NO	1.3±0.4	NA	1
1.2 wt % TE (1:2) 4-iPrCN-TAA/C8-Flu (70:30)	NO (Spin coating)	YES	4.3±0.3	~10	2
TE	NO (Spin coating)	NO	2.6-3.5	~40	3
1wt % TE	NO (Drop casting)	NO	0.3	~0	4
1 wt% TE (1:1) (iPVN)	NO (Drop casting)	YES	0.07	~0	4
n.r.-	NO (Spin coating)	NO	1.9		5

(CB) chlorobenzene, (TL) toluene, (TE) tetralin, (iPVN) isotactic poly(a-vinyl naphthalene and (4-iPrCN-TAA/C8-Flu) 4-isopropylcyano triarylamine/n-octyl Fluorene, 70/30 copolymer. n.r.: not reported.

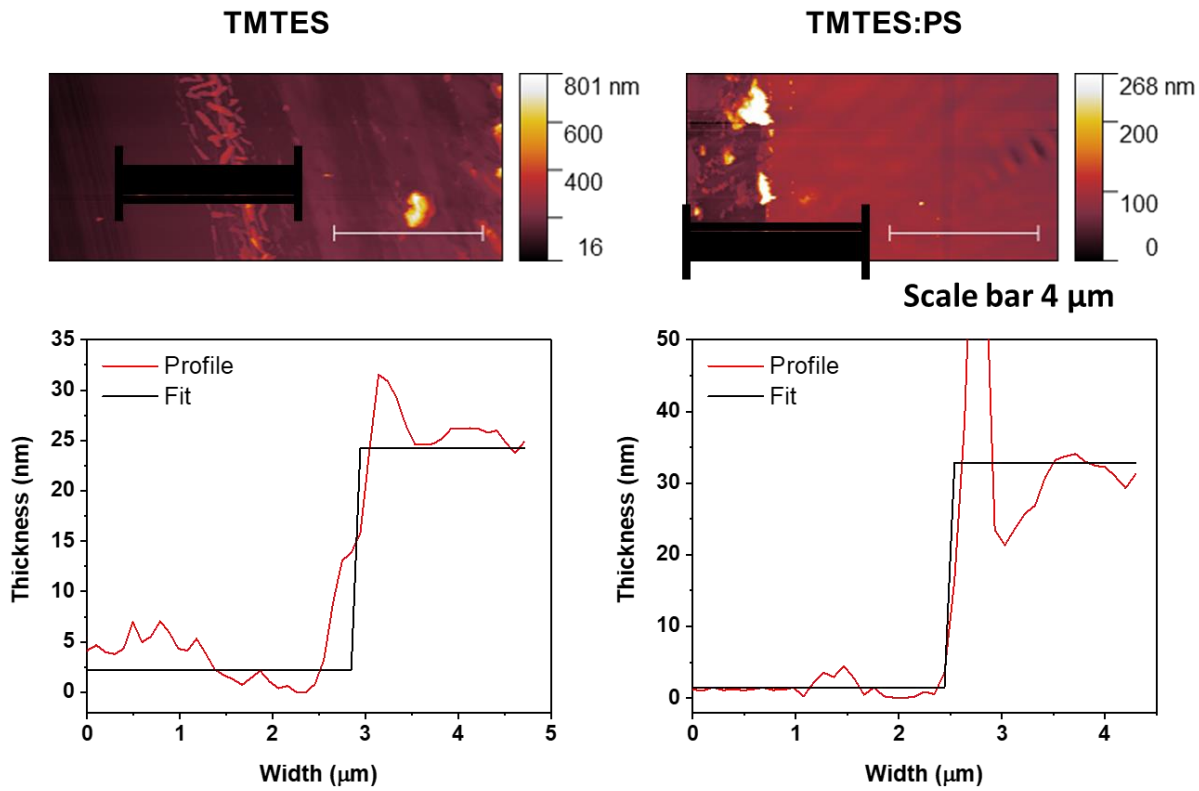

Figure S1. Topographic AFM images (top) and depth profiles (bottom) for thickness estimation of the TMTES and TMTES:PS thin films.

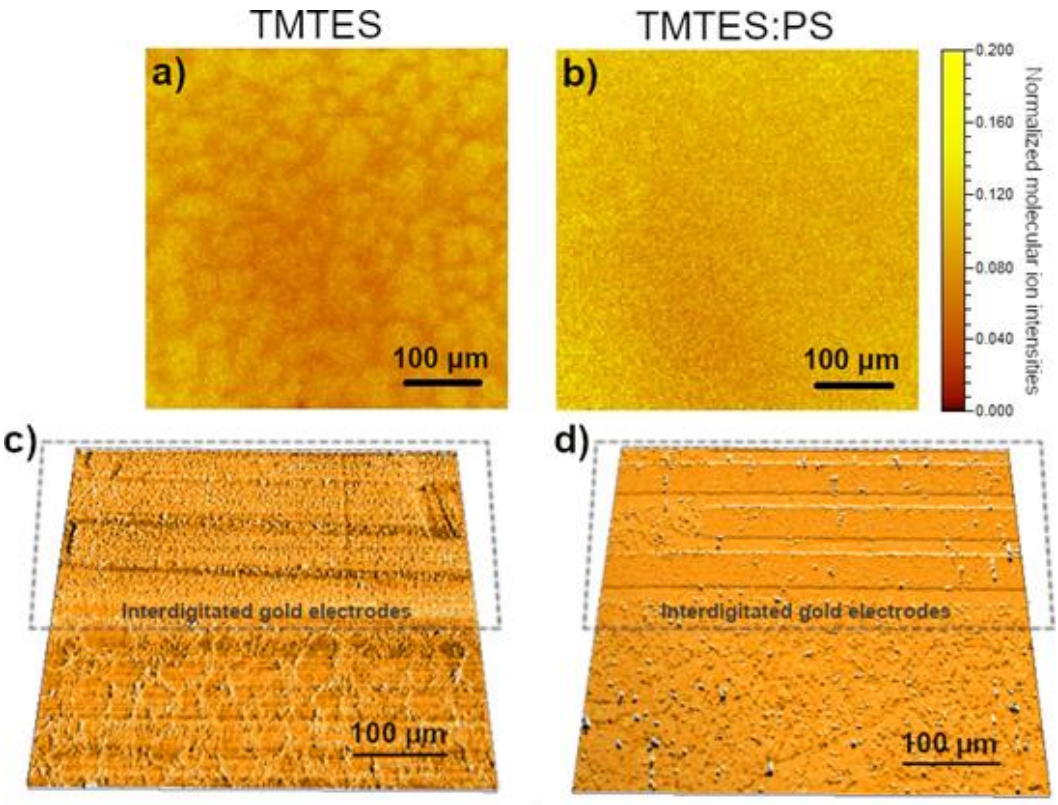

Figure S2. ToF-SIMS 2D surface chemical maps of TMTES and TMTES:PS thin films deposited by BAMS at high coating speed. Normalized (to total counts) sum of $Si_2C_{42}H_{50}^+$ (m/z = 610.34), $Si_2{}^{13}CC_{41}H_{50}^+$ (m/z = 611.35), $Si_2{}^{13}C_2C_{40}H_{50}^+$ (m/z = 612.35), $^{30}SiSi^{13}CC_{41}H_{50}^+$ (m/z=613.34), $^{30}SiSi^{13}C_2C_{40}H_{50}^+$ (m/z = 614.35), and $^{30}SiSi^{13}C_3C_{39}H_{50}^+$ (m/z = 615.35) secondary ion signals from (a) TMTES and (b) TMTES:PS surface acquired outside the interdigitated electrodes. 3D surface height profiles maps of c) TMTES and d) TMTES:PS films with the interdigitated gold electrodes.

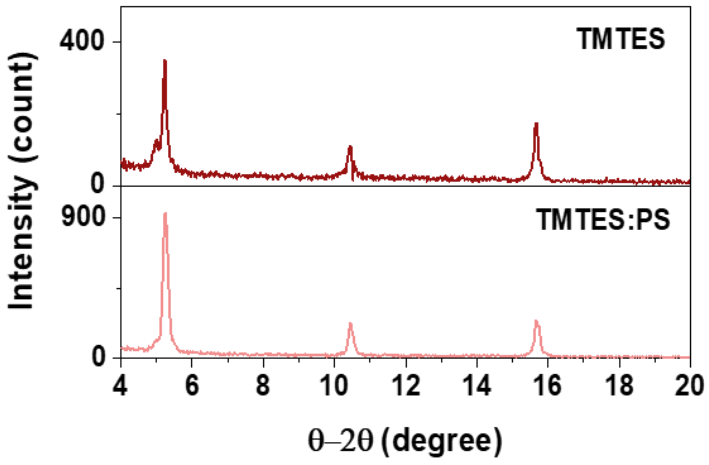

Figure S3. X-ray diffractograms of TMTES and TMTES:PS thin films deposited by BAMS.

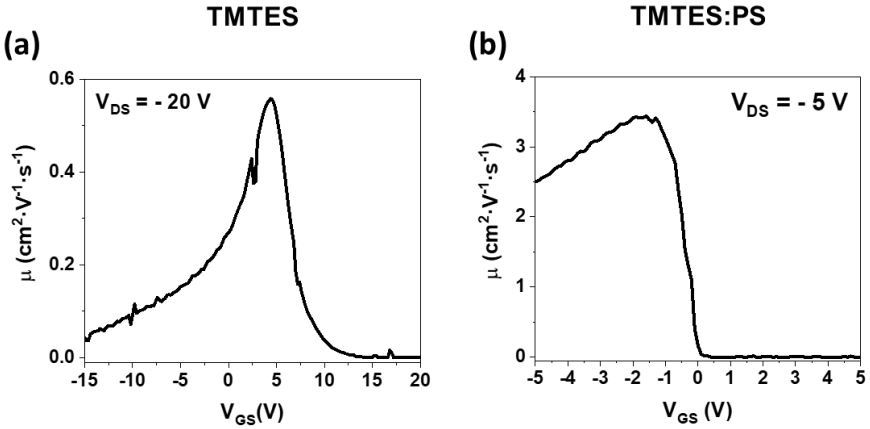

Figure S4. Dependence of charge carrier mobility on the applied gate voltage for OFETs based on (a) TMTES and (b) TMTES:PS.

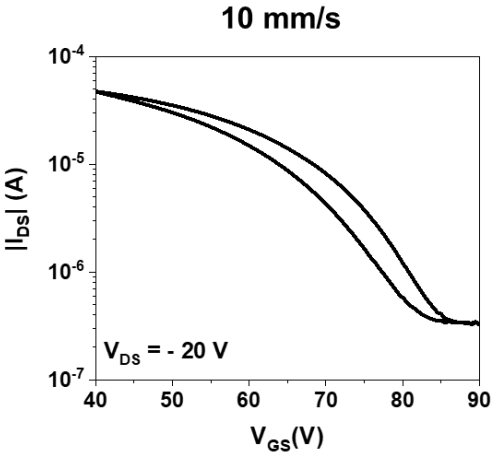

Figure S5. Transfer characteristics in saturation regime of TMTES OFETs measured 90 days after their fabrication

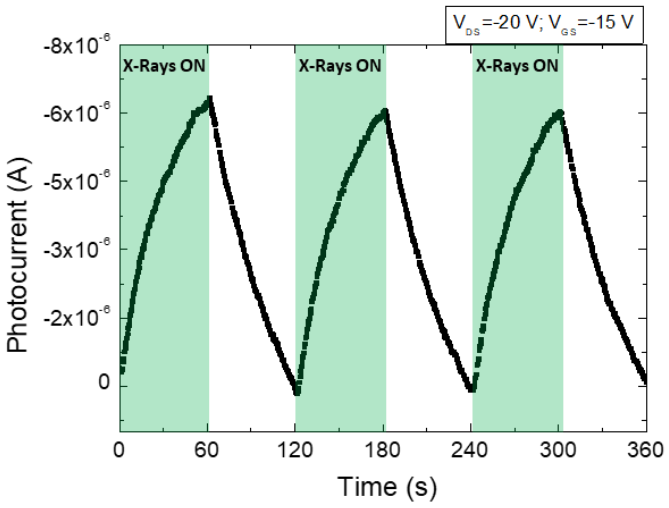

Figure S6. X-ray induced photocurrent response of a TMTES:PS BAMS-coated device upon three on/off switching cycles (green areas correspond to time windows of 60 s) employing a dose rate of 9.8 mGy s^{-1}.

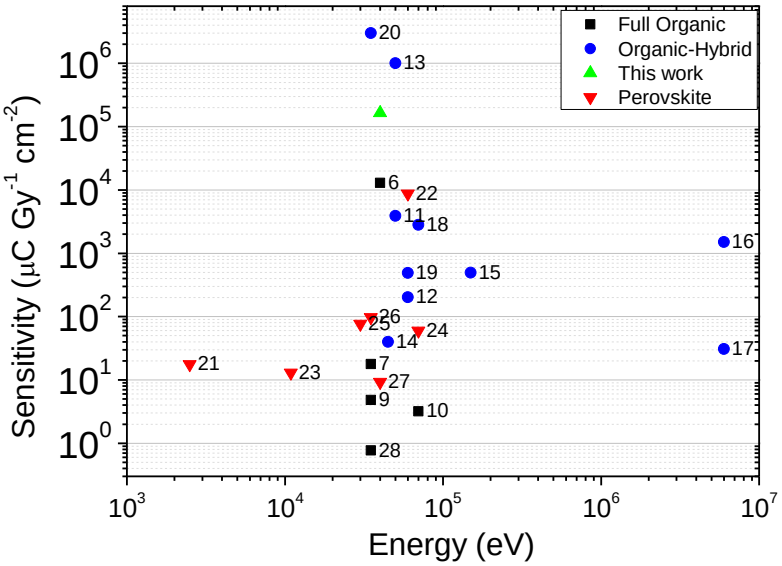

Figure S7. Comparison of the sensitivity values per unit area achieved in this work (green triangle), with those reported at the state of the art for thin-film detectors based on perovskite (red triangles), organic-hybrid (blue circles), and full-organic (black squares) active layers.[6-28]

Bibliography

[1] G. R. Llorente, M. B. Dufourg-Madec, D. J. Crouch, R. G. Pritchard, S. Ogier, S. G. Yeates, Chem. Commun. 2009, 3059.

[2] K. L. Mccall, S. R. Rutter, E. L. Bone, N. D. Forrest, J. S. Bissett, J. D. E. Jones, M. J. Simms, A. J. Page, R. Fisher, B. A. Brown, S. D. Ogier, Adv. Funct. Mater. 2014, 24, 3067.

[3] J. F. Chang, T. Sakanoue, Y. Olivier, T. Uemura, M. B. Dufourg-Madec, S. G. Yeates, J. Cornil, J. Takeya, A. Troisi, H. Sirringhaus, Phys. Rev. Lett. 2011, 107, 066601.

[4] M. M. Ibrahim, A. C. MacIel, C. P. Watson, M. B. Madec, S. G. Yeates, D. M. Taylor, Org. Electron. 2010, 11, 1234.

[5] A. Y. B. Meneau, Y. Olivier, T. Backlund, M. James, D. W. Breiby, J. W. Andreasen, H. Sirringhaus, Adv. Funct. Mater. 2016, 26, 2326.

[6] I. Temiño, L. Basiricò, I. Fratelli, A. Tamayo, A. Ciavatti, M. Mas-Torrent, B. Fraboni, Nat. Commun. 2020, 11, 2136.

[7] A. Ciavatti, L. Basiricò, I. Fratelli, S. Lai, P. Cosseddu, A. Bonfiglio, J. E. Anthony, B. Fraboni, Adv. Funct. Mater. 2019, 29, 1806119.

[8] A. M. Zeidell, T. Ren, D. S. Filston, H. F. Iqbal, E. Holland, J. D. Bourland, J. E. Anthony, O. D. Jurchescu, Adv. Sci. 2020, 7, 2001522.

[9] S. Lai, P. Cosseddu, L. Basiricò, A. Ciavatti, B. Fraboni, A. Bonfiglio, Adv. Electron. Mater. 2017, 3, 1600409.

[10] L. Basiricò, A. Ciavatti, I. Fratelli, D. Dreossi, G. Tromba, S. Lai, P. Cosseddu, A. Bonfiglio, F. Mariotti, C. Dalla Val, V. Bellucci, J. E. Anthony, B. Fraboni, Front. Phys. 2020, 8, 10.3389/fphy.2020.00013.

[11] H. M. Thirimanne, K. D. G. I. Jayawardena, A. J. Parnell, R. M. I. Bandara, A. Karalasingam, S. Pani, J. E. Huerdler, D. G. Lidzey, S. F. Tedde, A. Nisbet, C. A. Mills, S. R. P. Silva, Nat. Commun. 2018, 9, 2926.

[12] L. Mao, Y. Li, H. Chen, L. Yu, J. Zhang, Nanomaterials 2021, 11, 1832.

[13] Y. Gao, Y. Ge, X. Wang, J. Liu, W. Liu, Y. Cao, K. Gu, Z. Guo, Y. M. Wei, N. Zhou, D. Yu, H. Meng, X. F. Yu, H. Zheng, W. Huang, J. Li, Adv. Mater. 2021, 33, 2101717.

[14] H. Li, X. Shan, J. N. Neu, T. Geske, M. Davis, P. Mao, K. Xiao, T. Siegrist, Z. Yu, J. Mater. Chem. C 2018, 6, 11961.

[15] A. Ciavatti, R. Sorrentino, L. Basiricò, B. Passarella, M. Caironi, A. Petrozza, B. Fraboni, Adv. Funct. Mater. 2021, 31, 2009072.

[16] M. P. A. Nanayakkara, L. Matjačić, S. Wood, F. Richheimer, F. A. Castro, S. Jenatsch, S. Züfle, R. Kilbride, A. J. Parnell, M. G. Masteghin, H. M. Thirimanne, A. Nisbet, K. D. G. I. Jayawardena, S. R. P. Silva, Adv. Funct. Mater. 2021, 31, 2008482.

[17] H. M. Thirimanne, K. D. G. I. Jayawardena, A. Nisbet, Y. Shen, R. M. I. Bandara, C. A. Mills, G. Shao, S. R. P. Silva, IEEE Trans. Nucl. Sci. 2020, 67, 2238.

[18] K. D. G. I. Jayawardena, H. M. Thirimanne, S. F. Tedde, J. E. Huerdler, A. J. Parnell, R. M. I. Bandara, C. A. Mills, S. R. P. Silva, ACS Nano 2019, 13, 6973.

[19] J. Peng, K. Ye, Y. Xu, L. Cui, R. Li, H. Peng, Q. Lin, Sensors Actuators, A Phys. 2020, 312, 112132.

[20] A. Ciavatti, T. Cramer, M. Carroli, L. Basiricò, R. Fuhrer, D. M. De Leeuw, B. Fraboni, Appl. Phys. Lett. 2017, 111, 183301.

[21] J. Liu, B. Shabbir, C. Wang, T. Wan, Q. Ou, P. Yu, A. Tadich, X. Jiao, D. Chu, D. Qi, D. Li, R. Kan, Y. Huang, Y. Dong, J. Jasieniak, Y. Zhang, Q. Bao, Adv. Mater. 2019, 31, 1901644.

[22] J. Zhao, L. Zhao, Y. Deng, X. Xiao, Z. Ni, S. Xu, J. Huang, Nat. Photonics 2020, 14, 612.

[23] H. Tsai, F. Liu, S. Shrestha, K. Fernando, S. Tretiak, B. Scott, D. T. Vo, J. Strzalka, W. Nie, Sci. Adv. 2020, 6, eaay0815.

[24] H. Mescher, F. Schackmar, H. Eggers, T. Abzieher, M. Zuber, E. Hamann, T. Baumbach, B. S. Richards, G. Hernandez-Sosa, U. W. Paetzold, U. Lemmer, ACS Appl. Mater. Interfaces 2020, 12, 15774.

[25] J. Guo, Y. Xu, W. Yang, B. Xiao, Q. Sun, X. Zhang, B. Zhang, M. Zhu, W. Jie, ACS Appl. Mater. Interfaces 2021, 13, 23928.

[26] L. Basiricò, S. P. Senanayak, A. Ciavatti, M. Abdi-Jalebi, B. Fraboni, H. Sirringhaus, Adv. Funct. Mater. 2019, 29, 1902346.

[27] S. Demchyshyn, M. Verdi, L. Basiricò, A. Ciavatti, B. Hailegnaw, D. Cavalcoli, M. C. Scharber, N. S. Sariciftci, M. Kaltenbrunner, B. Fraboni, Adv. Sci. 2020, 7, 2002586.

[28] L. Basiricò, A. Ciavatti, T. Cramer, P. Cosseddu, A. Bonfiglio, B. Fraboni, *Nat. Commun.* 2016, *7*, 13063.

CHAPTER IV

ELECTROLYTE-GATED ORGANIC FIELD EFFECT TRANSISTORS: MODIFICATION OF THE ELECTROLYTE/GATE INTERFACE

4.1 TUNING OF THE GATE ELECTRODE/ELECTROLYTE INTERFACE IN EGOFET DEVICES

Nowadays, the design and development of biosensors have taken a centre stage in a wide range of applications, such as health care and disease diagnosis, environmental monitoring, water and food quality monitoring, and drug delivery.[1] In the recent decade, the field of diagnostics by a biosensor based on OFET devices is raising great interest in the scientific community.[2–7]

Electrolyte-Gated Organic Field-Effect Transistors (EGOFETs) were first reported by Kergoat *et al*.[8] EGOFETs are a special configuration of OFET, in which instead of using a conventional dielectric, an electrolyte media is employed and the gate contact is immersed into it. EGOFETs are excellent platforms for the development of biosensors because they operate in aqueous environment, at low voltages and can transduce and amplify surface phenomena into electronic signals.[7,9–12] EGOFETs work in accumulation mode, where the gate voltage induces the charging of the electrolyte-semiconductor interface, and it relies on the capacitive coupling between the gate electrode and the organic semiconductor (OSC) layer thought the electrolyte (**Figure 4.1a**).[13] The capacitance of the EGOFET is determined by two electrical double layers (EDLs),[8,14] which are formed by an array of charged particles and oriented dipoles at the gate electrode/electrolyte and electrolyte/OSC interfaces. The value of capacitance in the EDL is the storge charge at the surface of the interfaces for each unit of voltage, which is expressed by the following relationship:

$$C = \frac{Q}{V} \qquad (4.1)$$

where C is the capacitance, Q is the total charge stored at the surfaces and V is the electrical potential.[15]

In EGOFETs, the potential drop between the gate electrode and the channel interfaces occurs at the EDLs, while in OFETs occurs linearly along the dielectric material (**Figure 4.1b**). This makes EGOFETs highly sensitive to changes taking place at the interfaces and, hence, they can be applied to design sensors, where small modifications of the gate/electrolyte or electrolyte/OSC interfaces would produce important changes in the potential drop

distribution. Further, the low thickness of EDLs (i.e., sub-nano scale) results in a large capacity value in the order of 1-40 µF·cm^{-2}, which yields devices with low-voltage operation (< 1 V), crucial for biosensing applications.[10,16–18]

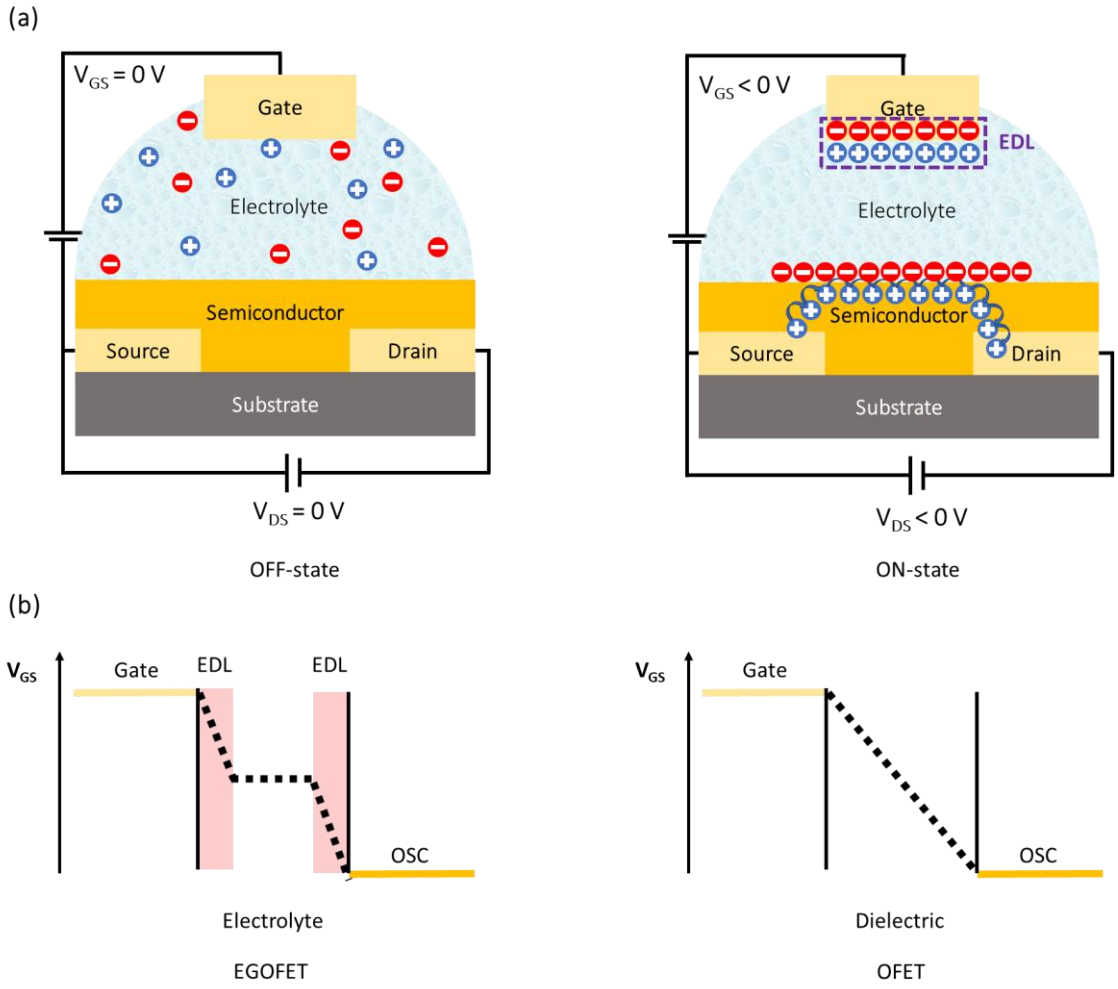

Figure 4.1. (a) Schematic simplified representation of the operation mechanism of a p-type EGOFET device in off-state and on-state. **(b)** Schematic diagram of the potential drop between the gate electrode interface and the channel interface in an OFET and EGOFET device.

Changes in the capacitance of the EDLs result in changes in the slope of the transfer characteristics of the EGOFETs. On the other hand, EGOFETs respond also to changes of the electrochemical potential at the OSCs/electrolyte and gate/electrolyte interfaces, which typically give rise to threshold voltage shifts in the devices.[7,9] The modification of the electrochemical gate potential also leads to changes in the flat-band potential.

The threshold voltage describes the voltage required to create a conducting channel, while the flat-band voltage (V_{FB}) corresponds to the voltage in which there is no electrical charge

in the OSC and, therefore, no voltage drop across it. Kergoat *et al*. proved a clear linear dependence between the threshold voltage and the flat-band potential.[19]

The flat-band potential can be described by the following equation:

$$V_{FB} = \frac{W_M - W_S}{q} - \frac{Q}{C} \qquad (4.2)$$

where W_M and W_S are the gate and semiconductor work functions, respectively, q is the charge of the electron, Q is the interface charge density, and C is the capacitance of the insulator layer (per unit area).

Therefore, surface engineering of the gate electrode, that is, the type of electrode material as well as its surface modification, has a direct impact on the EGOFET response since the electrode work function and the capacitance of the EDLs formed can be significantly modified.[20,21]

In this chapter, we investigated the impact of the gate surface modification by means of self-assembled monolayers (SAMs) of different chemical nature on the device response. In addition, in the second part of the chapter, we substituted the conventional gold gate electrode by home-made carbon composite electrodes to explore the potential of these electrodes in EGOFETs. Finally, the physical adsorption of surfactant molecules at the gate/electrolyte and electrolyte/OSC was explored. We found that EGOFETs can be an excellent tool to monitor the formation of monolayers at the electrode surface and, at the same time, that the use of high concentration of surfactants can be exploited to encapsulate the OSC and achieve long-term stabilization of the EGOFETs. All these experiments were performed on EGOFETs fabricated on flexible substrates.

4.2. MODIFICATION OF THE GOLD GATE ELECTRODE WITH SELF-ASSEMBLED MONOLAYERS

Article 10: Modification of the gate electrode by self-assembled monolayers in flexible electrolyte-gated organic field effect transistors: work function vs. capacitance effects.

In this paper, we reported a systematic research of the impact of the chemical functionalization of a coplanar gold gate electrode on the electrical performance of a flexible EGOFET based on dibenzotetrathiafulvalene:polystyrene blends (DB-TTF:PS).

Additionally, a new strategy to fabricate EGOFETs with coplanar gate electrodes was carried out.

Self-assembled monolayers provide an excellent approach for tuning the interfacial properties of metals and semiconductors and have been exploited for a wide range of applications. In organic transistors, SAMs have been applied to reduce the charge trapping at the SiO_2/OSC interface, to improve the crystallization of OSCs,[22–24] tune the surface wettability for patterning,[25] and to modify the work function of source and drain electrodes to improve charge injection/release.[21] However, the modification of the gate contact work function with SAMs in EGOFET devices was never explored before.

For this purpose, devices with coplanar gate electrodes were designed using Kapton as substrate. The coplanar configuration demanded the need to pattern the OSC to cover only the interdigitated source/drain area and to leave free the gate electrode. This was achieved by using a sacrificial layer to cover the gate electrode previously to the OSC deposition. The gate electrode was hence protected with a water-soluble polymer (i.e., Dextran). After the printing of the active layer using the bar-assisted meniscus shearing (BAMS) technique, the dextran layer was removed with water (**Figueres 4.2a**). The EGOFET based on a coplanar gate electrode displayed an electrical performance comparable with the classic top-gated configuration.

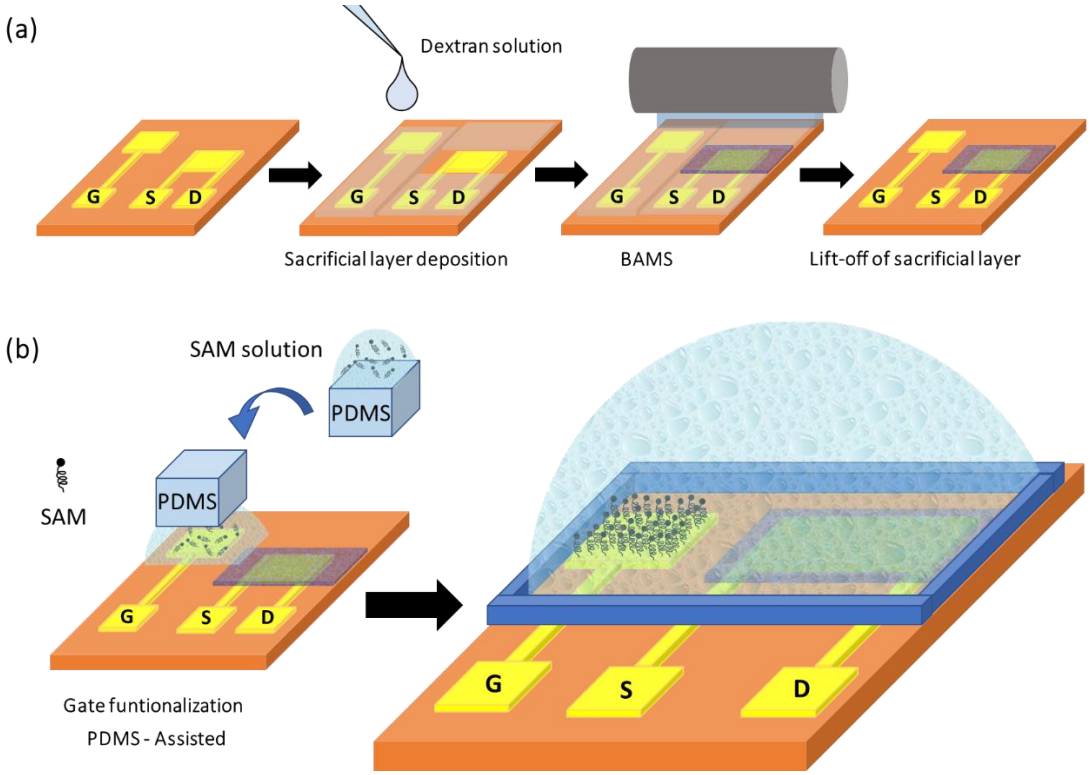

Figure 4.2. (a) Schematic representation of the semiconductor patterning process using the sacrificial layer approach. **(b)** PDMS- assisted printing for the gate functionalisation.

The functionalization of the gate electrode was carried out by poly(dimethylsiloxane) (PDMS)-assisted printing (Figure 4.2b). The thiolated molecules for SAM formation selected were: 2H,2H-perfluorodecanethiol (PFDT), 1-dodecanethiol (1DT), 4-methylthiophenol (MeTP), 4-aminothiophenol (ATP), 16-mercaptohexadecanoic acid (MHD), 4-fluorothiophenol (FTP) and 11-amino-1-undecanol (AUT). These molecules differ in their backbone length and their dipole moment.

The shift of the work function by the SAMs formation was investigated by Kelvin Probe Microscopy. The SAMs with non-polar or amide head group such as 1DT, MeTP, AUT, ATP exhibited a positive work function shift, while a negative work function shift was observed by FTP, PFDT and MHD, which were molecules with fluorinated or carboxylic terminal groups. As expected, the nature of the head group directly affected the change in the work function electrode. However, it is important to note that the MHD was a molecule with a strange behaviour since, although it is composed by a carboxylic terminal group, the long backbone chain makes it behave similar to an alkane molecule.

The EGOFETs with the gate functionalised displayed a clear change in the threshold voltage. However, the representation of the threshold voltage shift with respect to the work function shift did not show an obvious trend. In addition, the threshold voltage was also extracted in devices measured using a functionalised gold electrode immersed in the electrolyte instead of the coplanar electrode. In these gate electrodes the molecular density in the SAMs is much larger since they were prepared by incubation instead of by PDMS-printing. We observed that the threshold voltage shifts were significantly affected by the degree of functionalisation.

Additionally, the slope of the transfer characteristics (i.e., the plot I_{SD} vs V_{GS} in the linear regime) was affected by the gate functionalization in all these devices, which is indicative of a change in the device capacitance. The device capacitance was extracted directly from the transfer characteristics assuming that the value of the mobility of the semiconductor was constant. In general, the devices exhibited a drop of capacitance in the coplanar configuration. However, with the fluorinated PFDT and FTP SAMs the EGOFETs exhibited a gain of capacitance. This could be ascribed to a lower molecular coverage permitting an enhanced diffusion of ions through the SAM. On the other hand, the EGOFETs with the gate immersed exhibited a drop of capacitance for all the SAMs. Thus, again it was observed that the functionalization process played a role in the compactness of the SAM, which had a critical impact on the capacitance of the device. In general, the formation of the SAMs on the gate electrode led to a decrease on the device capacitance. However, other factors such as the packing of the SAMs and their polarizability were also crucial in order to understand the final device response.

Hence, it was concluded that the functionalization of the gate electrode with SAMs was a good strategy to modify the EGOFET response. The SAMs produced both a potentiometric and capacitive effects in the EGOFET, having the latter a stronger influence. This result is

interesting for the development of EGOFET sensors and points out the need of understanding the capacitive and potentiometric contributions in order to gain insights into the mechanisms involved.

4.3. CARBON PASTE ELECTRODES AS GATE CONTACTS IN EGOFETS

Article 11: Electronic performance of polymer carbon-paste nanoallotropes from 0D to 3D as novel gate electrodes in water-gated organic field-effect transistors.

In this paper, we reported the use of carbon composite electrodes (CPE) as gate contacts in EGOFETs. We explored the influence of the carbon filler, using carbon nanohorns (0D), carbon nanotubes (1D), reduced graphene oxide (2D) and graphite (3D), on the device electrical characteristics. As active layer, films of 2,8-difluoro-5,11-bis(triethylsilylethynyl) anthradithiophene:polystyrene (diF-TES-ADT:PS) deposited by BAMS were employed.

The CPEs were based on a nanocomposite of a conductor carbon nanoallotrope within an insulator polymer matrix. This type of electrodes have previously been used in analytical electrochemistry to develop biosensors.[26–28] The CPEs are non-toxic and environmentally friendly and, in addition, offer a series of desirable benefits, such as: i) robustness, ii) convenient electrical conductivity, iii) stable response in water media, iv) high specific surface area, v) facile tunability with a wide range of recognition elements and vi) the active surface of the electrode can be reset by simply polishing it.

The CPEs were hence prepared by dispersing the carbon materials in the insulation matrix (epoxy resin) **(Figure 4.3).** It is known that the properties of the electrode are strongly dependent on the nature, quantity and distribution of the conductor material.[29,30]

Previously, in our group it was reported the influence of the electrode electroactive area on the EGOFET electrical response using CPEs based on carbon nanotubes.[29] The electroactive area was tuned by the modification of the carbon nanotubes load, which exhibited a linear trend with the threshold voltage. In this work, we fixed the same electroactive area of the CPE to obtain the maximum conductivity and guarantee the mechanical properties of the nanocomposite. In this way, the electroactive device area dependence could be discarded and all the electrical changes could be attributed to the nature of the carbon filler.

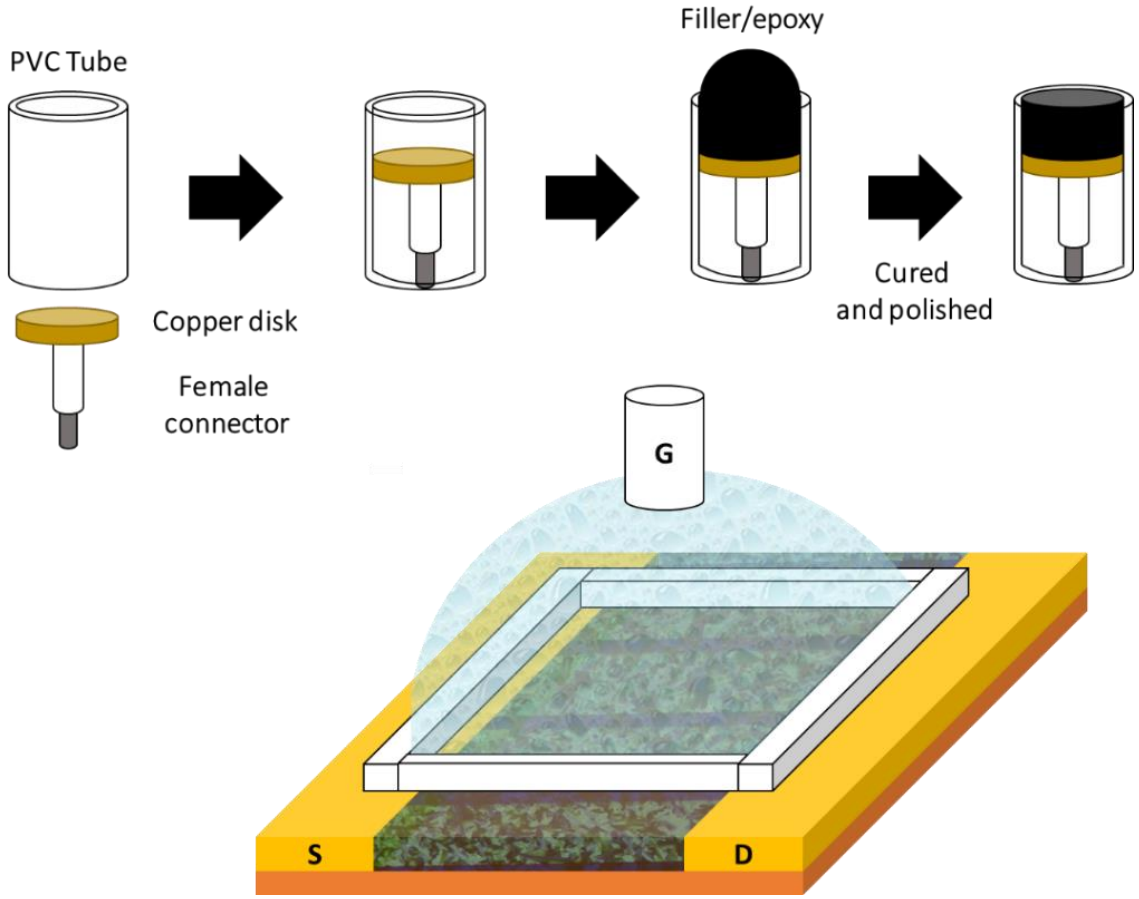

Figure 4.3. Methodology followed for the construction of a carbon paste electrode and schematic representation of the EGOFET configuration used with a carbon paste gate electrode.

The CPEs were characterised by electrochemical measurements to determine the electrical properties of the electrodes. The cyclic voltammetry revealed similar electrochemical performance and similar values of electroactive area as expected. However, it is important to note that the reduced graphene oxide exhibited a capacitive behaviour in the cyclic voltammogram. By electrochemical impedance spectroscopy (EIS) a relationship between the ohmic resistance of the system and the dimensionality of the electrodes was observed. Indeed, a significant resistance decrease with increasing the nanostructured dimension from 0D to 3D of the carbon material was observed. This trend was explained taking into account that the CPEs with higher dimensionality (3D) also had a higher load of conductive material (i.e., 16 % of 3D active material in front of 6% of 0D active material). In addition, a higher resistance to charge transfer was observed for CPEs based on reduced graphene oxide, which was an unequivocal sign of a more capacitive behaviour.

The final step was focused on the electrical measurements of the EGOFETs with the CPEs as gate contacts. The transfer characteristics of the EGOFETs displayed a good modulation of the source-drain current (I_{DS}), and the leakage current (I_{GS}) was low verifying that no

Faraday processes were taking place. The slope of the transfer characteristics showed similar values for all CPE gates and were similar to EGOFETs measured with the conventional gold electrodes. This indicated similar values of EDL capacitance. However, the transfer characteristics displayed a remarkable threshold voltage shift depending on the nature of the carbon filler or the load of conductive material in the paste. It should be noticed that the use of gate electrodes based on carbon materials with low dimensionality allowed to operate in a more positive voltage window than CPEs based on graphite.

The work function of the electrodes was evaluated by Kelvin Force Probe Microscopy in order to attempt to correlate the threshold voltage values with their work function. However, in our measurements conditions (25^{o}C and in air) no evident differences were observed in the work function of the materials. Therefore, the modulation of the threshold voltage was attributed to by the topological differences in the carbon materials, being an evident signal the different ohmic resistance observed in the electrochemical measurements.

Summarising, four different composite carbon-based electrodes were tested as non-conventional gate electrodes in EGOFETs. The performance of the electrodes were comparable to the one achieved with a conventional immersed gold gate electrode. In addition, we demonstrated that the electrical properties of the transistors can be customized by the choice of the carbon filler. The dimensionality or topography of the CPE was found to influence the threshold voltage and, thus, it is a useful tool to modulate the device properties.

4.4. EGOFET AS A TOOL TO MONITOR THE SURFACTANT MONOLAYER FORMATION ON A METAL ELECTRODE

Article 12: *Interplay between electrolyte-gated organic field-effect transistors and surfactants: a surface aggregation tool and protecting semiconducting layer.*

In this paper (***Article 12***), we investigated the modification of the EGOFET interfaces by the formation of self-assembled monolayers of surfactants. We demonstrated that EGOFETs can be exploited as a tool to monitor the surfactant monolayer formation on a polarised metal contact (i.e., the gate). Further, at higher surfactant concentrations it was found that surfactants assemble on the OSC surface protecting it.

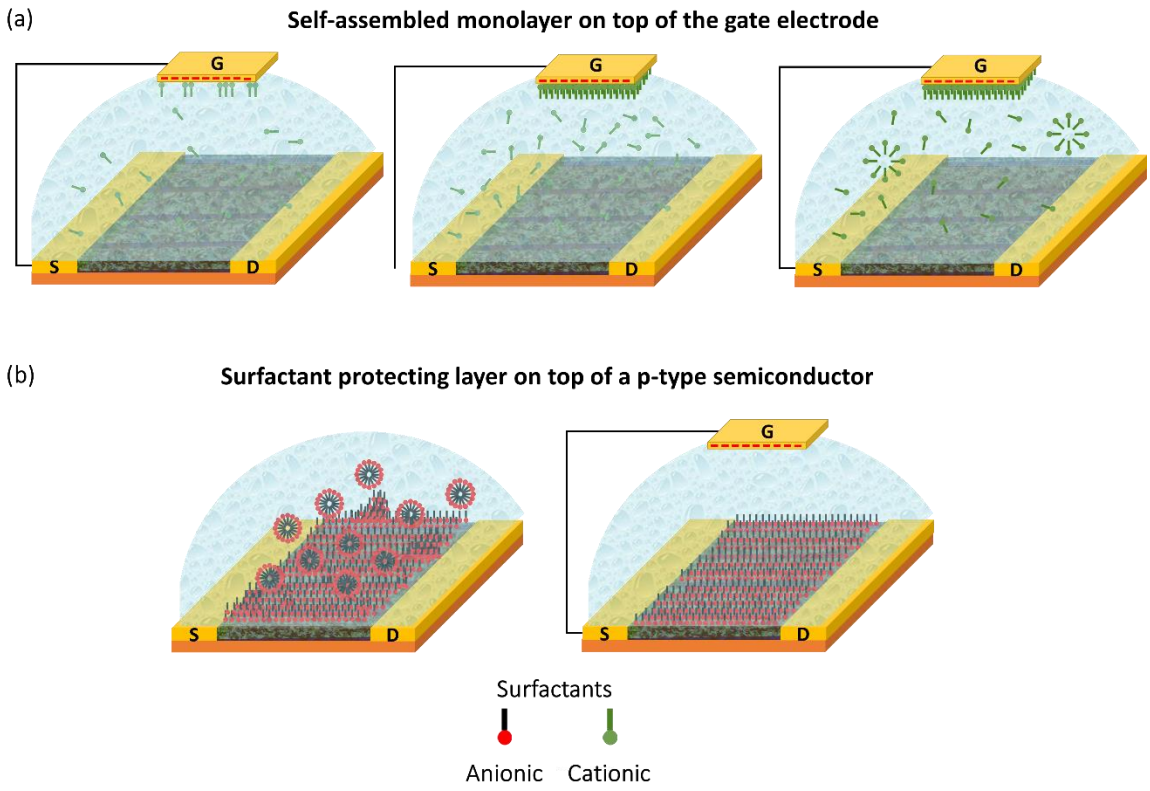

Figure 4.4. Schematic representation of the physical adsorption mechanism of surfactants on a p-type EGOFET. **(a)** Below the monolayer concentration, a cationic surfactant forms a self-assembled monolayer on the gate electrode. **(b)** Above the micelle concentration, anionic surfactants can be used to protect the OSC.

Surfactants are amphiphilic molecules with a hydrophilic polar head and a long hydrophobic backbone chain. The most exceptional property of surfactants is the capacity to form self-assembled structures at the interfaces and supramolecular structures in solution.[31] Here we investigated the monolayer formation of surfactants on top of the gate electrode (at the electrode/electrolyte interface). We selected devices based on blends of PS and the p-type OSC diF-TES-ADT and the n-type OSC N,N'-bis(n-octyl)-dicyano-perylene-3,4:9,10-bis-(dicarboximide) (PDI8CN2). As cationic and anionic surfactant molecules, we chose cetyltrimethylammonium bromide (CTAB) and sodium dodecyl sulfate (SDS), respectively.

The EGOFETs were measured at different concentrations of surfactants, cationic for the p-type EGOFET (i.e., gate negatively polarised) and anionic for the n-type one (i.e., gate positively polarised) (**Figure 4.4a,** for a p-type EGOFET). The EGOFET devices based on diF-TES-ADT:PS were tested introducing CTAB solutions from 1 nM to 1 mM in the electrolyte media. It was observed that the concentration of surfactant affected the EGOFET response. The increment of CTAB in the solution media produced a negative threshold voltage shift, while the slope of the transfer characteristics kept constant during the test. In addition, we

observed three different regimes. In the first regime from 1 nM to 100 nM the EGOFET devices did not exhibit any change since the low surfactant concentration did not cover a significant part of the surface of the gate electrode. The formation of a self-assembled monolayer on top of the gate electrode was observed between 100 nM to 10 μM, where the formation of the monolayer reduced the effective gate voltage on the OSC producing a threshold voltage shift towards more negative voltage values. A higher concentration of surfactant (> 10 μM) produced micelles in the solution, which did not affect the electrical performance of the EGOFET.

The monolayer formation was also confirmed by electrochemical and AFM measurements, Sub-microstructures were observed by AFM imaging and the electrochemical measurements using a redox probe revealed a drop of the peak current and an increase of the potential difference between the oxidation and reduction peak when the concentration of the surfactant increased in agreement with the passivation of the electrode.

The experiment was repeated employing the n-type EGOFET based on PDI8CN2:PS with the anionic surfactant. The results displayed the same three regimes. In this case, the monolayer formation was observed in the concentration range from 1 μm to 1 mM leading to a threshold voltage shift towards higher positive voltages. As in the previous case, the electrochemical and AFM measurements confirmed the presence of the monolayer on top of the gate electrode. Thus, EGOFETs represent a promising approach to detect the formation of monolayers on the electrode/electrolyte interface.

The second part of the work involved the formation of a protecting surfactant layer on the electrolyte/OSC interface. The growth of the surfactant layer consisted of releasing a drop of surfactant solution above its micellar concentration for 20 min followed by rinsing and drying with a nitrogen flow. As in the previous part, the formal charge of the head group played a role. In order to form a stable protecting layer during device operation, the charge of the carriers of the OSC had to be opposite to the formal charge of the surfactant head group.

The p-type EGOFETs based on diF-TES-ADT:PS were stabilized with a 50 mM solution of SDS. The protected films were electrically characterised by current monitoring exhibiting only a 10% current decrease after 10 hours of operation, while the non-treated EGOFETs exhibited more than 30 % of current drop.

Further, the n-type EGOFETs were stabilized using a 10 mM solution of CTAB. The devices revealed an enhanced stability in the current monitoring experiments comparable to what it was observed with the p-type EGOFETs passivated with SDS. The treated n-type EGOFETs exhibited a fast current increase in the first 30 minutes and then a constant current for 3 hours, while the non-treated n-type EGOFETs displayed an important drop of 90% of the current in the same period of time. It is important to note that the ultra-high stability

observed for the n-type EGOFETs is a great advance, since it is known that n-type EGOFETs suffer of much faster deterioration in water.[32]

The low operational stability of EGOFETs due to permeability of ions into the OSCs is one of the main limitations for long-term operability and their practical implementation. Here, EGOFETs with an extraordinary long-term stability in water environment was achieved by a simple and versatile approach using a surfactant encapsulation layer.

4.5 SUMMARY

In conclusion, we fabricated EGOFETs and studied the impact of modification of the gate electrode/electrolyte interface on the device electrical characteristics.

The functionalization of the gate electrode with a series of SAMs of different chemical nature was tested using a PDMS-assisted printed coplanar gate electrode and a conventional top gate functionalised by the incubation method. Our results showed that the functionalization of the gate produced threshold voltage shifts and capacitance changes. We observed that the capacitance effect had a more pronounced impact than the potentiometric one. We demonstrated that the device electrical properties can be tuned by surface engineering of the gate electrodes with SAMs, although the interplay between capacitive and potentiometric effects is complex and also dependent on the degree of the SAM functionalisation. Additionally, the development of a new strategy to fabricate flexible coplanar EGOFET with a patterned OSC was accomplished successfully.

Secondly, home-made carbon paste electrodes with excellent electronic properties were implemented as gate electrodes in EGOFETs as alternative to conventional Au electrodes. The carbon paste electrodes exhibited different potentiometric behaviour depending on the nature of the carbon nanomaterials, which was reflected by a threshold voltage shift in the EGOFET characteristics.

The previous works demonstrated hence that the modification of the gate electrode surface with SAMs or the modification of the nature of the gate using carbon paste electrodes are promising strategies to tune the EGOFET electrical characteristics.

Finally, EGOFETs were used to monitor the surfactant monolayer formation at the polarised gate electrode/electrolyte interface by registering the shift of the threshold voltage in the monolayer formation concentration range. This work proves the potential of using EGOFETs to investigate events occurring at the electrode surface. In addition, the treatment of the OSCs with higher surfactant concentrations led to the long-term stabilization of the EGOFETs due to the encapsulation of the OSC reducing the migration of ions inside the OSC.

The modification of the electrolyte/gate interface is a powerful tool to modify the electrical properties of EGOFETs, which can be used to improve the electrical characteristics, tune the operation voltage window of the EFOGET or follow adsorption processes at the electrode/electrolyte interface.

4.6. References

(1) Poimanova, E. Y.; Shaposhnik, P. A.; Anisimov, D. S.; Zavyalova, E. G.; Trul, A. A.; Skorotetcky, M. S.; Borshchev, O. V.; Vinnitskiy, D. Z.; Polinskaya, M. S.; Krylov, V. B.; Nifantiev, N. E.; Agina, E. V.; Ponomarenko, S. A. Biorecognition Layer Based On Biotin-Containing [1]Benzothieno[3,2- b][1]Benzothiophene Derivative for Biosensing by Electrolyte-Gated Organic Field-Effect Transistors. *ACS Appl. Mater. Interfaces* 2022, *14* (14), 16462–16476.

(2) Liao, J.; Si, H.; Zhang, X.; Lin, S. Functional Sensing Interfaces of PEDOT:PSS Organic Electrochemical Transistors for Chemical and Biological Sensors: A Mini Review. *Sensors (Switzerland)* 2019, *19* (2), 218.

(3) Torsi, L.; Magliulo, M.; Manoli, K.; Palazzo, G. Organic Field-Effect Transistor Sensors: A Tutorial Review. *Chem. Soc. Rev.* 2013, *42* (22), 8612–8628.

(4) Mulla, M. Y.; Tuccori, E.; Magliulo, M.; Lattanzi, G.; Palazzo, G.; Persaud, K.; Torsi, L. Capacitance-Modulated Transistor Detects Odorant Binding Protein Chiral Interactions. *Nat. Commun.* 2015, *6*, 6010.

(5) Mulla, M. Y.; Seshadri, P.; Torsi, L.; Manoli, K.; Mallardi, A.; Ditaranto, N.; Santacroce, M. V.; Di Franco, C.; Scamarcio, G.; Magliulo, M. UV Crosslinked Poly(Acrylic Acid): A Simple Method to Bio-Functionalize Electrolyte-Gated OFET Biosensors. *J. Mater. Chem. B* 2015, *3* (25), 5049–5057.

(6) Berto, M.; Diacci, C.; D'Agata, R.; Pinti, M.; Bianchini, E.; Lauro, M. Di; Casalini, S.; Cossarizza, A.; Berggren, M.; Simon, D.; Spoto, G.; Biscarini, F.; Bortolotti, C. A. EGOFET Peptide Aptasensor for Label-Free Detection of Inflammatory Cytokines in Complex Fluids. *Adv. Biosyst.* 2018, *2* (2), 1700072.

(7) Casalini, S.; Leonardi, F.; Cramer, T.; Biscarini, F. Organic Field-Effect Transistor for Label-Free Dopamine Sensing. *Org. Electron.* 2013, *14* (1), 156–163.

(8) Kergoat, L.; Herlogsson, L.; Braga, D.; Piro, B.; Pham, M. C.; Crispin, X.; Berggren, M.; Horowitz, G. A Water-Gate Organic Field-Effect Transistor. *Adv. Mater.* 2010, *22* (23), 2565–2569.

(9) Magliulo, M.; Mallardi, A.; Mulla, M. Y.; Cotrone, S.; Pistillo, B. R.; Favia, P.; Vikholm-Lundin, I.; Palazzo, G.; Torsi, L. Electrolyte-Gated Organic Field-Effect Transistor Sensors Based on Supported Biotinylated Phospholipid Bilayer. *Adv. Mater.* 2013, *25* (14), 2090–2094.

(10) Torricelli, F.; Adrahtas, D. Z.; Bao, Z.; Berggren, M.; Biscarini, F.; Bonfiglio, A.; Bortolotti, C. A.; Frisbie, C. D.; Macchia, E.; Malliaras, G. G.; Mcculloch, I.; Moser, M.; Nguyen, T.-Q.; Owens, R. M.; Salleo, A.; Spanu, A.; Torsi, L. Electrolyte- Gated Transistors for Enhanced Performance Bioelectronics. *Nat. Rev. Methods Prim.* 2021, *1*, 66.

(11) Berto, M.; Vecchi, E.; Baiamonte, L.; Condò, C.; Sensi, M.; Di Lauro, M.; Sola, M.; De

Stradis, A.; Biscarini, F.; Minafra, A.; Bortolotti, C. A. Label Free Detection of Plant Viruses with Organic Transistor Biosensors. *Sensors Actuators, B Chem.* 2019, *281*, 150–156.

(12) Zhang, Q.; Leonardi, F.; Casalini, S.; Mas-Torrent, M. Mercury-Mediated Organic Semiconductor Surface Doping Monitored by Electrolyte-Gated Field-Effect Transistors. *Adv. Funct. Mater.* 2017, *27* (46), 1703899.

(13) Ricci, S.; Casalini, S.; Parkula, V.; Selvaraj, M.; Saygin, G. D.; Greco, P.; Biscarini, F.; Mas-Torrent, M. Label-Free Immunodetection of α-Synuclein by Using a Microfluidics Coplanar Electrolyte-Gated Organic Field-Effect Transistor. *Biosens. Bioelectron.* 2020, *167*, 112433.

(14) Cramer, T.; Kyndiah, A.; Murgia, M.; Leonardi, F.; Casalini, S.; Biscarini, F. Double Layer Capacitance Measured by Organic Field Effect Transistor Operated in Water. *Appl. Phys. Lett.* 2012, *100* (14), 143302.

(15) Bard, A. J.; Faulkner, L. R. *Electrochemical Methods: Fundamentals and Applications*; John Wiley & Sons, 2001.

(16) Wang, D.; Noël, V.; Piro, B. Electrolytic Gated Organic Field-Effect Transistors for Application in Biosensors—A Review. *Electronics* 2016, *5* (1), 9.

(17) Leonardi, F.; Casalini, S.; Zhang, Q.; Galindo, S.; Gutiérrez, D.; Mas-Torrent, M. Electrolyte-Gated Organic Field-Effect Transistor Based on a Solution Sheared Organic Semiconductor Blend. *Adv. Mater.* 2016, *28* (46), 10311–10316.

(18) Kergoat, L.; Piro, B.; Berggren, M.; Horowitz, G.; Pham, M. C. Advances in Organic Transistor-Based Biosensors: From Organic Electrochemical Transistors to Electrolyte-Gated Organic Field-Effect Transistors. *Anal. Bioanal. Chem.* 2012, *402* (5), 1813–1826.

(19) Kergoat, L.; Herlogsson, L.; Piro, B.; Pham, M. C.; Horowitz, G.; Crispin, X.; Berggren, M. Tuning the Threshold Voltage in Electrolyte-Gated Organic Field-Effect Transistors. *Proc. Natl. Acad. Sci. U. S. A.* 2012, *109* (22), 8394.

(20) Wang, N.; Yang, A.; Fu, Y.; Li, Y.; Yan, F. Functionalized Organic Thin Film Transistors for Biosensing. *Acc. Chem. Res.* 2019, *52*, 277–287.

(21) Casalini, S.; Bortolotti, C. A.; Leonardi, F.; Biscarini, F. Self-Assembled Monolayers in Organic Electronics. *Chem. Soc. Rev.* 2017, *46* (1), 40–71.

(22) Janneck, R.; Heremans, P.; Genoe, J.; Rolin, C. Influence of the Surface Treatment on the Solution Coating of Single-Crystalline Organic Thin-Films. *Adv. Mater. Interfaces* 2018, *5* (12), 1800147.

(23) Li, S.; Guérin, D.; Lmimouni, K. Improving Performance of OFET by Tuning Occurrence of Charge Transport Based on Pentacene Interaction with SAM Functionalized Contacts. *Microelectron. Eng.* 2018, *195* (5), 62–67.

(24) Londhe, P.; Chaure, N. B.; Athawale, A. Interface Engineering of Gate Dielectrics with Multifunctional Self-Assembled Monolayers in Copper Phthalocyanine Based Organic Field-Effect Transistors. *Mater. Sci. Eng. B* 2021, *273*, 115397.

(25) Sang, B.; Yang, Y.; Shin, K.; Park, C. E. The Effect of Gate-Dielectric Surface Energy on Pentacene Morphology and Organic Field-Effect Transistor Characteristics. *Adv. Funct. Mater.* 2005, *15* (11), 1806–1814.

(26) Muñoz, J.; Baeza, M. Customized Bio-Functionalization of Nanocomposite Carbon Paste Electrodes for Electrochemical Sensing: A Mini Review. *Electroanalysis* 2017, *29* (7), 1660–1669.

(27) Švancara, I.; Vytřas, K.; Kalcher, K.; Walcarius, A.; Wang, J. Carbon Paste Electrodes in Facts, Numbers, and Notes: A Review on the Occasion of the 50-Years Jubilee of Carbon Paste in Electrochemistry and Electroanalysis. *Electroanalysis* 2009, *21* (1), 7–28.

(28) Muñoz, J.; Bastos-Arrieta, J.; Muñoz, M.; Muraviev, D.; Céspedes, F.; Baeza, M. Simple Green Routes for the Customized Preparation of Sensitive Carbon Nanotubes/Epoxy Nanocomposite Electrodes with Functional Metal Nanoparticles. *RSC Adv.* 2014, *4* (84), 44517–44524.

(29) Muñoz, J.; Leonardi, F.; Özmen, T.; Riba-Moliner, M.; González-Campo, A.; Mas-Torrent, M.; Baeza, M.; Mas-Torrent, M. Carbon-Paste Nanocomposites as Unconventional Gate Electrodes for Electrolyte-Gated Organic Field-Effect Transistors: Electrical Modulation and Bio-Sensing. *J. Mater. Chem. C* 2019, *7* (47), 14993–14998.

(30) Muñoz, J.; Brennan, L. J.; Céspedes, F.; Gun'ko, Y. K.; Baeza, M. Characterization Protocol to Improve the Electroanalytical Response of Graphene-Polymer Nanocomposite Sensors. *Compos. Sci. Technol.* 2016, *125*, 71–79.

(31) Tyrode, E.; Rutland, M. W.; Bain, C. D. Adsorption of CTAB on Hydrophilic Silica Studied by Linear and Nonlinear Optical Spectroscopy. *J. Am. Chem. Soc.* 2008, *130* (51), 17434–17445.

(32) Porrazzo, R.; Luzio, A.; Bellani, S.; Bonacchini, G. E.; Noh, Y. Y.; Kim, Y. H.; Lanzani, G.; Antognazza, M. R.; Caironi, M. Water-Gated n-Type Organic Field-Effect Transistors for Complementary Integrated Circuits Operating in an Aqueous Environment. *ACS Omega* 2017, *2* (1), 1–10.

ARTICLE 10: MODIFICATION OF THE GATE ELECTRODE BY SELF-ASSEMBLED MONOLAYERS IN FLEXIBLE ELECTROLYTE-GATED ORGANIC FIELD EFFECT TRANSISTORS: WORK FUNCTION VS. CAPACITANCE EFFECTS

AUTHORS: Francesca Leonardi, Adrián Tamayo, Stefano Casalini and Marta Mas-Torrent

PUBLICATION: RSC advances 8 (48), 27509 (2018)

ARTICLE 11: Electronic Performance of Polymer Carbon-Paste Nanoallotropes from 0D to 3D as Novel Gate Electrodes in Water-Gated Organic Field-Effect Transistors

AUTHORS: Adrián Tamayo, Jose Muñoz and Marta Mas-Torrent

PUBLICATION: Advanced Electronic Materials 6 (7), 2000431 (2020)

ARTICLE 12: INTERPLAY BETWEEN ELECTROLYTE-GATED ORGANIC FIELD-EFFECT TRANSISTORS AND SURFACTANTS: A SURFACE AGGREGATION TOOL AND PROTECTING SEMICONDUCTING LAYER

AUTHORS: Qiaoming Zhang, Adrián Tamayo, Francesca Leonardi, Marta Mas-Torrent

PUBLICATION: ACS Applied Materials & Interfaces 13 (26), 30902 (2021)

CHAPTER V

CONCLUSIONS

In this thesis, we studied fundamental aspects in the fabrication of crystalline organic semiconductor (OSC) layers by solution shearing for their implementation in organic field-effect transistors (OFETs). Special attention has been paid to the use of blends of OSCs and insulating polymers and on establishing correlations morphology/structure-performance. The application of OFETs as X-rays detector were investigated and their response optimised. Finally, development of high-performance electrolyte-gated OFETs (EGOFETs) has been pursued with the aim at understanding the interfaces in this more complex architecture.

The research conducted and presented in this thesis has led to the following conclusions:

i) The control of polymorphism and morphology of the OSC films can be carried out by tuning the ink formulation and deposition parameters. In general, the deposition of the OSC using the Bar-Assisted Meniscus Shearing (BAMS) leads to kinetic polymorphs. However, at low coating speeds the thermodynamic polymorph can be formed. It should also be highlighted that one polymorph can be obtained in different morphologies. The polymorphism and morphology have a great impact on the OFET performance.

ii) The blending of the OSC with an insulating polymer has a beneficial impact on the processability and electrical performance of the polycrystalline OSC layer. During the deposition, a vertical phase separation takes places in which the OSC crystallises on top of a PS layer. This process enhances the OSC crystallisation and the PS bottom layer reduces the interfacial charge traps.

iii) In particular, the p-type OSC DB-TTF blended with polystyrene (PS) has been studied. This OSC displays a rich polymorphism. In general, in all the employed deposition conditions the kinetic γ phase was formed, which exhibited an excellent device performance with a maximum mobility in the range 0.1-0.3 $cm^2 \cdot V^{-1} \cdot s^{-1}$ when the morphology of the DB-TTF:PS film was optimised. In addition, the thermodynamic α phase was formed when using a low shearing speed. This was the first time that this polymorph was obtained as thin film. The devices based on this polymorph exhibited a mobility of 0.05 $cm^2 \cdot V^{-1} \cdot s^{-1}$, lower than the γ phase.

iv) OFETs based on Ph-BTBT-C_{10}, which is a promising asymmetric p-type OSC, have been successfully fabricated. The devices based on films of Ph-BTBT-C_{10}:PS exhibited an enhanced performance compared with the devices based on only the OSC. The films deposited at high coating speeds showed an isotropic mobility of 0.2 $cm^2 \cdot V^{-1} \cdot s^{-1}$ for the

pristine films and 1.3 $cm^2 \cdot V^{-1} \cdot s^{-1}$ for the Ph-BTBT-C_{10}:PS films. On the other hand, OFETs prepared at low coating speed based on Ph-BTBT-C_{10}:PS and Ph-BTBT-C_{10} displayed lower mobilities (0.04 $cm^2 \cdot V^{-1} \cdot s^{-1}$) with a high anisotropic character.

X-ray diffraction measurements showed that the OSC crystallises following the bulk bilayer structure instead of the thin film layer structure typically obtained by spin coating on surface without performing an annealing step. However, the prepared films showed some molecular disorder that could be detrimental to the device mobility.

v) The addition of a small percentage of fluorinated PS (i.e., PFS) for processing OSC:PS blends has been shown to be a promising tool to enhance the device bias stress and shelf stability. Thanks to the high hydrophobicity of PFS, the water penetration towards the OSC films is reduced. In particular, in blended films of TIPS-pentacene:PS 4:1, it was found that the replacing of 20% of PS with PFS provided devices with a time stability increase of up to 250 % and enhanced bias stress stability, without compromising significantly the device mobility (i.e., mobility of 0.5 $cm^2 \cdot V^{-1} \cdot s^{-1}$).

vi) OFET devices represent a promising platform to be applied as direct X-ray detectors since they can be fabricated at low cost and on flexible substrates. Our studies employing solution-sheared OSC films shed light on the main parameters affecting the X-ray photoresponse. The sensitivity values were affected by the morphological characteristics of the OSC films and electrical characteristics of the OSC. In p-type films, it was observed that a higher grain density resulted in an increment in the electron charge traps (i.e., minority charges) which was beneficial to the photosensitivity since promoted the hole-electron dissociation. Additionally, the reduced hole traps (i.e., majority charges) at the OSC/SiO_x interface produced by the vertical stratification of the OSC blends, led to an improvement in the device mobility, and, in turn, in the X-ray sensitivity.

The OFET devices based on TIPS-pentacene:PS and TMTES-pentacene:PS blends exhibited ultra-high sensitivity values $3 \cdot 10^9$ and $4 \cdot 10^{10}$ $\mu C \cdot Gy^{-1} \cdot cm^{-3}$, respectively. This is the highest sensitivity achieved for OFETs and surpasses the performance of commercial detectors based on inorganic semiconductors.

vii) Electrolyte gated organic field-effect transistors (EGOFETs) are devices raising a lot of interest in sensing applications since they operate in water environment. Remarkably, the modification of the gate electrode/electrolyte interface has a strong impact on the device performance. Changes at this interface can lead to potentiometric changes that are translated into threshold voltage shifts, or/and capacitance changes.

viii) The functionalisation of metals with self-assembled monolayers (SAMs) is a well-known approach to modify the metal work function. The functionalization of the gold gate electrode with SAMs in EGOFETs resulted in a significant shift in the threshold voltage but also in a capacitance change of the electrical double layers. It was found that both the chemical nature of the SAM (i.e., dipole) and also the packing density were influencing on

the device response. A poor layer compactness SAM caused a smaller drop in capacitance. Due to the interplay between these effects, clear correlations between the metal work function and the device response was not possible to carry out.

ix) Carbon paste electrodes based on carbon nanohorns, nanotubes, reduced graphene oxide and graphite, were exploited as new non-toxic reusable gate electrodes in EGOFETs. The devices exhibited mobilities comparable to the ones found with conventional gold gate contacts. The nature of the carbon material directly affected the threshold voltage of the EGOFET and, thus, it could be used as a tool to adjust the device window voltage. Considering that the electrode work functions were not significantly different between the different carbon electrodes, the changes observed were ascribed to changes in the intrinsic ohmic resistance of the carbon paste electrodes.

The best electrical performances were found using carbon paste electrodes based on reduced graphene oxide. These EGOFETs displayed a high reproducibility and negligible hysteresis.

x) It was demonstrated that EGOFETs can be exploited for monitoring events happening at the gate electrode/electrolyte interface. In particular, the adsorption of cationic (anionic) surfactants at the gold gate electrode of p-type (n-type) EGOFETs was investigated. A shift of the threshold voltage was observed by the shielding produced by the surfactant adsorption at the gate electrode. Hence, the EGOFET devices permit to determine the surfactant concentration required for a monolayer formation.

xi) In addition, the formation of cationic (anionic) surfactant layers on top of n-type (p-type) OSCs was found to lead to EGOFET devices that showed an increased long-term stability. This passivation of the OSCs prevented the migration of ions inside the OSC that causes deterioration of the device electrical properties.